THE DEVELOPMENT OF INSTRUMENTATION AND MODEL TESTING FOR THE LOAD DISTRIBUTION IN A DRILLED PIER

A THESIS

Presented to

The Faculty of the Graduate Division

By

Samuel Patton Clemence

In Partial Fulfillment

of the Requirements for the Degree

Doctor of Philosophy in the School of Civil Engineering

Georgia Institute of Technology

June, 1973

THE DEVELOPMENT OF INSTRUMENTATION AND MODEL TESTING FOR THE LOAD DISTRIBUTION IN A DRILLED PIER

Approved:

W. F. Brumund, Chairman

R. H. Brown

B. B. Mazanti

Date approved by Chairman: 5/22/73

ACKNOWLEDGMENTS

The writer wishes to gratefully acknowledge all those who helped in completion of this work. Special thanks go to Dr. W. F. Brumund for his encouragement and guidance throughout the whole project. Thanks are also extended to Dr. B. B. Mazanti and Dr. Russell H. Brown for their help as advisors and serving as reading committee members.

Special thanks are also extended to Professor G. F. Sowers for his suggestions and helpful advice during the writer's stay at Georgia Tech.

The kind help of Mr. Roland Brown, machinist, Mr. Ray Joyner, electronics technician, and Mr. Larry Westbrooks, assistant machinist, was also sincerely appreciated.

The financial assistance of the Shell Oil Company and the Ford Foundation is also acknowledged.

TABLE OF CONTENTS

APPENDIX Page

LIST OF TABLES

LIST OF ILLUSTRATIONS

SUMMARY

The increasing use of digital computers in the design of civil engineering structures has greatly expanded the engineer's capability to use more sophisticated analyses. The evaluation of these advanced design techniques is dependent on information from the field. Information from full scale structures or large scale models is required to evaluate the design performance. One of the basic steps required is development of suitable instrumentation to measure the loads in a structure or large scale model.

The objectives of this study were to develop a load cell and suitable instrumentation for use in a large scale model and to evaluate the load distribution in a model pier foundation. The load cell developed was a four-column sensor with the capability of measuring the six components of force: axial force, biaxial bending, torsion and shear forces in orthogonal planes. The cell was then used in the study of the load distribution in a large scale model concrete pier. The pier was preplaced with the tip resting on a simulated rock base. A homogeneous layer of sand at a relative density of 75 percent was placed around the pier. The load distribution along the pier shaft and the amount of skin friction developed were measured using Carlson cells and strain gages.

A rational method of predicting the skin friction was developed using laboratory direct shear tests and hyperbolic representation of the shear force-deflection curve of the sand-concrete interface.

The measured load distribution along the pier indicated a large transfer of load near the pier tip due to the effect of the simulated rock boundary.

The direct shear test and hyperbolic model procedure for predicting the skin friction were within sixteen percent of the measured value. An empirical correction applied to the model to account for the rigid boundary effect of the rock layer improved the prediction to within one percent of the measured load. The measured side friction was approximately ten percent of the total applied load. This amount of skin friction represents the lower bound for the expected value of skin friction for a concrete pier in sand, because of the smooth pier surface utilized.

CHAPTER I

INTRODUCTION

The use of digital computers in the design and analysis of civil engineering structures has rapidly expanded the engineer's capability to use more sophisticated systems of analysis. The applicability of these analyses is dependent on how closely the theoretical models approximate the actual field situation. The best means of determining the validity of the theoretical model is through measurements of the performance of full scale civil engineering structures. This type of information is most vital today, since most of the interest is focused on the computational and design technique with only a small amount of feedback from the field.

One of the earliest investigations of a full scale structure was conducted at the Massachusetts Institute of Technology. During the construction of the Hayden Library at MIT, the actual foundation loads were measured and compared with the design [1]. The measured dead loads were found to be nearly equal to the design value. The live loads, however, were less than 20 percent of the design value. The Russians have also conducted full scale studies. In 1970, Babichev and Yushin [4] measured the live loads and dead loads for two five-story apartment buildings in Salavat and Ufa, Russia, and

compared these measurements with what was predicted. Their study indicated that the measured live loads were from 10 to 25 percent over estimated by the design loads. These cases point out the need for more large scale studies. H. S. Ward, of the National Research Council of Canada, stated [56] in August, 1971:

> If full advantage is to be taken of the potential of the computational power now available, Civil Engineers should now focus far more attention than in the past on measuring the performance of completed structures.

In order to measure the performance of full scale structures and their foundations, reliable measurement techniques must be developed. One aspect of this study included the design, development and testing of a load cell which, built in prototype, would be suitable for placing in a full size structure to measure six components of force applied from the structure to the foundation. The study also included the evaluation of a number of different types of instrumentation which might be used to determine the load distribution along the shaft of a drilled pier. A major portion of this study was to integrate all this instrumentation into one large scale model of a pier foundation and show how the data could be used to verify an analytical model which was developed to describe the load distribution in a pier foundation.

A proposed sequel to this study would be the actual inclusion of the proposed load cell and instrumentation of the foundation into a full scale structure for the measurement

of loads and distribution through the foundation.

Column Load Sensors

The first portion of this project was concerned with the development of a load sensor which could be incorporated into a structure with properties as similar as possible to those of the replaced structural element. The cell would be capable of measuring six components of force: axial force, biaxial bending, torsion, and shear forces in two orthogonal planes.

Model Pier and Instrumentation

The major portion of this study was devoted to the instrumentation of a large scale model pier and to the prediction and behavior of the pier in a homogeneous sand. The pier foundation chosen for the study was one about a quarter-scale size of the typical pier foundations used in the Atlanta area. The combined model load cell and pier foundation comprised a large scale (one-quarter) model of what might be included in an actual building. The typical soil conditions in Atlanta, Georgia, consist of residual micaceous silty sands and sandy silts overlying a granite-gneiss rock. A common design assumption for the piers is to assume they act as end bearing members with little or none of the load being carried in skin friction along the sides of the pier. The model study was made with the twofold objective of (1) determining a suitable means of instrumenting a pier

foundation for field use, and (2) the development of a rational, simple means of predicting skin friction developed along a pier and confirming the procedure by a large scale model test.

CHAPTER II

REVIEW OF THE LITERATURE

The review of literature is separated into two parts: (1) structural load measurement devices, and (2) pier foundations.

Structural Load Measurement Devices

The need for reliable measurements of the loads imposed on foundations has led to the recent development of several types of load cells. Babichev [3], used hollow steel cylinders inserted between a continuous concrete grillage beam and the pile foundation to study the load distribution. The deformations were recorded by four sets of instruments: resistance strain gages, dial indicators, a comparator, and photoelastic strain gages. Eccentricities of load were allowed for by providing three measurements at 120° intervals around the tube. Only axial loads were measured by this system. The system worked quite well and was employed for approximately one year of study. In 1968, a more sophisticated cell was developed by Gupta [18] at the Imperial College, University of London. Gupta's cell was capable of measuring all six components (i.e., three force and three moment components) of the reaction at a support. This cell consisted of three tripods arranged such that their apexes formed the nodes

of an equilateral triangle. Each tripod consisted of tubular sections of an aluminum alloy with four electrical resistance strain gages mounted on the central part. The tripods were mounted on top and bottom steel plates. The most recent development was by Vanderbilt [50], at the University of Illinois, in which two types of load cells were developed to measure the structural reaction of large scale model concrete floor slabs. These two cells, a hollow cylinder type and a tripod type, were instrumented with electrical strain gages and were capable of measuring three orthogonal force components.

The hollow cylinder dynamometer consisted of an eight-inch length of aluminum tube with top and base plates, with a load capacity of 20,000 pounds. Three pairs of electric resistance strain gages were mounted on the hollow cylinder. During calibration of the hollow cylinder dynamometer, it was noted that while loading in any one direction, small strains were present on the gages in the other two directions, indicating some tubular shell action in this type of dynamometer. The tripod of load cell consisted of a steel base plate, three tubular legs and a steel ball seat, with a load capacity of 15,000 pounds. An active pair of strain gages was mounted on each leg at mid-height and was quite similar in construction to that of Gupta's cell.

Several pile and pier type load cells have been developed by Whitaker and Cooke [60] and Fellenius and

Haagen [17]. These will be described in the instrumentation section. A rather unusual earth pressure cell for the measurement of normal and shear stresses in a soil mass has been developed by Arthur and Roscoe [2]. With the exception of Babichev [3], none of the above described load cells have been developed for the purpose of full scale measurements of the transfer of load from a structure to the foundation. The load cell proposed in this study was developed to have the potential of being used for full scale measurement in the field.

Pier Foundations

Drilled pier foundations have been extensively used for the foundations of large structures. The development of suitable excavation equipment and construction technique in the 1940's and 1950's have made this type of foundation quite popular throughout the world. With the increasing use of this type of foundation, field tests and model studies were undertaken to investigate the behavior of these piers. The behavior with respect to the amount of load resisted by side friction in cohesive soils was extensively studied. A complete summary of the tests performed throughout the world from the early 1950's to 1970 has been presented by O'Neill and Reese [38].

Full Scale Tests

The earliest full scale tests were performed on

uninstrumented piers, the side friction was computed from the measured ultimate load and an assumed bearing capacity for the tip. Several of the later investigators did provide instrumentation on the piers to more completely define the load distribution. One of the earliest investigators using instrumentation, DuBose [15], performed a series of field tests on relatively small diameter drilled piers in layered clay with electrical load cells at the base. DuBose concluded that the skin friction played a major role in supporting the test loads. Whitaker and Cooke [59], conducted a comprehensive series of tests on instrumented shafts in London clay. The tests were conducted on twelve straight and belled shafts with electrical load cells at the bottom of the straight shafts and at the top of the bell. The test results indicated settlements of 10-20 percent of the diameter were required to produce complete base failure. A reduction factor for the shear strength along the sides of the pier was found to be approximately 0.44. Other studies have recently been conducted throughout the world. Mohan and Jain [35] and Mohan and Chandra [34] have conducted tests on uninstrumented piers with various shapes in the black cotton soils of India. The results were similar to those of Whitaker and Cooke. Woodward, Lundgren and Boitano [62] compared the results of driven pipe piles with drilled piers. The pipe piles developed about twenty percent more load resistance than the drilled shafts. Reese and others [43, 38, 55] have conducted extensive tests

on full scale drilled piers in the Beaumont clay and clay shale. These test piers were extensively instrumented and carefully tested. The results indicated that the drilled shafts resist an appreciable portion of the applied load in side friction. The side resistance varied along the shaft being generally smaller at the top and the bottom of the shaft. The magnitude of side stresses that could ultimately be developed depended on the construction procedure used (i.e., wet bore hole or dry bore hole), on the disturbance that occurred during drilling, and on the amount of soil softening that took place due to the adsorption of water from the setting concrete. The side resistance was found to be mobilized with much less pier movement than was base resistance with the result that side resistance was greater than base resistance at the design load. The Mustran instrumentation system used by Barker and Reese [5] was found to be very effective. This "Mustran" system consisted of strain cells in which foil gages were bonded to a vertical machined rod. The rod was connected rigidly between two end caps, approximately seven inches apart, covered with a heavy rubber sheath and embedded in the concrete. Reese found these cells to be reliable and suitable for measuring the load distribution. "Tell Tales" and a Gloetzl cell were also used with poor results.

Field tests were performed by Watson [58] on 18-inch diameter drilled piers in residual saprolitic soils. In some

of Watson's piers ice was placed in the bottom of the hole to insure that the applied load would only be carried in side friction. The results indicate that a substantial portion of the applied loads were carried in side friction, and a procedure for the design of piers in saprolitic soils is proposed. This procedure requires direct shear tests or triaxial shear tests on undisturbed samples to determine the adhesion component of the skin friction. To determine the design values for the friction component and lateral pressures, Watson recommends instrumented field tests on full scale piers.

There is a notable lack of reported results on drilled shafts in sands and silts. Martins [30] reported the results of compression tests of uninstrumented drilled shafts in sandy soil, from which he inferred that the shaft resistance is produced by soil in the fully active state along the periphery of the shaft. A study by Horner [21] on uplift resistance of short drilled shafts has indicated that the average side friction in partially saturated sandy silt is equal to about one-half the product of the effective overburden pressure, the tangent of the angle of internal friction of the soil and the pier area. Sowa [44] conducted tests on the pulling capacity of concrete cast in-situ bored piles. The tests were conducted on piles 15 inches and 21 inches in diameter and ranging in length from 10 to 40 feet, both in cohesive and cohesionless soils. He concluded that the

coefficient of lateral pressure in sandy soils was so variable that a predicted value is not reliable, and field tests are required to establish the lateral pressures.

Recently, Touma and Reese [49] conducted a series of load tests on instrumented bored piles in sand. Their tests indicated that the contribution of base resistance to total capacity is significant only in the case of dense sand. However, the deformation required to mobilize base resistance was about five to ten percent of the tip diameter; this amount of deformation is usually more than ordinary structures can tolerate. The ultimate side resistance was mobilized at deformations less than 0.5 inch. The deformations required for ultimate capacity by Touma and Reese are similar to previously reported results by Whitaker and Colman [61], Watson [58], Vesic [52], and others.

The number of investigations for skin friction and end bearing in pile foundations is far too numerous to discuss. However, there are a number of studies that have provided considerable insight into the general problem. An excellent summary of investigations in load transfer in pile-soil problems has been presented by Vesic [51]. Kerisel [25] has investigated the load transfer from piles in sand with large scale models in homogeneous sand masses. The results indicated that the skin friction does not continue to increase with depth, but the rate of increase with depth decreases. Vesic [52] in large scale model tests has observed that the

skin friction may become constant below depths of 15 to 20 pile diameters. It was also shown that values of relatively low skin friction immediately above the pile tip can be attributed to arching or stress relief in a zone extending to possibly three pile diameters above the pile point. Watt et al. [57] conducted full scale tests on three cast in place concrete piles, 24 inches in diameter. The soil types were a plastic clay, silty clay and glacial till. The piers were cast with a void space under the tip to measure the skin friction. An interfacial frictional device consisting of concrete plates mounted on a hydraulic jack was used to predict the skin friction from the tests. The authors concluded that the skin friction was dependent on the lateral pressure between the soil and hardened concrete, thus the use of the interfacial device is dependent on some means of determining the lateral pressure distribution.

Model Tests

Most of the design criteria for large diameter piles and piers is based on the results of full scale tests or large scale models. Although full scale models are expensive, they are, at the present time, the only reliable method of obtaining quantitative information on the behavior of piles and drilled piers. One of the basic reasons for this as pointed out by Jimenez Salas [24], is because of our inability to completely satisfy similitude requirements in model testing. In model piers and piles, this problem manifests itself by the

inability to model the mass density of the soil, which is one of the major forces acting on the pier or pile. Kerisel [25] has indicated that the sensitivity of a granular mass to compaction and subsequent disturbance may be more accentuated in model tests than for relatively large scales. Also, in *driving model piles*, a scaling effect due to densification must be expected since overburden pressures are much more reduced in the model and consequently expansion of the bulk of soil may affect a larger volume of soil. Vesic [54] has proposed four principal reasons for questioning the validity of model tests: (1) There are significant differences in the nature of the shear phenomenon in sand for different stress ranges. In the lower ranges, shear in dense sand is accomplished primarily through volume expansion or dilatancy. At higher stresses the shearing deformation occurs primarily through breakage of particles. (2) Experimental results have indicated that the displacements needed to develop the ultimate load along the shaft are practically independent of pile size. At the same time, the displacements required to reach ultimate load at the point were found to be roughly proportional to the pile size. (3) The extent of a zone of "arching" above the pile tip is due to the failure of the tip and is not proportional to the pile diameter and thus could not be scaled. (4) The compressibility of sand varied with pressure. The influence of the compressibility of the sand was found to be quite significant. Progressive rupture has

also been found to influence the tests. De Beer [14] indicated this influence: "In dense sand layers it must be expected that the progressive rupture phenomenon cannot be reduced to scale, so that in order to obtain the same state of stress with a larger footing, larger distortions must be induced."

With the above reservations in mind, several model tests will be discussed which have produced significant contributions to the behavior of piles and piers in sand. Mazurkiewicz [31] conducted model tests on preplaced piles in sand, primarily to investigate the phenomenon of negative skin friction in sandy soils. The author tabulates 27 theoretical expressions that have been proposed for the coefficient of lateral earth pressure, for different methods of placing the piles and types of loading. Also included in the tabulation are the corresponding expressions for the coefficient of friction. The conclusions from the model tests indicate that the skin friction stress does not increase proportionately with depth. The tests also indicated that a number of skin friction capacities can be defined depending on the sequence of loading and whether the friction is positive or negative.

Tjechman's [48] studies extended the work by Mazurkiewicz but used driven piles in place of the preplaced piles. Various densities of sand were tested. The studies generally confirmed the previous work by Mazurkiewicz. The author also

found that the positive skin friction was approximately twice that of the negative resistance. Also the skin friction along the shaft was not proportional to depth or effective overburden pressure. Parker and Reese [39] conducted tests on two-inch diameter pipe piles with an embedded length of 96 inches. The piles were preplaced and the sand compacted in layers around the piles. The study was conducted on axially loaded and laterally loaded piles. Triaxial shear tests were conducted on the sand and a hyperbolic model [26] was used to formulate the stress-strain curve. Correlation factors were developed to relate the skin friction transfer on the pile and the stress-strain characteristics of the sand. The resulting correlation factors were applied to previously published tests by Vesic [52] and other large scale tests. The author concluded that the proposed method of prediction accurately represented the load transfer for the two-inch diameter piles. The results also indicated that the shear transfer is not a linear function of depth. The proposed criterion was recommended for design problems with caution since only limited checks have been made.

In summary, the complexity of the behavior of pier and pile foundations was quite aptly stated by Meyerhoff [32].

> In spite of much research on deep foundations, such as piles, piers and caissons, their rational design still presents considerable difficulty. This is largely due to the fact that the bearing capacity and settlement of deep foundations depend not only on the original soil properties and the characteristics of the foundation, but also to a

great extent on the change of the soil properties by installing the foundations. This change depends on many interrelated factors, such as the type, size, layout and method of installation of the foundations, as well as the structure, strength and deformation properties of the soil and groundwater conditions.

CHAPTER III

HYPOTHESIS

The design of drilled pier foundations in many parts of the country is quite conservative. The major reasons for these conservative designs are: (1) imperfectly known structural loads, (2) in many instances, no account is taken of the ability of the pier to resist load by side friction.

The first objective of this project was the development of a load cell having superior properties to those currently available. This cell would be capable of accurately determining column loads, moments and shears. The concept for this new load sensor was to use four cylindrical elements with load transfer plates on the top and bottom. These four elements would have eight strain gages each, and the elements would be spaced so as to provide equivalent stiffness characteristics for the section of column it would replace. The cell would be developed in model form and tested to determine its accuracy and reliability.

Several studies, previously cited, indicated that significant load transfer can occur through side friction in piers even when the magnitude of tip movement is minimal. A method of estimating this side friction load transfer might be through use of a series of concrete-soil interface direct

shear tests. These tests would be conducted at varying confining pressures and the results represented by a hyperbolic relationship for the interface characteristics. Using this representation for the interface characteristics, and applying it to segments of a pier foundation, a design procedure for determining the load transfer in skin friction could be developed. The method used to compute the displacement of each segment would include the elastic compression as well as the tip movement of the pier. The procedure is illustrated in Figure 1. The pier is divided into N segments, preferably equal, along the length of embedment of the pier. Quite often, the top few feet of the embedded pier are not included in the contribution of skin friction due to the disturbance from drilling and the construction process. The deflection or movement at the center of each segment will be the movement of the pier tip plus the elastic deformation of the pier below the considered point.

Referring to Figure 1, the deflection at the midpoint of any segment can be found by:

$$\Delta_N = \delta_B + \frac{KPL}{2NAE} \qquad (1)$$

where

K = 1, 3, 5, 7, 9, etc. (where K = 1 for the nth segment)

N = number of segments

δ_B = deflection of tip

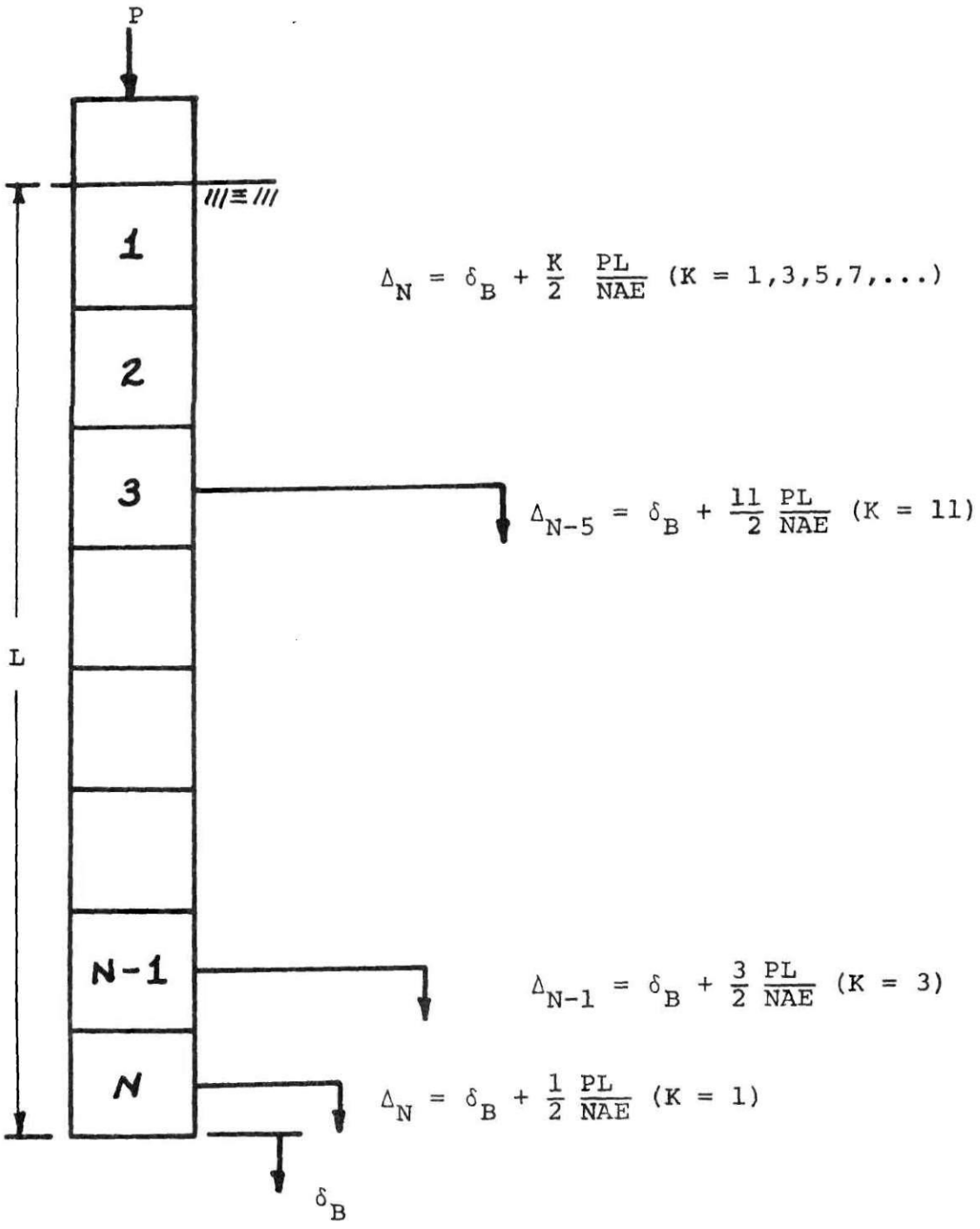

Figure 1. Calculation of Deflection for Pier Segments

P = applied load

A = area of pier

E = modulus of elasticity of pier

Δ_N = deflection at center of nth segment.

The proposed procedure for finding side friction would then be as follows:

(a) Direct shear tests between concrete and soil at varying confining pressures representative of those along the pier would be performed.

(b) Formulation of the hyperbolic model of interface behavior. The model can then be used to estimate the shear transfer at any confining pressure.

(c) Divide the pier into several segments.

(d) Estimate the amount of movement that the pier might undergo due to axial shortening and tip movement.

(e) Using the hyperbolic model, estimate the shear transfer for each segment.

(f) Sum up the shear transfer for all the segments to find the total load transferred through side friction.

A detailed description of the hyperbolic model is given in Appendix A.

The final objective of this project was to confirm the postulated design procedure by a large scale model test. An extensively instrumented "end-bearing" pier was constructed

and tested to verify this design procedure as a viable means of estimating the magnitude and distribution of shear transfer that actually occurs in full scale piers.

CHAPTER IV

DEVELOPMENT OF LOAD SENSOR

The development of a suitable load sensing device involves satisfying several requirements. One of these major requirements is that the device be quite safe with respect to failure. Each element of the device must be carefully considered and the factor of safety against any failure mode must be insured. Since the load sensing device will normally replace a portion of the structural element, the cell must be very safe against failure from all possible load applications. Additionally, the load sensor, when included in the structure, must behave as an integral part of the structure. The sensor must approximate as closely as possible, the behavior of the structural member that the load sensor is replacing. The load sensor must also reliably sense the applied loads and not be affected by any load combination or artifacts from the structure.

In order to verify the reliability and behavior of the load sensor, a model cell was constructed and tested in a manner which would simulate the actual loading conditions in the field.

Dimensional Analysis

In order to verify the validity of the model load

sensor, an extensive dimensional analysis was undertaken. This analysis is shown in Appendix B for both static loading and dynamic loading conditions.

This dimensional analysis indicates that the following dimensionless products should be considered:

$$\Pi_1 = \Delta/\ell \tag{2}$$

$$\Pi_2 = I/\ell^4 \tag{3}$$

$$\Pi_3 = \sigma/E \tag{4}$$

$$\Pi_4 = A/\ell^2 \tag{5}$$

The scale chosen for the model was one-quarter scale ($\lambda = 1/4$) giving:

$$\overline{\Delta} = \Delta/4 \tag{6}$$

$$\overline{I} = I/256 \tag{7}$$

$$\overline{F} = F/16 \tag{8}$$

$$\overline{A} = A/16 \tag{9}$$

$$\overline{\ell} = L/4 \tag{10}$$

where

$\bar{\Delta}$ = Model Dimension

I = Moment of Inertia

F = Force

A = Area

L = Length

This result is for the static case and a geometric reduction of the prototype is possible. The dynamic case was also evaluated in Appendix B. The requirements of the dimensional analysis for the dynamic loading case cannot be completely satisfied.

For this particular study, the static case of loading was considered of primary interest and the model load cell was designed and constructed based on the scale factors given in equations 6 through 10.

Basic Model Load Cell

Configuration

The requirement of matching the behavior of the load cell and structural element could not be completely satisfied. The properties that were considered most important to match: axial stiffness, moment of inertia and shear stiffness were approximated by choice of load sensor size and spacing. Figures 2 and 3 give the final configuration and dimensions of the model load cell.

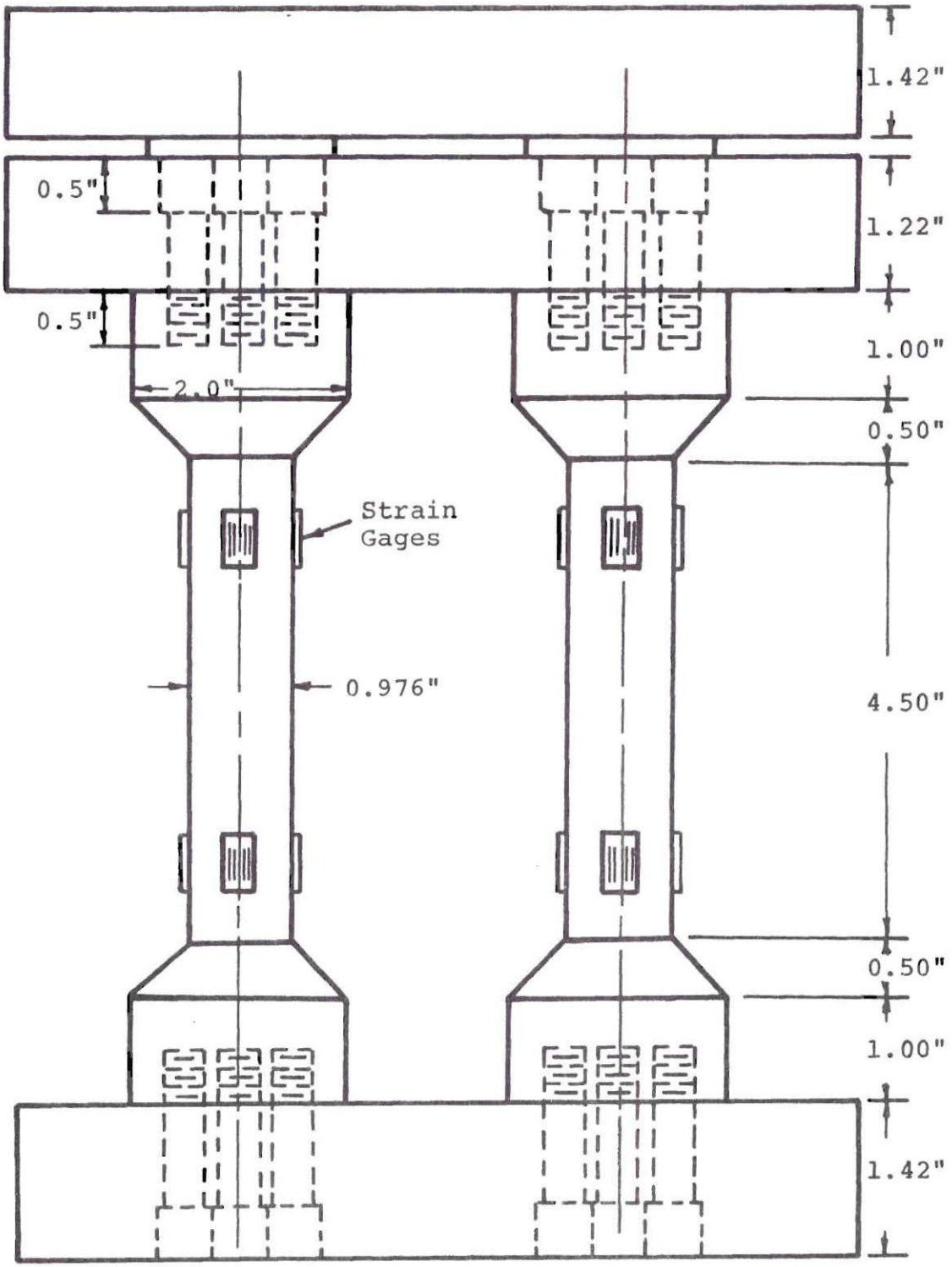

Figure 2. Model Load Cell

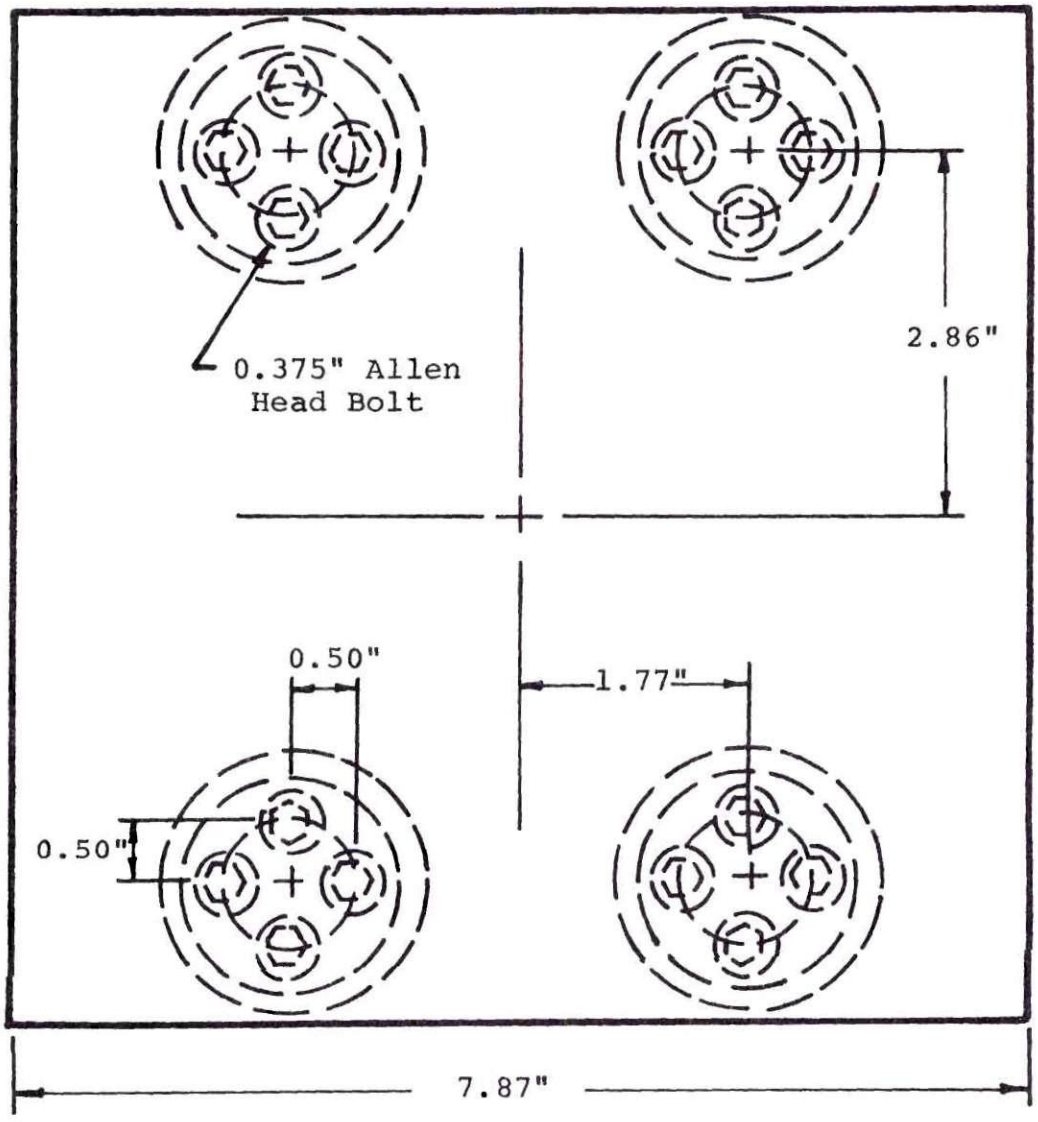

Figure 3. Model Load Cell (Plan View)

Material

The choice of high strength steel for the load sensor elements was necessary in order to insure an adequate factor of safety and to provide sufficient strain at the expected stress levels which could be suitably monitored by the strain gages. The most suitable steel found was a hot rolled, heat treated steel manufactured under the trade name of "Maxell 3-1/2." This steel has a yield strength of 103,000 psi. The steel used in the model load cell was of a higher yield strength (150,000 psi) than that used for the design, it was felt that the higher strength added a factor of safety for overstressing in the laboratory testing program.

Structural Analysis

The analysis was based on matching the axial stiffness, moment of inertia and shear stiffness of the load sensor with that of the replaced structural element. Table 1 gives an example of matching the properties of the column and load cell.

Axial Deflection. The amount of strain selected for suitable sensitivity was 2,500 microinches/inch. This amount would provide resolution for accurate determination of the loads. The strain level and choice of steel dictated the diameter required for the load sensors. Since the area and type of steel were determined by consideration of other factors, the axial deflection of the replaced portion of column and load cell could not be matched. As indicated in Table 2, the deflection of a column 12.5 feet in length

Table 1. Example of Matching Properties of Column, Load Cell and Model Load Cell

Interior Column	Load Cell	Model Load Cell
W14 x 500	Sensor Area - 48.4 in^2	(One-quarter scale)
Area - 147 in^2	Fy Steel - 103,000 psi	Sensor Area - 3.90 in^2
Fy Steel - 36,000 psi	I major - 8250 in^4	Fy Steel - 150,000 psi
I major - 8250 in^4	I minor - 2880 in^4	I major - 24.60 in^4*
I minor - 2880 in^4	E = 30 x 10^6 psi	I minor - 9.54 in^4*
E = 30 x 10^6 psi		E = 31.0 x 10^6 psi
Design Loads	**Design Loads**	**Design Loads**
Axial - 3,000,000 lbs.	Same as column	Axial - 187,500 lbs.
Shear - 80,000 lbs. major 40,000 lbs. minor		Shear - 5,000 lbs. major 2,500 lbs. minor
Biaxial - 315,000 ft. lb. major		Biaxial - 4,930 ft. lb. major
Bending - 165,000 ft. lb. minor		Bending - 2,580 ft. lb. minor

*Reduced amounts due to space limitation of plates.

Table 2. Deflection/Unit Load for Column and Load Cell

Deflection	Column (12.5 ft.)	Load Cell (10 ft. + load cell height)	Percentage Difference
Axial	3.40×10^{-8} in/lb	3.96×10^{-8} in/lb	16.4%
Bending and Shear:			
Major Axis	9.45×10^{-8} in/lb	9.39×10^{-8} in/lb	0.6%
Minor Axis	12.94×10^{-8} in/lb	16.17×10^{-8} in/lb	25.0%

(The shape factors used for the column were: 1.0 for the major axis, and 6/5 for the minor axis)

(10 feet plus 2.5 feet for the cell) compared with a ten-foot column and a 2.5-foot cell (considering the deflection in the necked down portion of the sensor only) were within 17 percent.

This difference was considered not excessive in comparison with the increased sensitivity of the load cell. The steel used in the model load cell was of a higher yield strength (150,000 psi) than that used for the design; it was felt that the higher strength steel added a factor of safety for overstressing in the laboratory testing program.

Moment of Inertia. The spacing of the load cell sensors was adjusted such that the moments of inertia about the major and minor axes of the cell could be matched exactly with those of the column.

Shear Deflection. In most structural members, the deflection due to shear is neglected due to the dominance of the bending deflection. However, in the case of deep sections without large spans the shear deflection can become as significant as the deflection due to bending.

The shear deflection of the load cell sensors will be the same in all directions since the members are circular in cross section. However, in the case of the column, in the major axis direction the shear is resisted primarily by the web area, while in the minor axis direction the flanges resist the shear. As shown in Table 2, the values for shear deflection are different for each axis. The shape factors for the

column are also included in Table 2. Comparing the total deflection due to bending and shear, it can be seen that the total deflection (bending and shear) in the major axis is within one percent of that for the column and within 25 percent of the column for the minor axis.

Consideration was given to rectangular sensor elements which could have been arranged in a manner which would very closely match the column section, since the resistance to shear for the rectangular elements depends on the orientation of the elements; however, the difficulty of machining and the possibility of nonuniform stress distribution in the rectangular section favored use of the simpler circular cross-section.

During the construction of the model load cell, it was found that the base plates were not large enough to allow the full spacing required to match the amount of inertia about the major axis of the column. The reduced spacing is given in Figure 3.

Construction and Instrumentation

The construction of the one-quarter scale model load cell was accomplished in the machine shop at the Georgia Institute of Technology. The details of construction and the instrumentation are included in Appendix B.

Each load sensor was instrumented with eight strain gages attached at appropriate locations. The optimum position

for these gages was determined by an experimental stress analysis utilizing a photoelastic technique. The details of the technique and results are also outlined in Appendix B. The results indicated that the location of the gages should be a minimum of 0.5 inches from the enlarged portion of the sensor to ensure that there would be no effect from the stress concentration produced by the change in shape of the sensor (Figure 2).

Results of Tests and Discussion

The testing program for the model load cell was conducted in several steps: (a) Preliminary loading of a single sensor to check the gage sensitivity and to determine the modulus of elasticity of the sensors, (b) Axial loading of the model to evaluate the performance of the entire load cell, and (c) Eccentric loading to evaluate the performance of the load cell in biaxial bending. The additional modes of loading, i.e., horizontal and torsional, were not investigated due to lack of time. The details of each testing program and results are given in Appendix B; only a brief outline of these tests and results will be discussed.

Preliminary Tests

The results of these tests indicated that the difference in strain for axial loading between gages was small and that the sensitivity to bending would be excellent.

The compression tests for the modulus of elasticity

indicated an average value of 31.0×10^6 psi.

Axial Loading Tests

A total of 71 tests were performed on the cell using various techniques to eliminate bending in the sensor elements. The final configuration is shown in Figure 2 and the details discussed in Appendix B. The addition of the top plate with four spacers centered over each sensor proved to be the most suitable configuration. The top plate deflects, but the axial load is transmitted to the sensors with a small amount of bending. The final tests indicated that the model load cell can accurately measure the axial component of load within two percent up to a load of 250,000 pounds. This accuracy is consistent over a series of tests and is also obtained in the eccentric mode of loading also.

Eccentric Loading

The final series of tests was conducted to determine the ability of the model cell to sense the biaxial bending moments. A series of five tests was conducted with eccentric loads up to 100,000 inch-pounds applied to the load cell at various positions. The results of the tests indicate that the load cell can reliably measure the biaxial bending moment within seven percent. The details of the tests are given in Appendix B.

It is recommended that the future development of the cell will include the testing and modification to accurately measure the horizontal and torsional components.

CHAPTER V

MODEL PIER STUDY

General

In order to verify the postulated procedure for including the skin friction in the design of drilled piers, a large scale model test was conducted on a concrete pier. The model test technique was chosen as a means to verify the design procedure rather than a field test because the soil properties, construction technique and instrumentation can be more closely controlled in a model type test.

The model pier selected for the testing was 16 inches in diameter and 15 feet long. A model of this size was chosen to minimize test artifacts and the limitations of model testing indicated by Vesic [54] and others [14]. The model pier was constructed in place in a large test pit used for a previous research project [52] and located adjacent to the soils laboratory at the Georgia Institute of Technology. The pit dimensions are 8 feet, 4 inches in diameter and 22 feet deep. The side of the pit is corrugated steel backed with approximately eight inches of concrete. The arrangement of the pit, excavation and filling sequences are shown in Figure 4. The use of a large diameter test pit minimized the influence of confining effects or disturbance from the

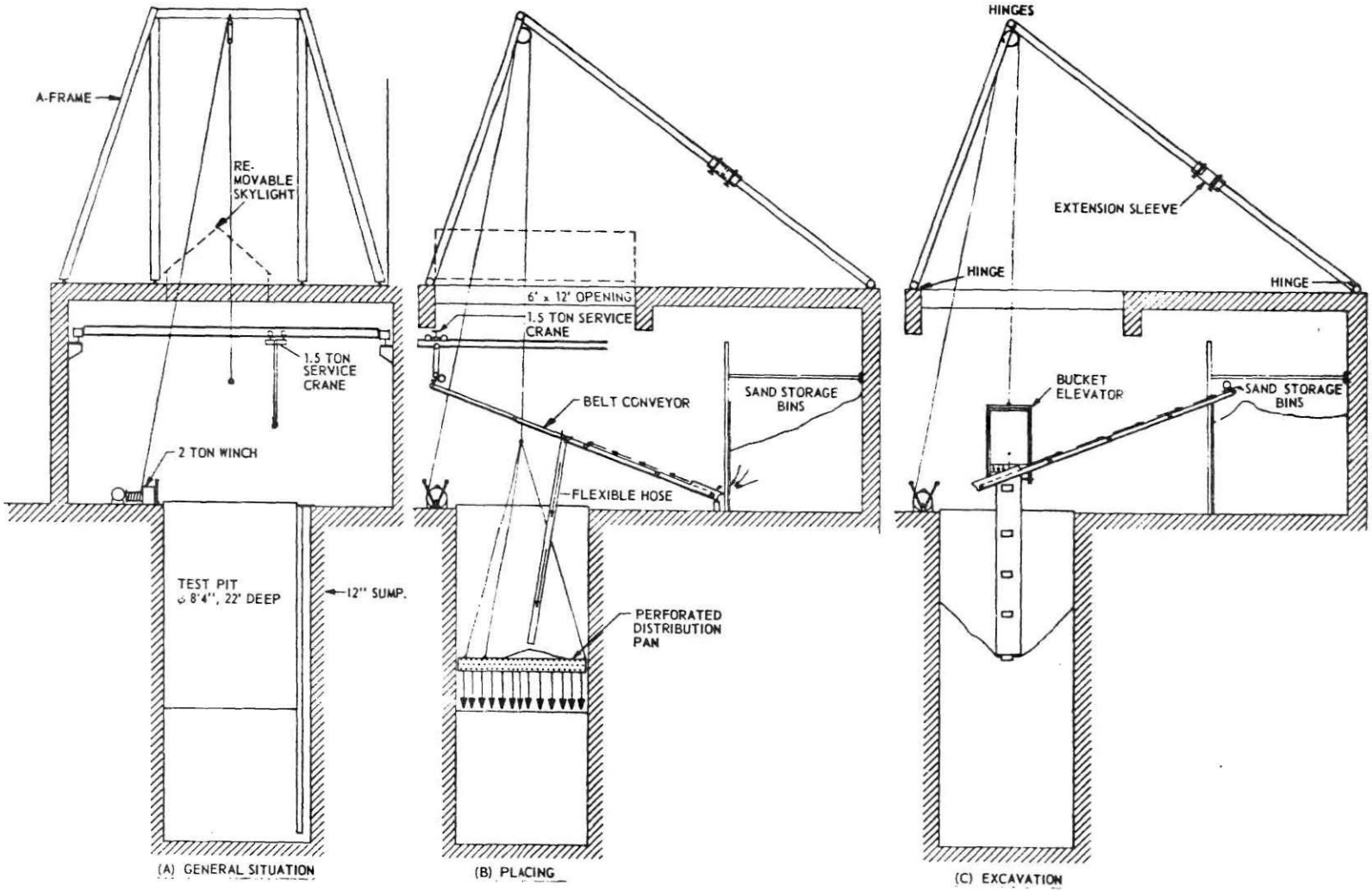

Figure 4. Testing Area During Different Phases of Operation (After Vesic [52])

side walls.

Figure 5 shows a cross section of the test pier and gives an overall view of the test pit and instrumentation.

In order to accurately determine the tip loads, a 200,000 pound capacity hydraulic ram was placed at the base of the pit. The pier tip rested on this ram which provided a means of measuring the tip load of the pier throughout the test program. The top of the pier was loaded by a 400,000 pound capacity ram reacting against a steel reaction frame. The pier was instrumented at several levels along the pier shaft which provided a means of determining the load distribution in the pier. The complete system consisted of a model load cell to determine the applied load; instrumentation along the pier shaft to measure the distribution of the load; and the 200,000 pound capacity hydraulic ram at the pier base to measure the tip load. The area from the bottom of the pit up to the level of the pier base was filled with concrete blocks stacked in a close knit arrangement to simulate a sound rock base upon which the pier was resting. The construction of the pier is outlined in Appendix C.

Materials

The pier concrete was designed for a 28-day strength of 5,000 psi, a five- to six-inch slump, and a water cement ratio of 0.5. The maximum size aggregate used was 0.75 inch. The first pour from the bottom to 2.5 feet used Type 1

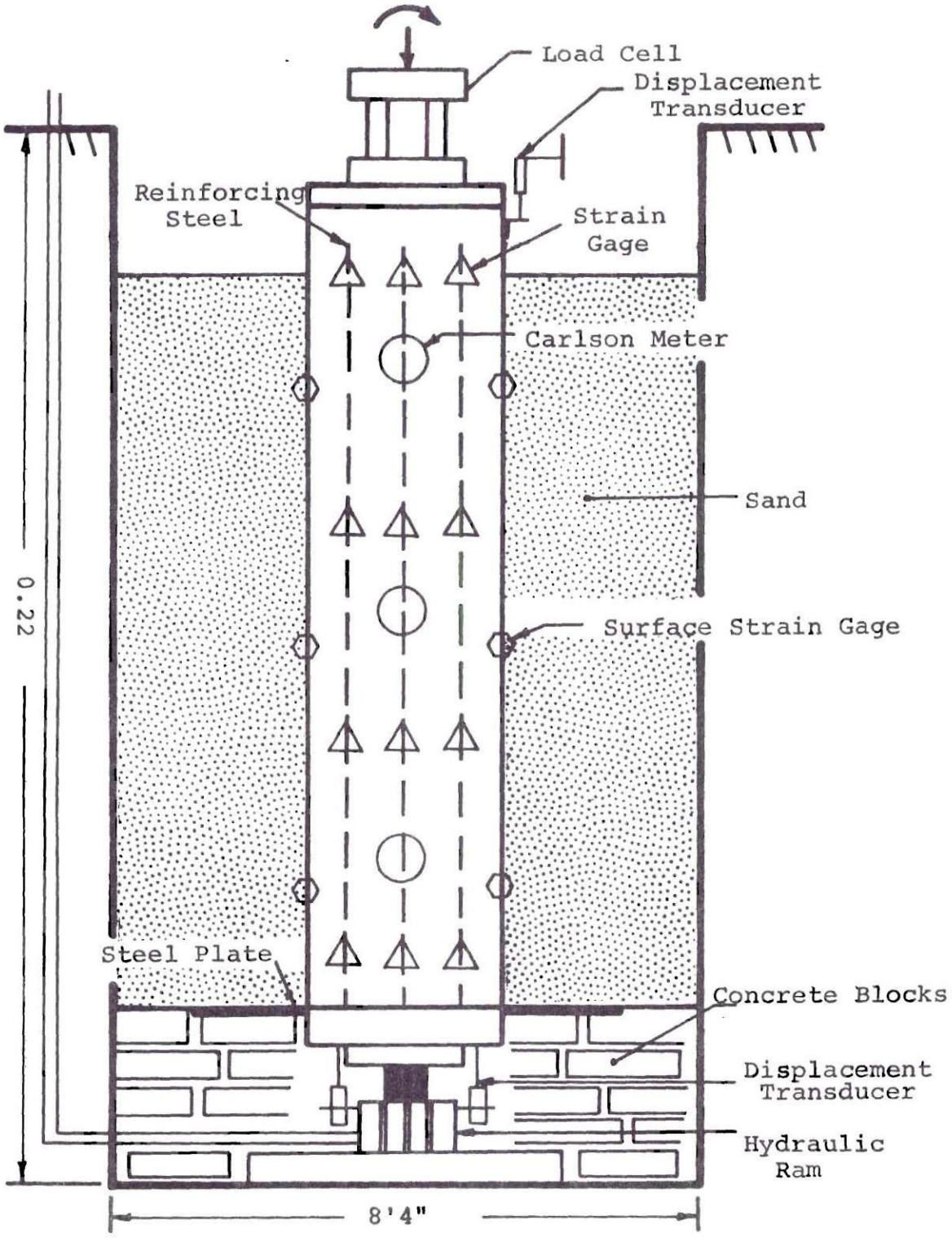

Figure 5. Cross Section of Experimental Model and Instrumentation

Portland cement and the original mix design. The remaining three pours used Type 1A air-entraining cement. This was the only type cement available at the time of pouring. The details of the concrete design are included in Appendix D.

Reinforcing Steel

The reinforcing consisted of six number six, 15-feet long vertical bars. The bars were equally spaced around a 10-inch diameter circle. The concrete cover on the longitudinal bars was 3-3/16 inches. Horizontal hoop ties were spaced one diameter (16 inches) apart along the length of the bars. The concrete cover on the hoop ties was 2-3/16 inches. The amount of steel used was slightly more than one percent of the total cross section area as recommended by O'Neill and Reese [38].

Sand

The sand used was a Chattahoochee River sand previously used in studies by Vesic [52]. The properties of the sand are given in Appendix D.

Instrumentation Required

The types of instrumentation used in model and full-scale piers is varied and the success is also variable depending on the type of project and manner in which the instrumentation is placed. References [6, 7, 13, 20 and 42] indicate types of instrumentation that can be used in piers and piles and discuss the applicability of each. From a study

of the above references, one fact became apparent: To insure a successful set of results from a series of tests, one must have several independent systems of measurement. This provides a backup type of arrangement such that if one system fails to operate correctly, then the alternate system will provide the information. Also evident from previous studies was the detrimental effect of moisture or water vapor on any electrical type of system. Moisture proved to be the major cause of failure for the instrumentation schemes reported.

With the above facts in mind, the following instrumentation systems were used for the model pier:

1. A series of SR-4 strain gages bonded to the reinforcing steel of the pier at four levels along the pier shaft.
2. Three Carlson concrete stress meters (PC 800) placed at the third points along the shaft in the center of the pier.
3. Concrete SR-4 strain gages (six-inch gage length) placed at three levels on the surface of the concrete pier.
4. A 200,000 pound Simplex hydraulic ram placed at the base of the pier and connected by high pressure hose to a Bourdon pressure gage at the top of the pier, which allowed the ram pressure to be monitored throughout the test.
5. Two linear variable differential transformers

(LVDT's), G. L. Collins Model SS-207, attached to the ram body at the base of the pier, to measure the tip displacement of the pier.

6. The model load cell described in Chapter IV was placed at the top of the pier to monitor the amount of axial load and biaxial moment applied at the top of the pier.

The instrumentation system consisted of three separate means of measuring the load in the pier: The strain gages on the steel and concrete were a purely electrical means, the Carlson meters utilized the deflection of a diaphragm converted to an electrical output, and the 200,000 pound hydraulic ram was a purely hydraulic system to sense the base load. The duplication of measurements was felt to be imperative to insure suitable results. The details of placing the instrumentation systems are included in Appendix E.

Location of Instrumentation

The instrumentation was placed along the pier shaft to describe the load distribution as completely as possible.

The Carlson stress meters were placed approximately at the third points of the pier: 2.5 feet, 7.5 feet and 12.5 feet and in the center of the reinforcing steel cage.

The reinforcing steel gages were placed at four levels along the pier shaft: 1.67 feet, 6.17 feet, 10.17 feet and 14.17 feet below the top. The top and bottom levels were placed close to the pier extremities such that the measured

load and applied load could be compared.

The concrete strain gages were placed at three levels along the pier shaft: 3.83 feet, 8.50 feet and 13.17 feet from the pier top. These gages were placed at approximately the same level as the Carlson meters to compare the load results from each.

The LVDT system at the pier tip provided a means of monitoring the bottom movement of the pier. The deflection of the pier top was measured by three 0.0001-inch micrometer dial gages resting on metal brackets epoxyed to the sides of the pier. These two systems provided a means of accurately sensing the top deflection of the pier as well as the tip movement. Figure 5 shows the location of the instrumentation and the pier dimensions.

Placement of Sand

The sand was placed by the "raining" method using an 8-foot diameter perforated pan held a minimum of 30 inches above the surface. The experimentation and technique for this method of sand placement is discussed by Vesic [52]. The details of the sand placing and measurement of densities is included in Appendix C.

The results of the density measurements are shown in Figure 6. The densities were lower at the sides of the pit and at the edge of the pier. The variation of densities will be discussed in Chapter VIII.

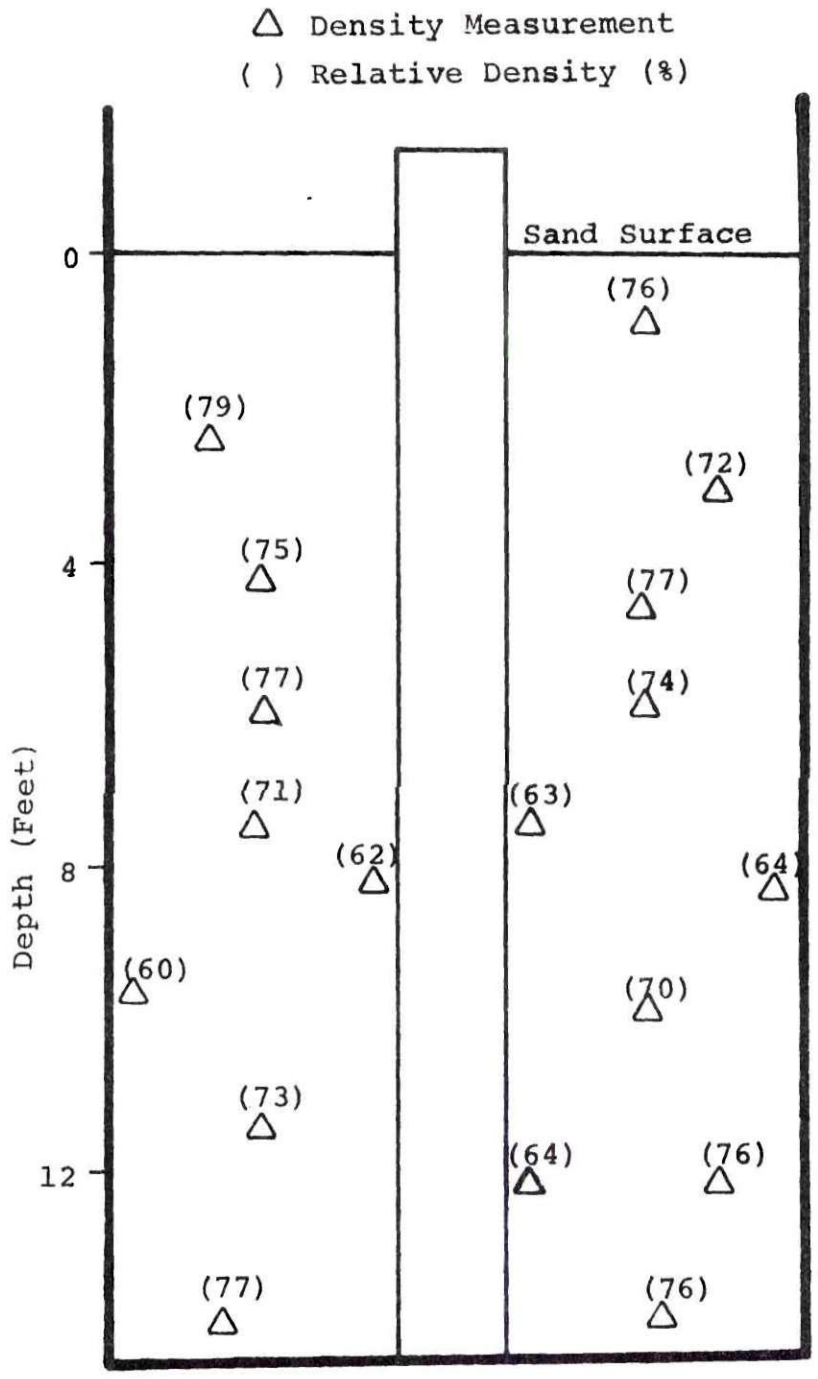

Figure 6. Relative Density Measurements of Sand in Test Pit

Completed Test System

Figure 7 is a view of the model pier surrounded by the sand with the top deflection gages in place for testing. Figure 8 shows the monitoring equipment and arrangement during testing.

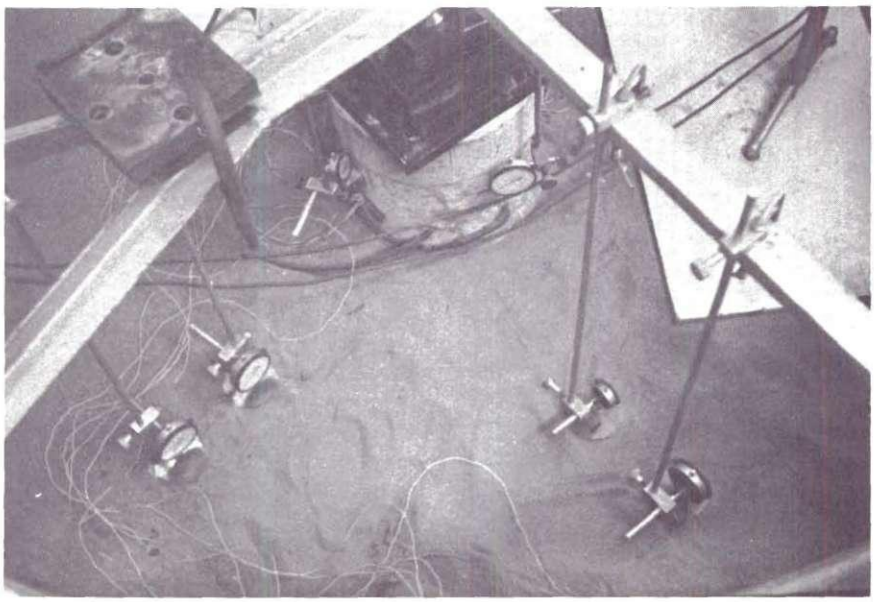

Figure 7. View of Micrometer Dial Gages in Test Pit

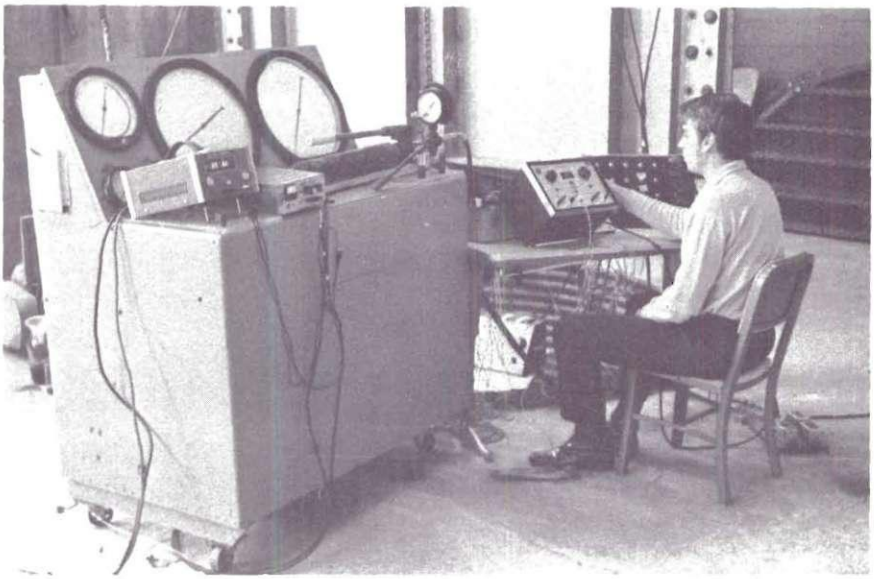

Figure 8. Test Being Conducted on Pier

CHAPTER VI

TEST PROCEDURE FOR PIER TESTS

Direct Shear Tests

A series of direct shear tests were conducted prior to testing the model pier in order to define the interface characteristics of the pier concrete surface and the sand. The direct shear tests were performed in a manually operated, two-part shear device. The cross section of the box is circular, with a 2.50-inch diameter. The upper and lower halves of the box are 0.49-inches deep. The movement of the upper half of the box is measured with a 0.0001 inch micrometer dial gage. The shear force is measured by a calibrated proving ring. The rate of shear is controlled manually, and the applied rate for the tests was 0.05 inches/minute. Normal loads, calculated to be those on the pier shaft at depths of 5, 10 and 15 feet below the ground surface were applied either directly with dead weights or with a lever arm arrangement to produce the required load. The bottom portion of the box was filled with a concrete block, cast in the box using the same paste proportions of the model pier mixture. The model pier surface was very smooth due to the paraffin coating inside surface of the pier form. To simulate this surface, a piece of glass was placed on top of the mixture cast in the

direct shear box to produce a smooth surface. The upper half of the box was filled with the Chattahoochee River sand at a specific relative density. The weight of the sand required was computed based on the box volume and the desired relative density. The sand was compacted in layers in the box until full. The desired normal load was then placed on the sand. The box halves were then separated approximately 0.05 inch and the test run. The deflections and loads were noted until failure was reached. Table 3 presents a summary of the direct shear test program.

Table 3. Direct Shear Test Program

Test Number	Concrete Surface Type	Relative Density of Sand (%)
1	Rough	75
2	Rough	75
3	Rough	75
4	Rough	65
5	Rough	65
6	Rough	65
7	Smooth	65
8	Smooth	65
9	Smooth	65

Tests on Model Pier

Preliminary Test

A preliminary test was conducted on the pier after

curing and prior to placing the sand around the pier. This test was made to check the operation of the instrumentation and loading devices. The pier was loaded to a maximum of 39,000 pounds in 10,000 pound increments, with readings taken at each load increment. The maximum load of 39,000 pounds was then maintained constant on the pier for a twenty-four hour period. All of the instrumentation was then read at the end of the twenty-four hour loading period. The load was removed and the pit was then filled with sand.

Eccentric Load Tests

This test series was conducted first and consisted of five tests. The procedure for all the tests was the same and is enumerated below.

Before loading, all the instrumentation was checked to see if it was functioning correctly. The steel and concrete strain gages were all initially set to a common reading by adjusting the resistors on the switching boxes. The micrometer dial gages on the pier were set at zero and the initial pressure of the bottom ram was read and noted. The position of the pier tip was indicated by the voltage output from the LVDT's. This voltage was noted and maintained constant throughout the test by manually adjusting the pressure to the bottom ram. The top load was incrementally (usually 10,000 or 20,000 pound increments) applied to the pier with the Simplex 400,000 pound ram using a manually operated hydraulic pump. The approximate load was noted on the pressure gage to

the top ram. The exact load was then found by reading the strain gage output from the model load cell. The exact amount of eccentricity of load was also determined from the load cell readings. After finding the exact load, the reinforcing steel strain gages, concrete strain gages and Carlson stress meters along the pier shaft were read. The digital voltmeter indicating the pier tip position was monitored throughout the test to ensure the tip remained stationary, to simulate an unyielding support. The micrometer dial gages attached to the pier were then read and recorded. The time required at each load increment for reading data was approximately 10 to 20 minutes, with the entire test taking two to four hours to complete. The pressures on the top and bottom rams stayed constant throughout all the tests and the loads were satisfactorily maintained for the duration of each increment.

All of the pier tests were conducted simulating field conditions as much as possible. The loads were applied incrementally with readings taken at each increment of loading. The top load was applied through a series of spreader plates to ensure the load would be applied uniformly, such as the load through a base plate at the base of a column.

Concentric Load Tests

This series consisted of one test with the load being applied to the center of the pier within $\pm$ 0.10 inches. The concentric loading was accomplished by trial and error. The pier was loaded to 20,000-30,000 pounds and the load cell

strain gages were read and the amount of eccentricity computed. The load was removed, the top ram shifted in the correct direction and reloaded. The eccentricity was again noted until the ram was properly centered. The tests were conducted in the same manner as the eccentric loading.

Ultimate Load Test

The final test was conducted with a concentric load on the pier. The load was applied in increments and the tip of the pier was allowed to move. The ultimate skin friction was determined from the maximum applied load. Table 4 presents a summary of the model test program.

Table 4. Model Pier Tests

Test	Type of Loading
Preliminary	Concentric (Load maintained for 24 hours)
1	Eccentric
2	Eccentric
3	Eccentric
4	Eccentric
5	Eccentric
1C	Concentric
Ultimate Load	Concentric

CHAPTER VII

TEST RESULTS

Direct Shear Tests

Table 5 is a summary of the test results and properties of the sand-concrete interface. The force deflection curves for the direct shear tests are shown in Figures 9, 10, and 11. The figures are presented in the same order as the tests were conducted: Figure 9, rough concrete with the sand placed at a relative density of 75 percent; Figure 10, rough concrete with the sand placed at a relative density of 65 percent; Figure 11, smooth concrete with the sand placed at a relative density of 65 percent.

The force deflection curves for the direct shear tests converted to hyperbolic form are shown in Figures 12, 13, and 14.

The relationship between the initial tangent modulus, E_i, and normal stress for the direct shear tests is shown in Figure 15.

Tests on Model Pier

Preliminary Test

Prior to sand placement, the pier was loaded and a check on all the instrumentation was made. The results of this test are shown in Table 6.

Table 5. Results of Direct Shear Tests

Test Number	Relative Density %	σ_n (psi)	c (psi)	ψ^a (degrees)	$E_i{}^b$ (pci)	$R_f{}^c$
Rough Concrete:						
1	75	1.30	0	40.3	417	0.90
2	75	2.62	0	44.2	611	0.88
3	75	3.93	0	44.2	870	0.87
			average	42.9		
4	65	1.50	0	39.4	352	0.88
5	65	2.24	0	37.2	473	0.85
6	65	3.37	0	38.0	618	0.85
			average	38.2		
Smooth Concrete:						
7	65	1.50	0	32.2	393	0.87
8	65	2.24	0	30.0	646	0.88
9	65	3.37	0	29.0	695	0.83
			average	30.4		

a. Coefficient of wall friction between sand and concrete

b. $E_i = \frac{\text{Initial Tangent Modulus (psi)}}{\text{Area of Shear Surface (sq. in.)}} = E_i$ (pci)

c. R_f = Ratio of Measured τ_f to Predicted τ_{ult}

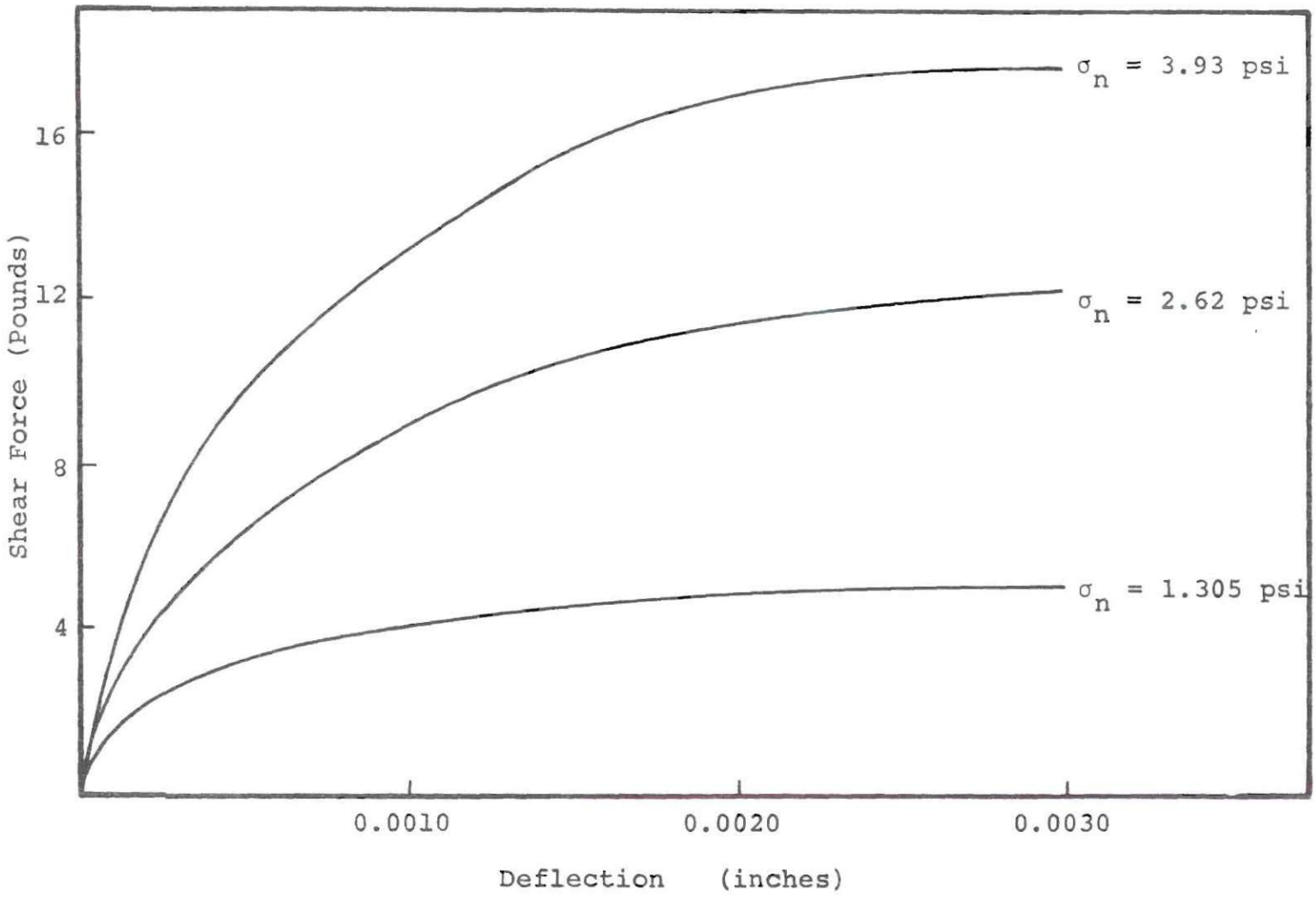

Figure 9. Direct Shear Tests for Rough Concrete, D_R = 75%

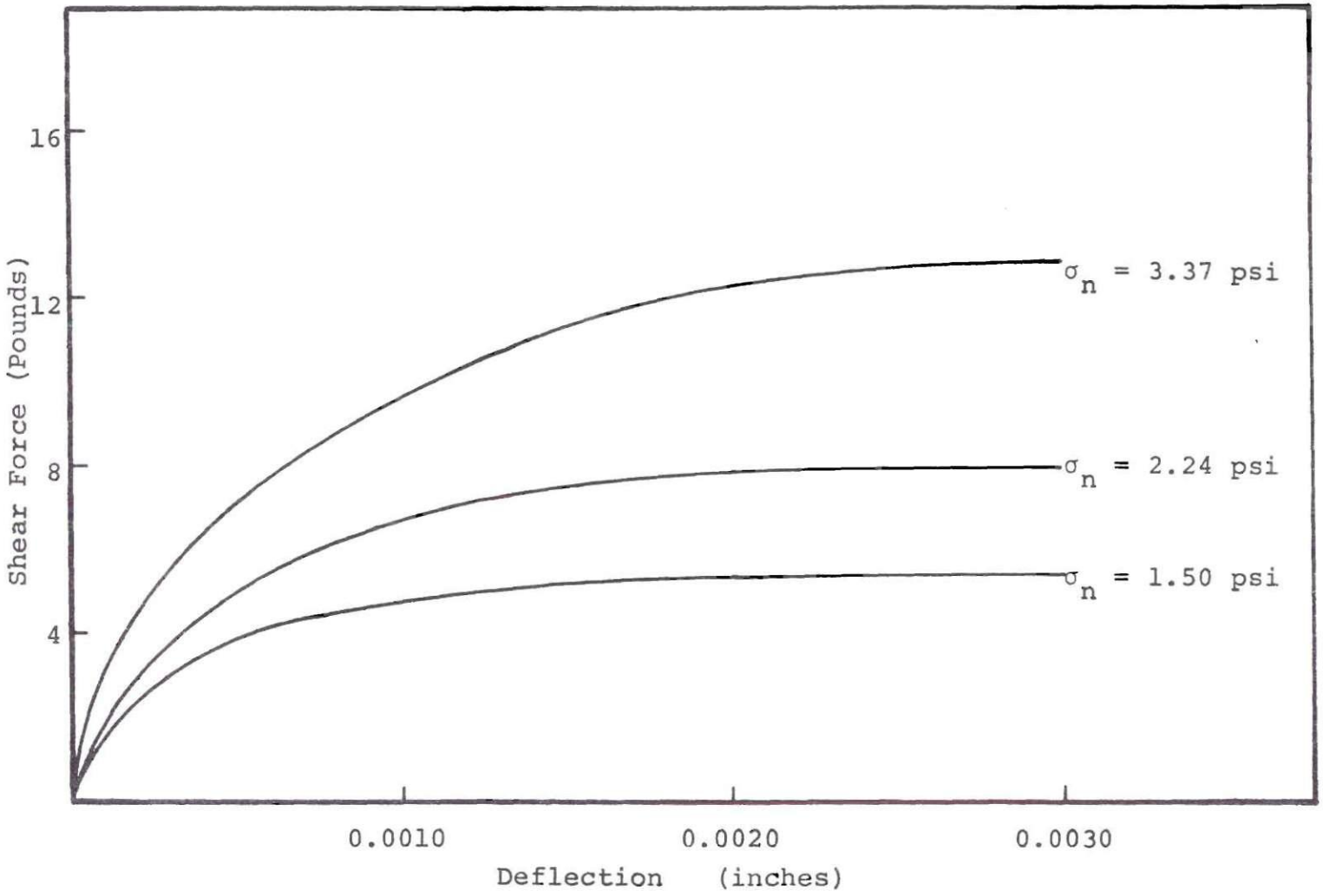

Figure 10. Direct Shear Tests for Rough Concrete, D_R = 65%

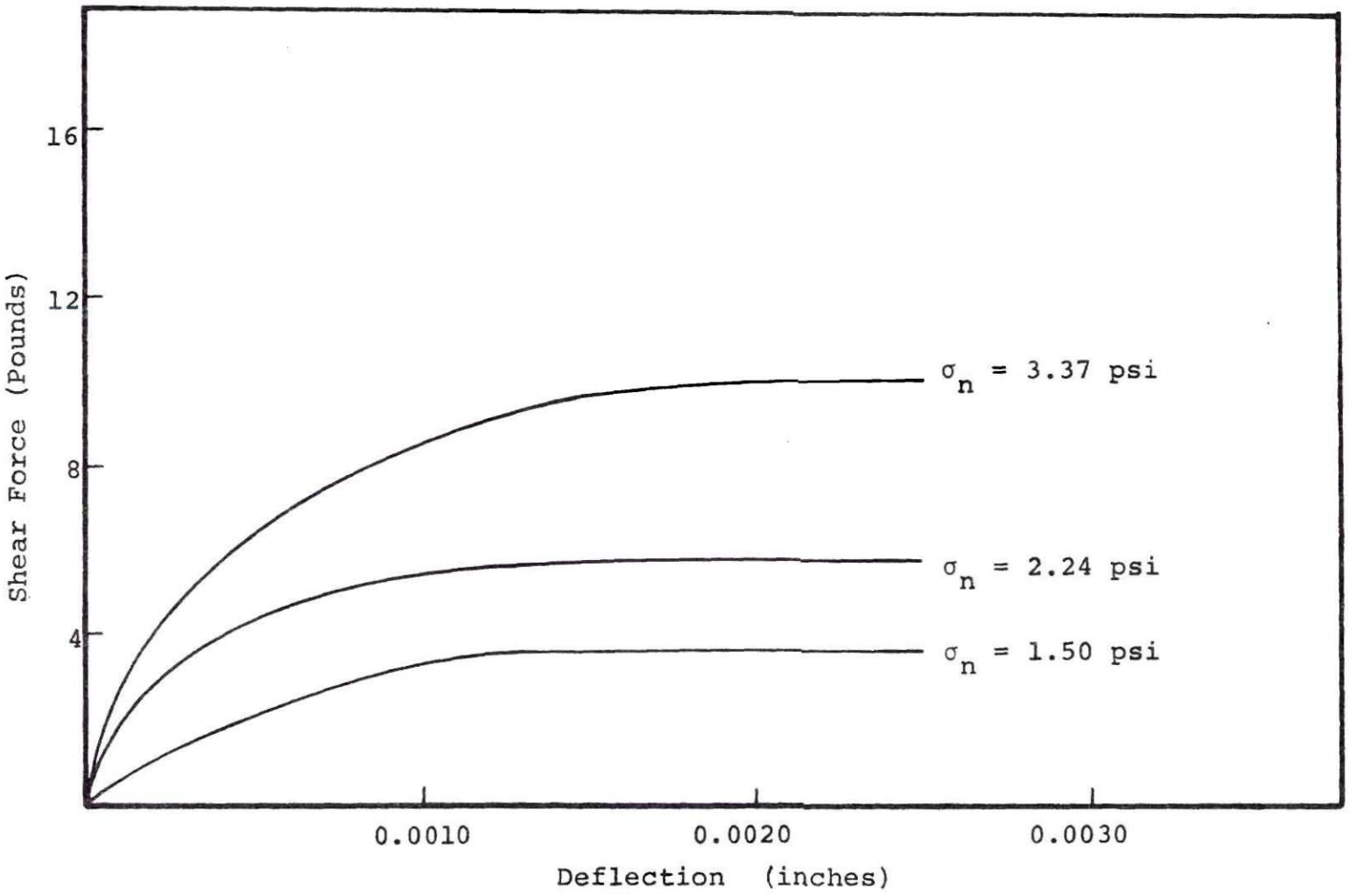

Figure 11. Direct Shear Tests for Smooth Concrete, D_R = 65%

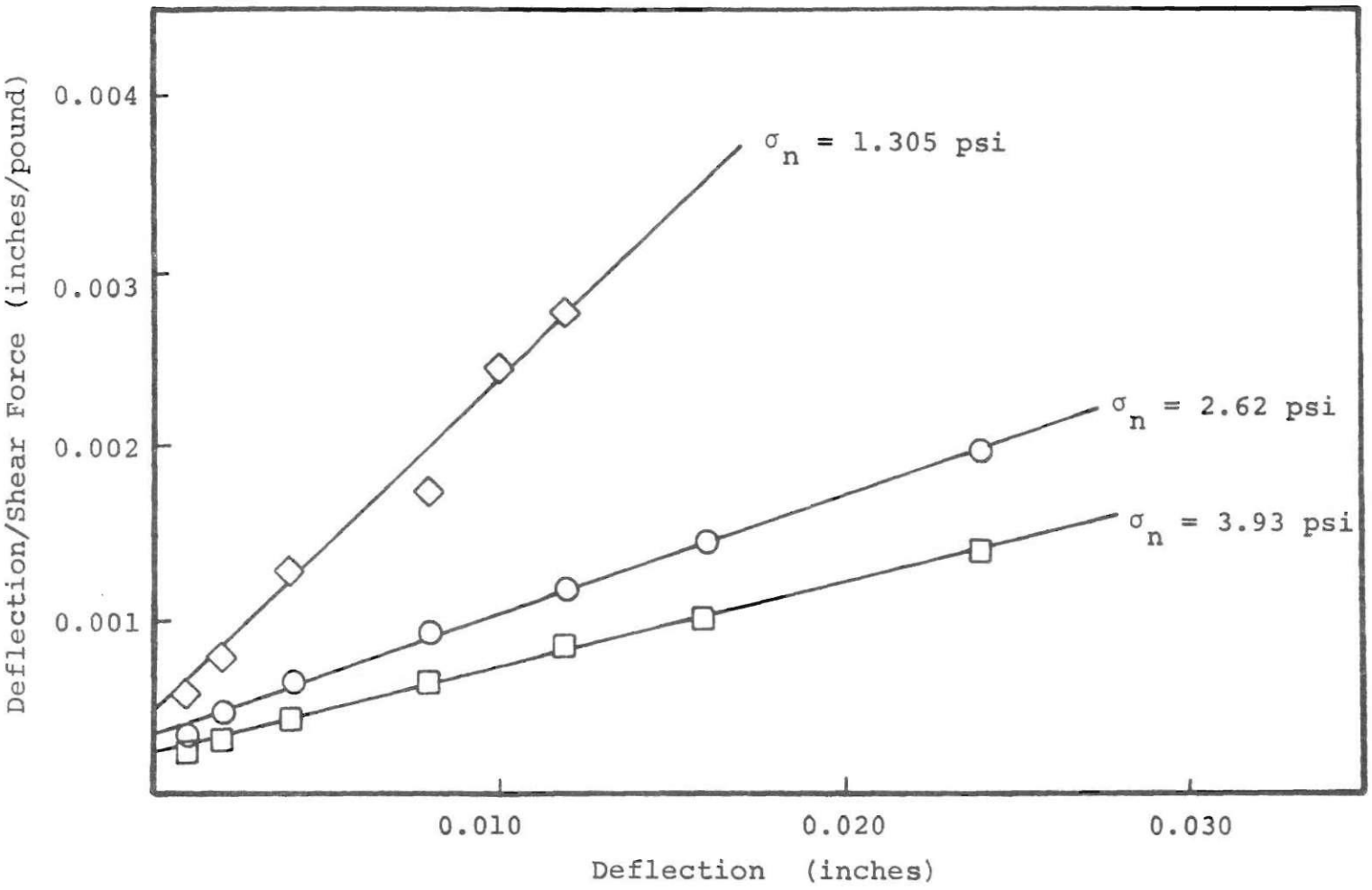

Figure 12. Transformed Hyperbolic Shear Force - Deflection Curves for Series 1,2 and 3 Rough Concrete, D_R = 75%

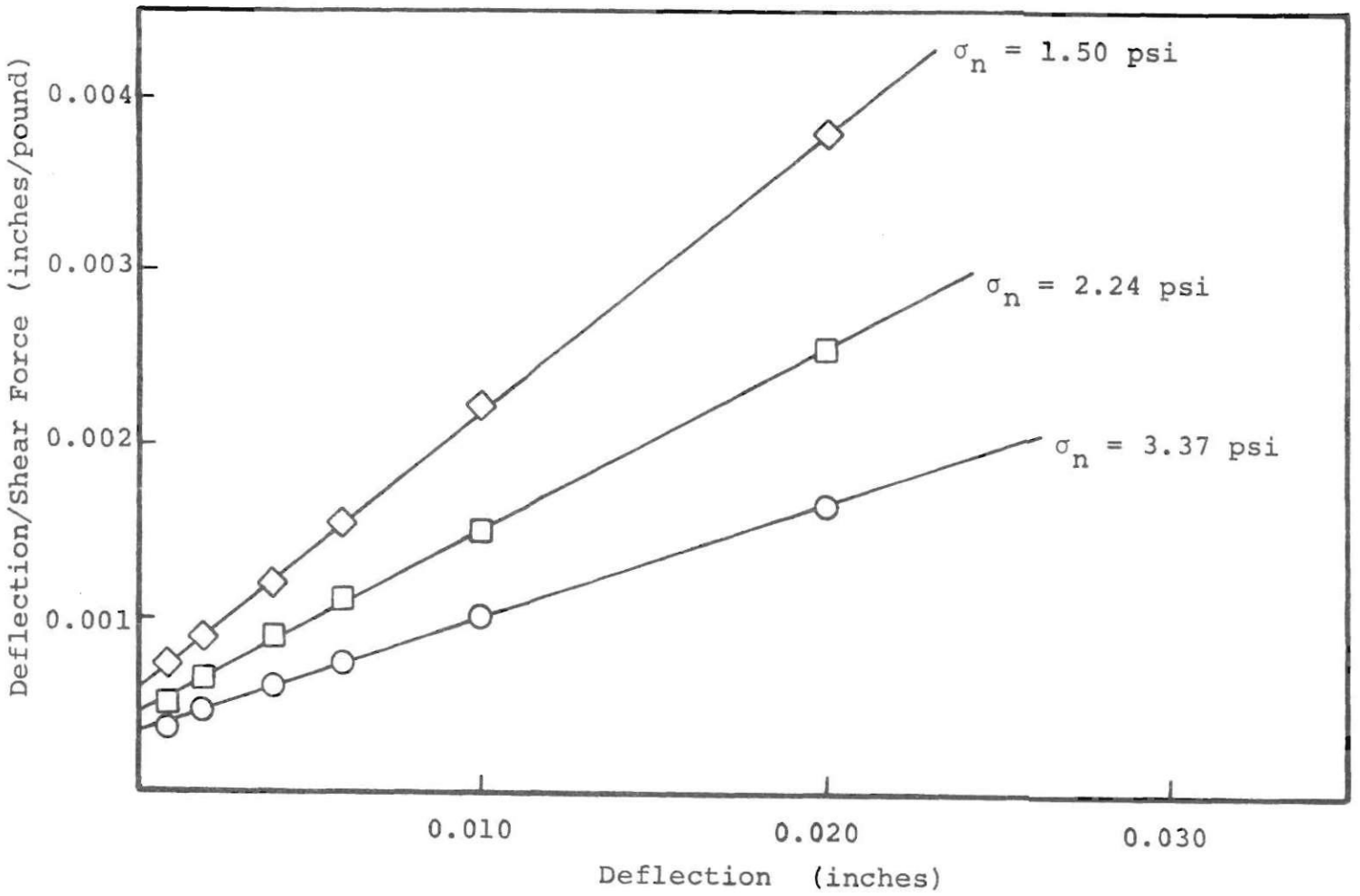

Figure 13. Transformed Hyperbolic Shear Force - Deflection Curves for Series 4, 5 and 6, Rough Concrete, D_R = 65%

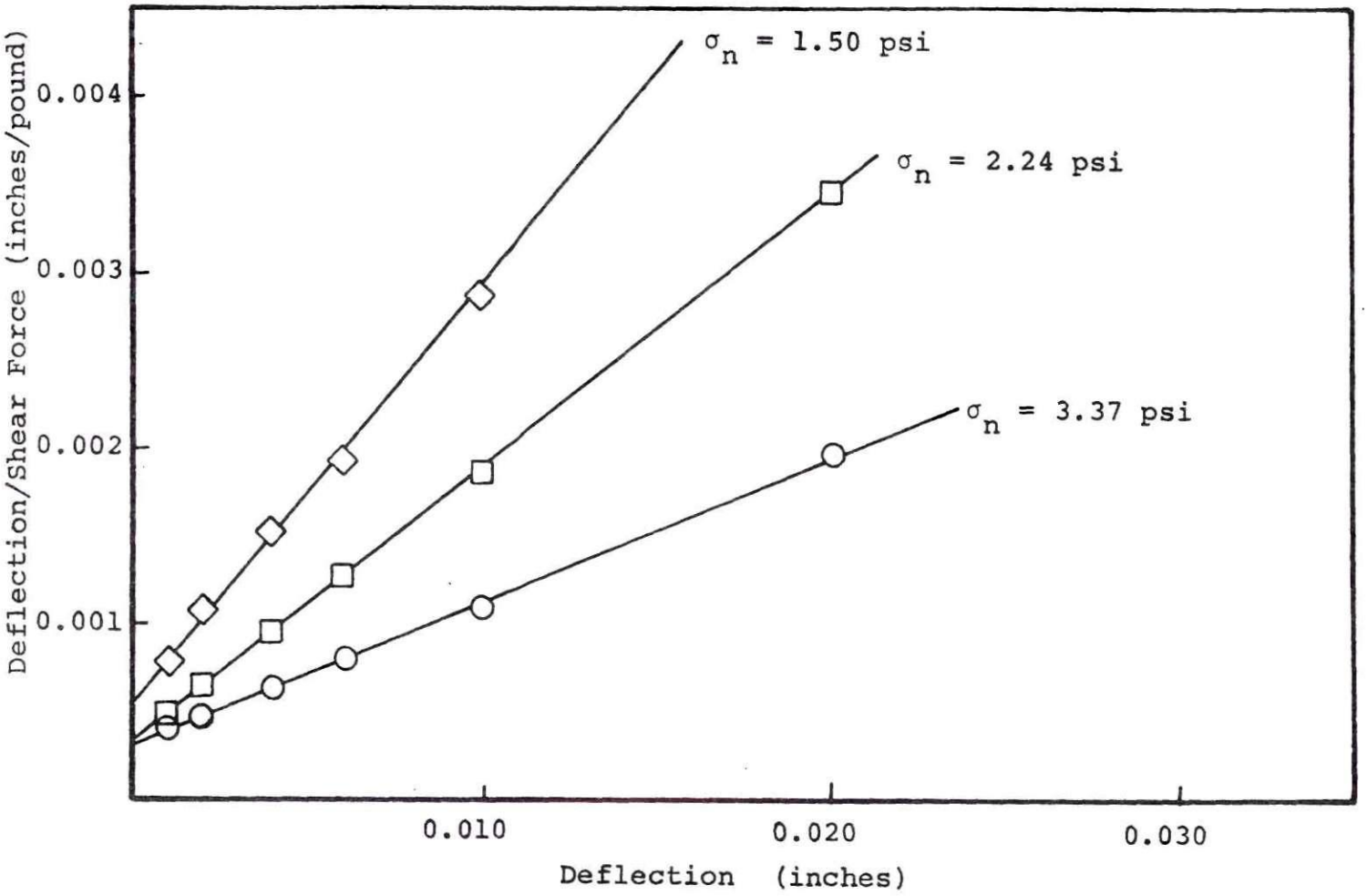

Figure 14. Transformed Hyperbolic Shear Force - Deflection Curves for Series 7, 8 and 9, Smooth Concrete, D_R = 65%

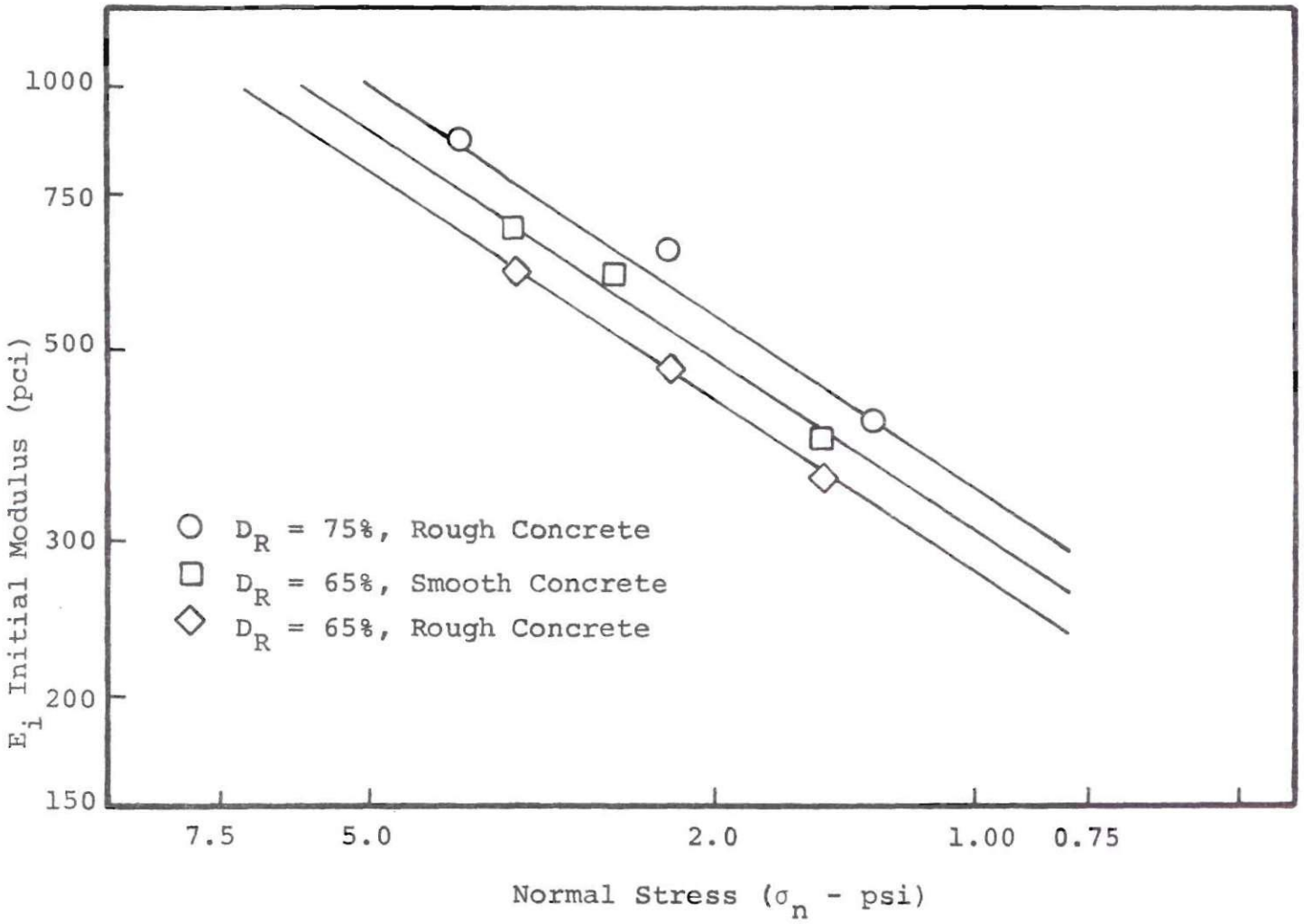

Figure 15. Linear Relationship of E_i and Normal Stress in Logarithmic Coordinates

Table 6. Measured Load in Pier Based on Indicated Strains; Preliminary Test (no sand)

Assumed: Concrete Modulus of Elasticity - 2.60×10^6 psi
Reinforcing Steel Modulus of Elasticity - 30×10^6 psi

Using Strain From Reinforcing Steel Gages:

Top Load (lbs)	Tip Load (lbs)	Level 1[a] (lbs)	Level 2 (lbs)	Level 3 (lbs)	Level 4 (lbs)
39,000	39,000	38,500	35,600	36,700	39,400

Using Strain From Concrete Strain Gages:

Top Load (lbs)	Tip Load (lbs)	Level A[b] (lbs)	Level B (lbs)	Level C (lbs)
39,000	39,000	37,700	30,400	21,100

Using Stress From Carlson Meters (Average Area = 201 sq. in.):

Top Load	Tip Load	#1[c] (lbs)	#2 (lbs)	#3 (lbs)
39,000	39,000	43,300	75,500	56,000

Note:

Distance From Top of Pier:

a) Level 1 - 1.67 ft.
Level 2 - 6.17 ft.
Level 3 - 10.17 ft.
Level 4 - 10.67 ft.

b) Level A - 3.83 ft.
Level B - 8.50 ft.
Level C - 13.17 ft.

c) #1 - 3.34 ft.
#2 - 8.17 ft.
#3 - 13.09 ft.

Eccentric Load Tests

The results of the eccentric load tests on the model pier are shown in Tables 7 through 10. The load distribution for the eccentric load tests are shown in Figures 16 through 20.

Concentric Load Test

The results of the concentric load test are also included in Tables 7 through 10. The load distribution for the concentric load test is shown in Figure 21.

Ultimate Load Test

The maximum load sustained in skin friction with no tip support was 10,300 pounds.

Table 7. Pier Load Distribution from Reinforcing Steel Strain Gages

Test Number	Applied Load (lbs)	Tip Load (lbs)	*Level 1 (lbs)	Level 2 (lbs)	Level 3 (lbs)	Level 4 (lbs)
1	16,800	14,500	18,500	16,700	16,000	14,880
	33,930	34,000	32,180	33,920	--	34,500
	54,440	48,000	54,200	54,200	51,700	50,050
	72,910	65,800	72,100	69,770	70,900	68,500
	84,580	76,000	86,800	82,200	84,600	80,400
	93,630	82,750	91,800	92,850	90,500	87,000
2	17,690	11,700	16,090	14,960	13,720	12,500
	36,340	29,500	35,070	33,400	33,900	33,400
	58,250	50,500	57,800	59,520	56,500	56,500
	85,680	76,500	86,400	85,200	83,300	82,800
	96,030	85,300	--	93,600	91,900	88,800
3	26,570	18,700	28,500	25,600	23,770	23,290
	37,200	28,100	--	38,160	35,170	34,600
	56,410	46,100	55,380	53,050	49,670	50,050
	74,580	64,000	72,650	68,640	--	65,620
	93,660	83,000	95,150	92,800	89,900	86,950
4	18,480	13,600	--	19,000	--	14,300
	39,390	32,500	--	38,750	34,600	33,300
	58,730	51,600	58,350	55,950	--	54,800
	77,590	68,300	76,800	78,000	--	75,600
	97,380	87,400	95,000	93,400	95,750	90,600
	108,770	97,900	108,400	106,600	104,250	101,150
5	19,010	12,000	20,300	20,300	17,880	14,880
	38,190	30,900	35,170	33,340	--	31,600
	58,140	51,000	59,520	55,950	51,320	50,800
	78,160	67,300	--	78,100	69,780	69,780
	96,730	86,600	--	94,700	92,850	88,200
1c	18,530	14,000	19,040	17,830	17,880	16,140
	38,480	32,800	36,910	38,750	36,340	35,070
	59,080	51,300	--	60,790	56,620	53,630
	78,510	70,000	77,400	76,250	73,840	72,100
	100,290	90,100	--	98,300	94,700	92,250

*See note, Table 6.

Table 8. Pier Load Distribution from Concrete Strain Gages

Test Number	Applied Load (lbs)	Tip Load (lbs)	*Level A (lbs)	Level B (lbs)	Level C (lbs)
1	16,800	14,500	--	16,200	14,400
	33,930	34,000	32,100	--	--
	54,440	48,000	52,600	--	--
	72,910	65,800	75,100	--	69,100
	84,580	76,000	85,200	--	--
	93,630	82,750	--	--	--
2	17,690	11,700	** --	--	--
	36,340	29,500	--	--	--
	58,250	50,500	--	--	--
	85,680	76,500	--	--	--
	96,030	85,300	--	--	--
3	26,570	18,700	24,900	--	--
	37,200	28,100	--	--	--
	56,410	46,100	--	--	--
	74,580	64,000	72,600	--	--
	93,660	83,000	--	--	--
4	18,480	13,600	19,300	--	--
	39,390	32,500	--	--	--
	58,730	51,600	55,300	--	--
	77,590	68,300	80,900	--	--
	97,380	87,400	91,600	--	--
	108,770	97,900	105,900	--	--
5	19,010	12,000	--	--	--
	38,190	30,900	--	--	--
	58,140	51,000	--	--	--
	78,160	67,300	84,200	74,900	--
	96,730	86,600	--	94,300	--
1c	18,530	14,000	18,100	--	14,500
	38,480	32,800	37,900	--	--
	59,080	51,300	60,000	--	50,700
	78,510	70,000	79,500	--	--
	100,290	90,100	--	96,800	92,200

*See note, Table 6.

**Switching box not functioning properly.

Table 9. Pier Load Distribution as Indicated by Carlson Meters (Assuming an Effective Area of 201 Square Inches)

Test Number	Applied Load (lbs)	Tip Load (lbs)	No. 1*	No. 2	No. 3
1	16,800	14,500	58,000	52,900	47,000
	33,930	34,000	70,600	85,200	68,700
	54,440	48,000	85,700	115,500	91,500
	72,910	65,800	107,500	140,300	113,100
	84,580	76,000	111,000	160,000	120,600
	93,630	82,750	117,700	171,000	130,300
2	17,690	11,700	49,600	55,400	41,800
	36,340	29,500	67,000	96,900	75,800
	58,250	50,500	83,400	135,000	100,400
	85,680	76,500	109,200	173,000	109,000
	96,030	85,300	117,000	187,000	123,000
3	26,570	18,700	55,500	64,400	59,200
	37,200	28,100	62,200	85,500	74,400
	56,410	46,100	82,500	118,200	99,500
	74,580	64,000	93,500	145,500	125,500
	93,660	83,000	114,000	172,000	146,000
4	18,480	13,600	34,600	56,300	31,200
	39,390	32,500	56,300	107,500	58,400
	58,730	51,600	72,700	150,000	87,000
	77,590	68,300	86,500	163,000	109,500
	97,380	87,400	96,500	193,000	135,000
	108,770	97,900	113,000	208,000	164,000
5	19,010	17,000	--**	39,000	37,200
	38,190	30,900	--	84,500	76,400
	58,140	51,000	--	122,000	101,500
	78,160	67,300	--	149,000	122,000
	96,730	86,600	--	176,500	146,000
1C	18,530	14,000	--	40,500	39,400
	38,480	32,800	--	83,000	77,500
	59,080	51,300	--	103,000	124,000
	78,510	70,000	--	153,000	141,000
	100,290	90,100	--	185,500	146,500

*See note at end of Table 6.
**Initial reading unstable.

Table 10. Summary of Load Eccentricity, Skin Friction, and Deflection in Pier Tests

Test Number	Top Load (lbs)	Eccentricity (inches) x	Eccentricity (inches) y	Bottom Load (lbs)	Skin Friction (lbs)	Top Deflection (inches)
1	16,800	0.57	0.61	14,500	2,300	--
	33,930			34,000	--	--
	54,440			48,000	6,440	--
	72,910			65,800	7,110	--
	84,580			76,000	8,580	--
	93,630			82,750	10,880	0.056
	17,690	0.58	0.70	11,700	5,990	0.012
	36,340			29,500	6,840	0.027
	58,250			50,500	7,750	0.043
	85,680			76,500	9,180	0.048
	96,030			85,300	10,730	0.055
3	26,570	0.59	0.74	18,700	7,870	0.018
	37,200			28,100	9,100	0.026
	56,410			46,100	10,310	0.039
	74,580			64,000	10,580	0.046
	93,660			83,000	10,660	0.054
4	18,480	0.34	0.75	14,600	3,880	0.0110
	39,390			33,500	5,890	0.0266
	58,730			52,600	8,130	0.0382
	77,590			69,300	8,290	0.0481
	97,380			88,400	8,980	0.0566
	108,770			97,900	10,870	0.0619
5	19,010	0.04	0.29	12,000	7,010	0.0162
	38,190			30,900	7,290	0.0248
	58,140			50,000	8,140	0.0381
	78,160			67,300	10,860	0.0498
	96,730					0.0605
1C	18,530	0.04	0.10	14,000	4,530	0.0123
	38,480			32,800	5,680	0.0257
	59,080			51,300	7,780	0.0366
	78,510			70,000	8,510	0.0456
	100,290			90,100	10,190	0.0536

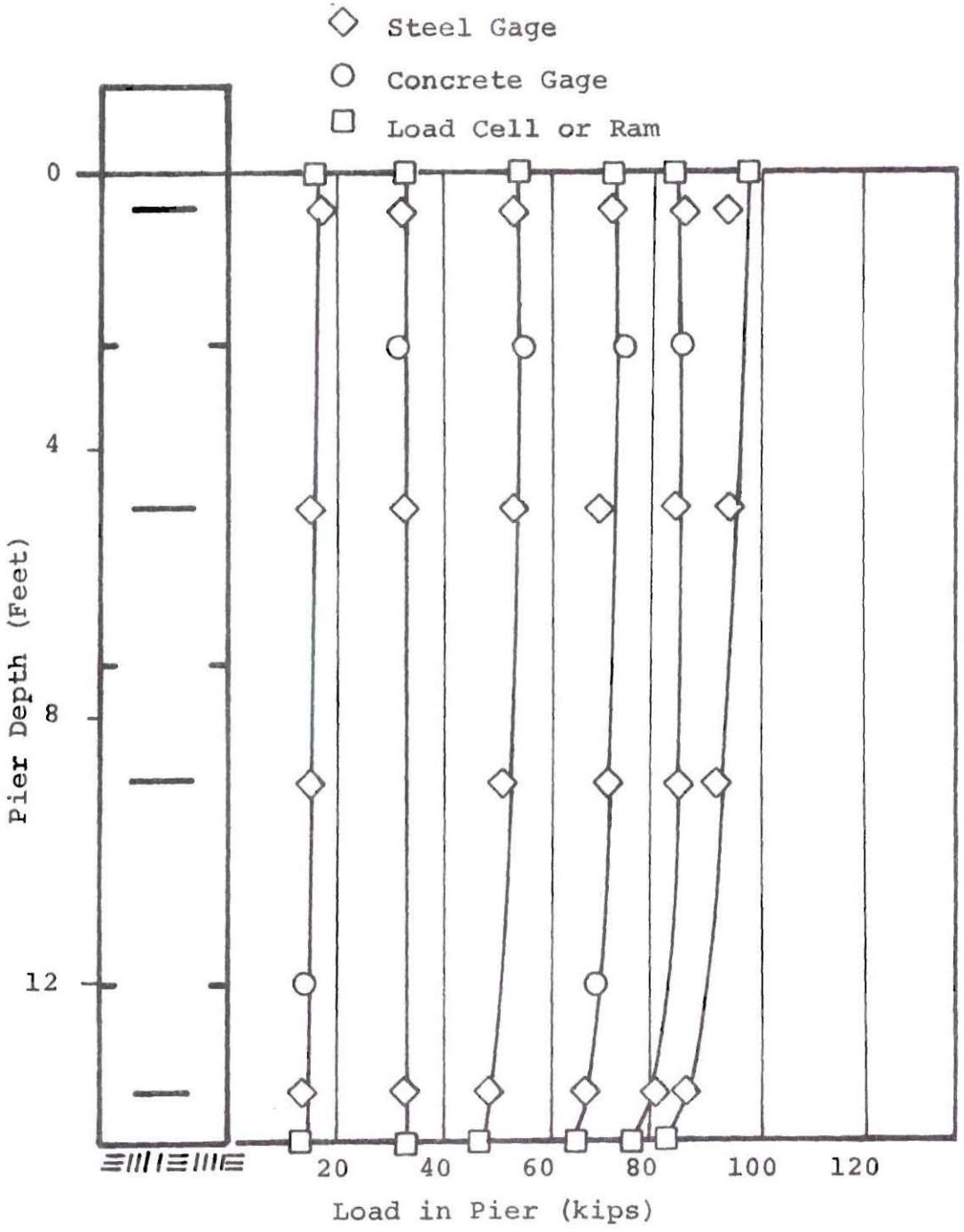

Figure 16. Measured Loads in Pier Shaft For Various Levels of Applied Load, Test 1

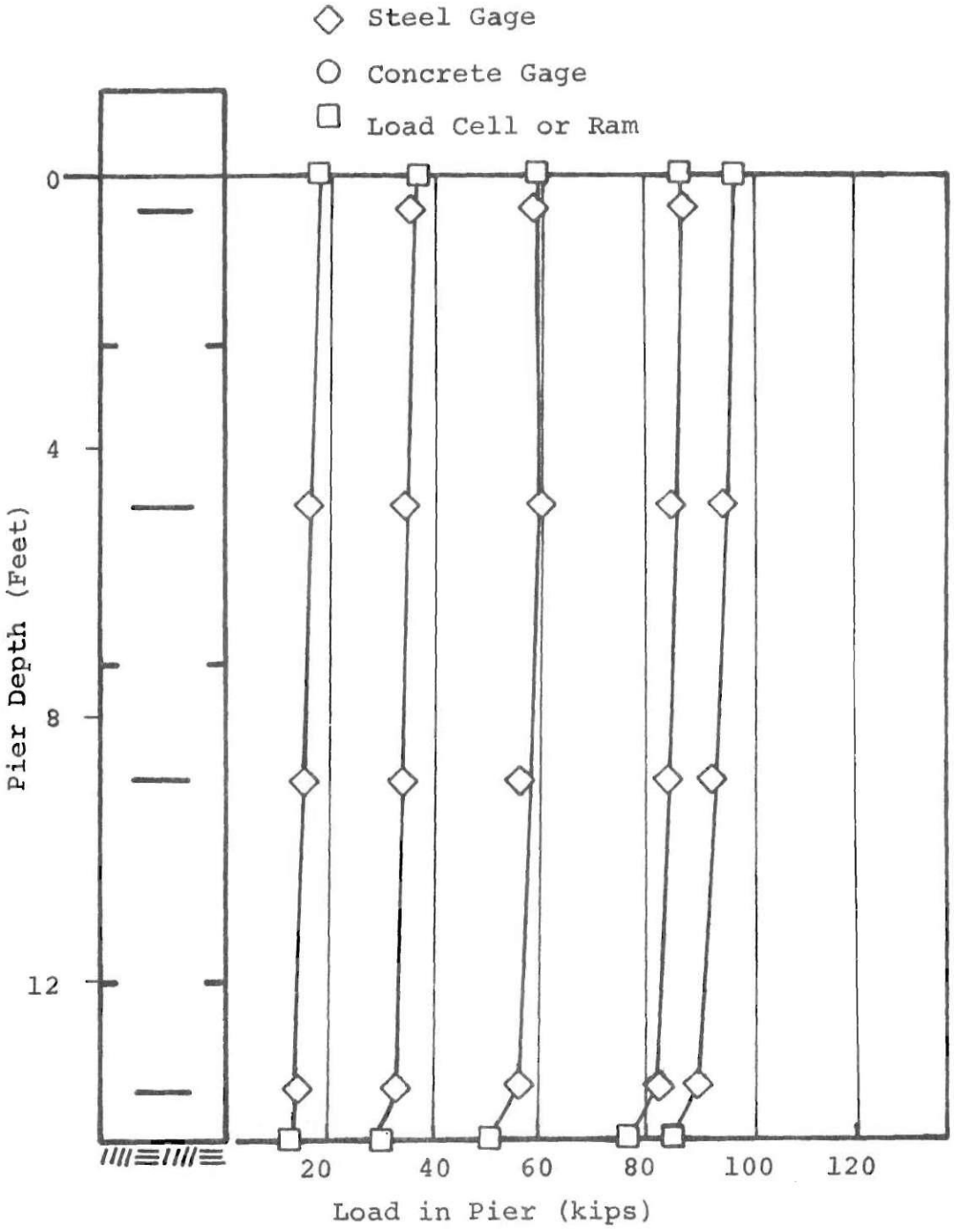

Figure 17. Measured Loads in Pier Shaft for Various Levels of Applied Load, Test 2

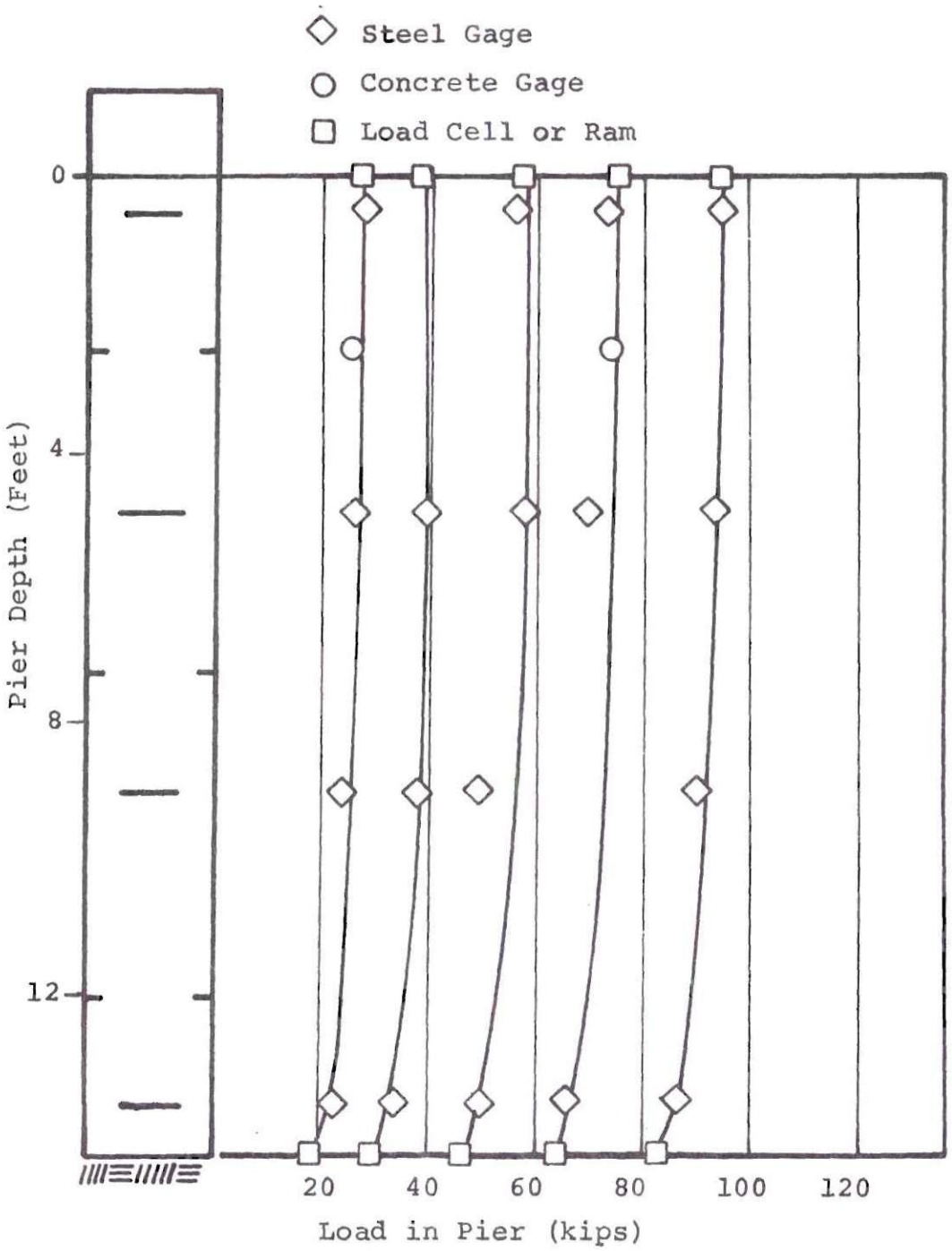

Figure 18. Measured Loads in Pier Shaft for Various Levels of Applied Load, Test 3

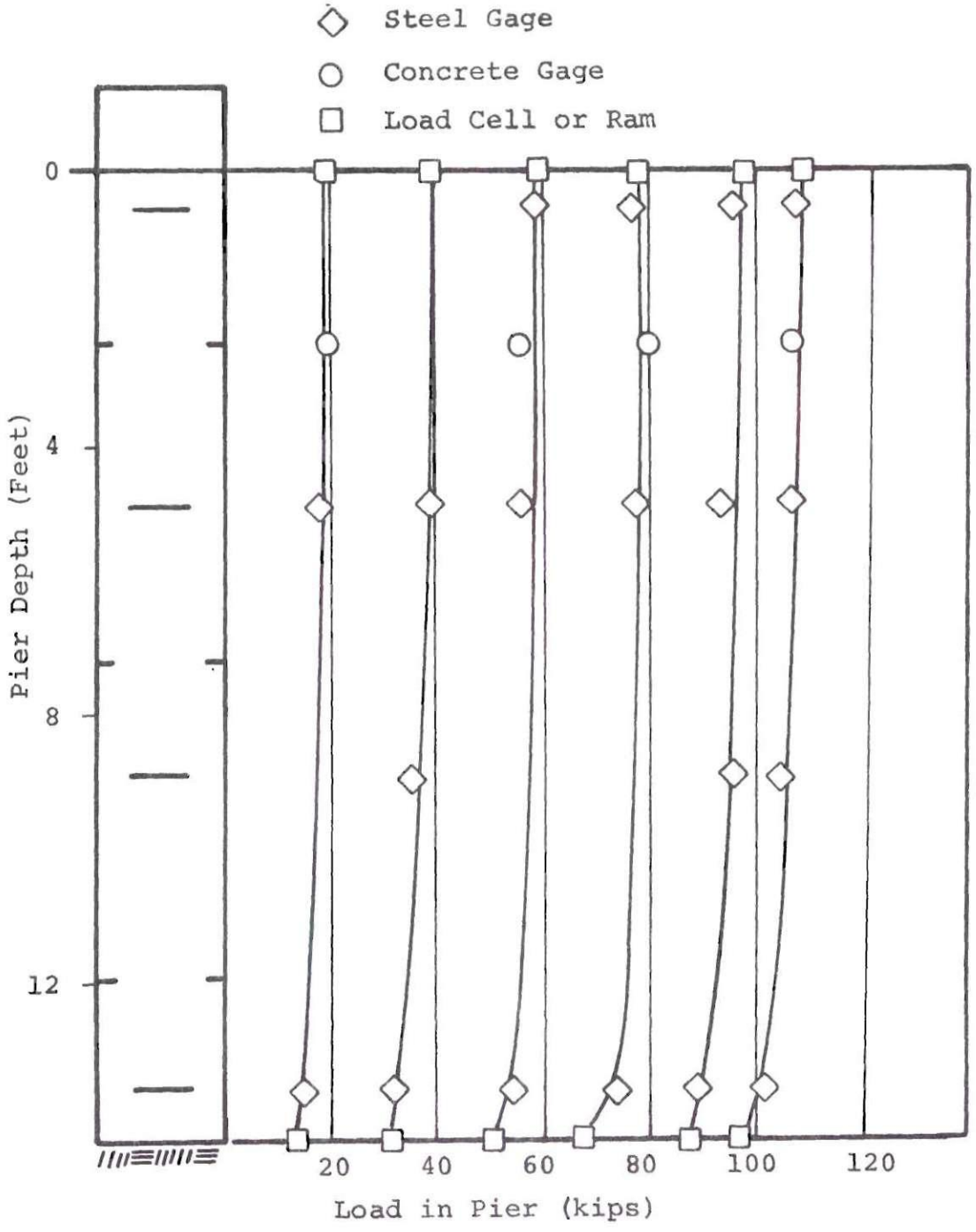

Figure 19. Measured Loads in Pier Shaft for Various Levels of Applied Load, Test 4

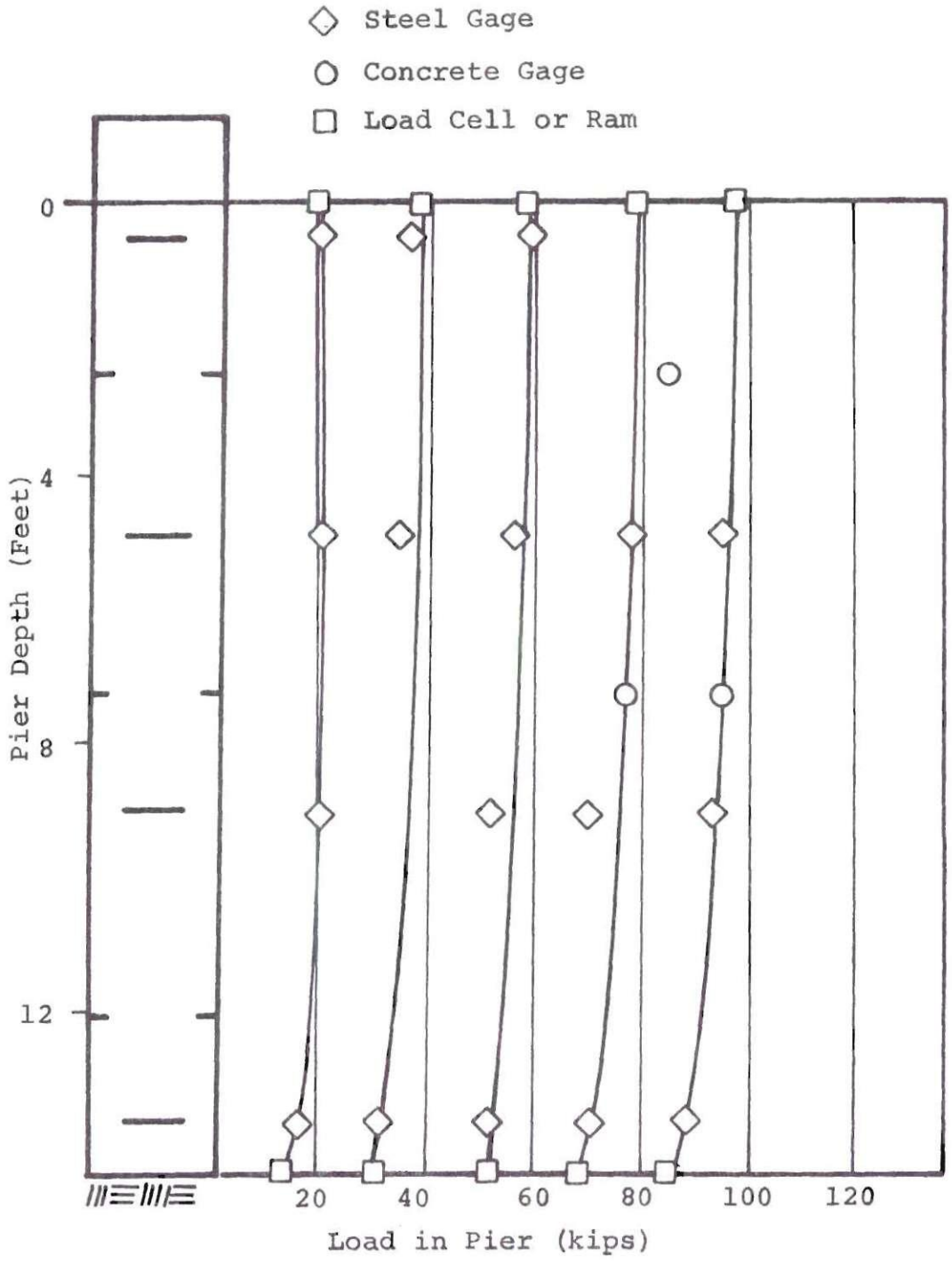

Figure 20. Measured Loads in Pier Shaft for Various Levels of Applied Load, Test 5

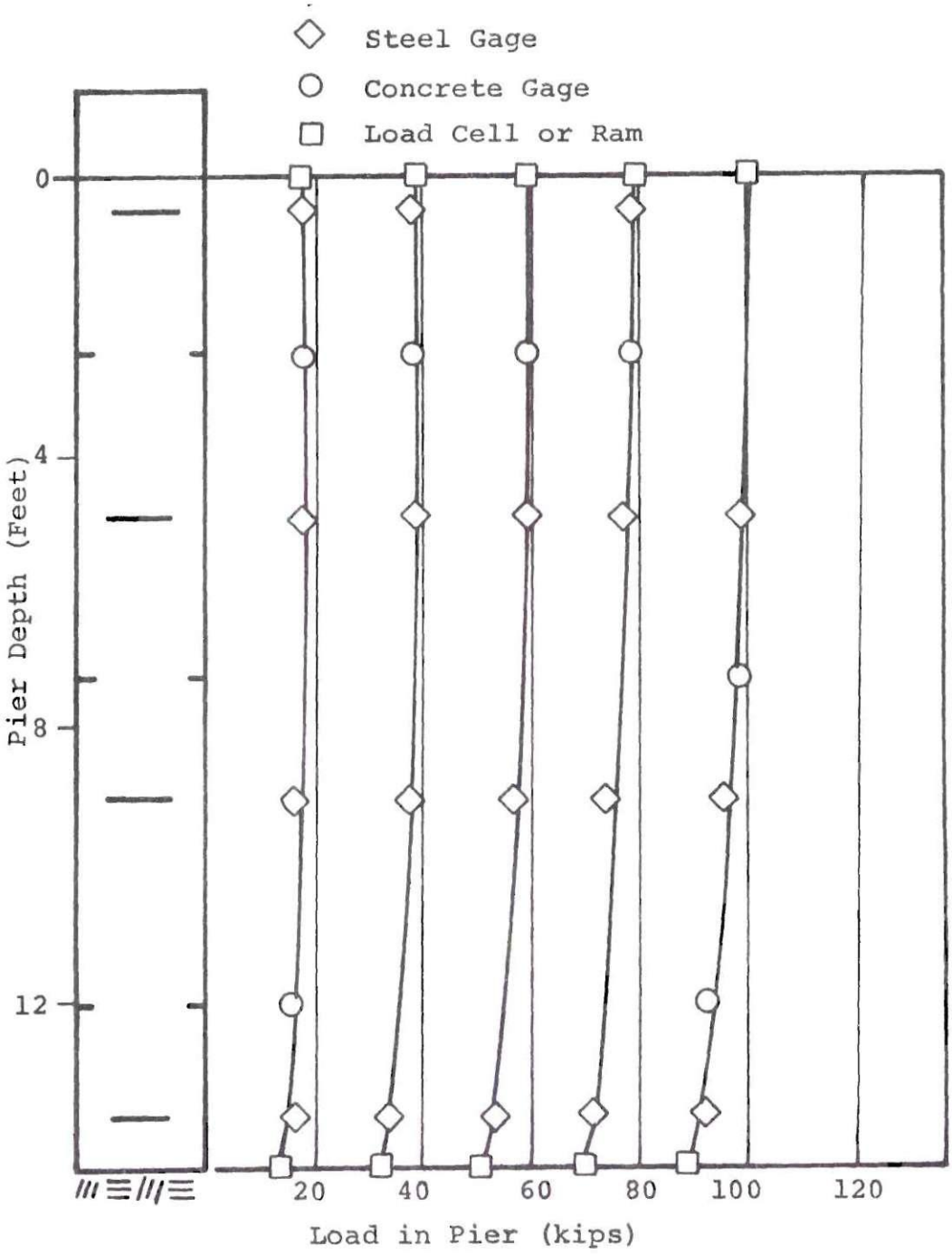

Figure 21. Measured Loads in Pier Shaft for Various Levels of Applied Load, Test 1C

CHAPTER VIII

DISCUSSION OF RESULTS

Direct Shear Tests

Based on the data from the load-deflection curves, Figures 9, 10, and 11, the hyperbolic model relations for each of the types of tests are as follows:

(1) Rough Concrete, Relative Density of 75 percent:

$$\tau = \frac{\delta}{1/E_i + \frac{0.946}{\sigma_n}} \tag{11}$$

(2) Rough Concrete, Relative Density of 65 percent:

$$\tau = \frac{\delta}{1/E_i + \frac{1.118}{\sigma_n}} \tag{12}$$

(3) Smooth Concrete, Relative Density of 65 percent:

$$\tau = \frac{\delta}{1/E_i + \frac{1.47}{\sigma_n}} \tag{13}$$

As indicated in equations 11 and 12 and Figures 9 and 10, the interface behavior is not sensitive to the relative density of the sand. The effect of surface roughness on the

shear transfer relation is significant. A "rough surface" is one in which the size of the grains or projections on the surface are greater than or equal to the average grain size of the soil placed against the surface. The interfacial shear between a rough surface and the soil may occur in the soil mass and not at the interface. The effect of the surface roughness on the difference in shear transfer for a rough and smooth surface may be as much as 20 percent.

The smooth surface used for the direct shear tests was formed by casting the concrete against a glass plate with a lubricant. The values of Ψ and R_f are shown in Table 5. The values of the coefficient of friction at a relative density of 65 percent were: $\Psi = 38° 12'$ for the rough concrete and $\Psi = 30° 25'$ for the smooth. The coefficient of friction for the rough concrete was equal to the angle of internal friction for the sand. The values from triaxial tests on the same Chattahoochee River sand by Vesic [52] at confining pressures less than 10 psi at approximately the same density were 38° 42'. This agrees well with the direct shear value and an average $\phi = 38° 12'$ was used. This condition was also found by Potyondy [40], that for all practical conditions, the coefficient of friction for rough concrete is equal to the apparent angle of shearing resistance of the sand. The value for the smooth concrete for these tests is a reduction of approximately 20 percent. Potyondy indicates a reduction of 11 percent, which agrees with that

found by Brumund [9]. The larger increase may be due to the difference in sand gradation and surface texture of the concrete.

The value of the initial tangent modulus for the hyperbolic relation was determined from a log-log plot of the initial tangent modulus versus normal stress. The relationship for several densities is shown in Figure 15. The values of E_i obtained from this study compared with typical values from Duncan and Chang [16], for a uniform, fine, silica sand at a confining pressure of 1.5 psi are shown in Table 11.

Table 11. Comparison of Initial Tangent Modulus, E_i, for Fine, Uniform Silica Sand and Chattahoochee River Sand

Sand	σ_n (psi)	E_i (pci)
Fine, Uniform Silica Sand (Duncan and Chang (16))	1.5	330
Chattahoochee River Sand	1.5	360

The direct shear test results and hyperbolic model agreed with previous studies [52, 16], and were used for predicting the skin friction transfer in the model pier tests.

Preliminary Pier Tests (No Sand)

The results of the preliminary pier tests are shown in Table 6. The measured load from the reinforcing steel strain gages was within ten percent of the applied load at all four strain gage levels in the pier. The indicated strain from the bottom level of gages with an applied load of 39,000 pounds was 55 microinches/inch. The calculated strain, based on elastic theory, for the same gage level was 56 microinches/inch. The measured strains from the concrete strain gages were not as consistent as those of the reinforcing steel gages. The two lower levels of concrete gages indicated much lower strains than the reinforcing steel gages.

The measured loads from the Carlson stress meters were much higher than the applied loads with the exception of meter number one. Subsequent test results indicated that the measured loads from meter number one were also higher than the applied loads. The measured loads from all the meters were so much in excess of the applied, that the values from the meters were not used in the load distribution results.

Model Pier Tests

An examination of Figures 16 through 21 indicates little shear transfer of load in the upper portion of the pier, as evidenced by an almost constant load at each

instrumented section. To examine the magnitude of shear transfer in various portions of the pier more closely, the measured shear stress distribution is shown in Figures 22 through 27. The measured values shown in Figures 22 through 27 were determined by dividing the measured amount of shear transfer along a section of the pier by the area of the pier over which the shear load was transferred. These figures were plotted for the maximum applied loads.

Instrumentation

Reinforcing Steel Strain Gages

The strain gages on the reinforcing steel proved to be the most reliable of the instruments in the pier. A total of 24 gages were used on the steel and four of the gages were found to be defective after placing the concrete. Unfortunately, two of the four defective gages were located in the top level of the steel; this left fewer gages for a comparison of the applied load and indicated strain at the top of the pier.

The major drawback of the monitoring system was the twenty-channel switching box used for the gages. The readings from the gages would occasionally be erratic due to the position of the switch on the channel selector. Care in switching was taken to ensure that the switch was placed at the same position on the channel throughout each test.

Examination of Tables 7 and 8 indicates some values

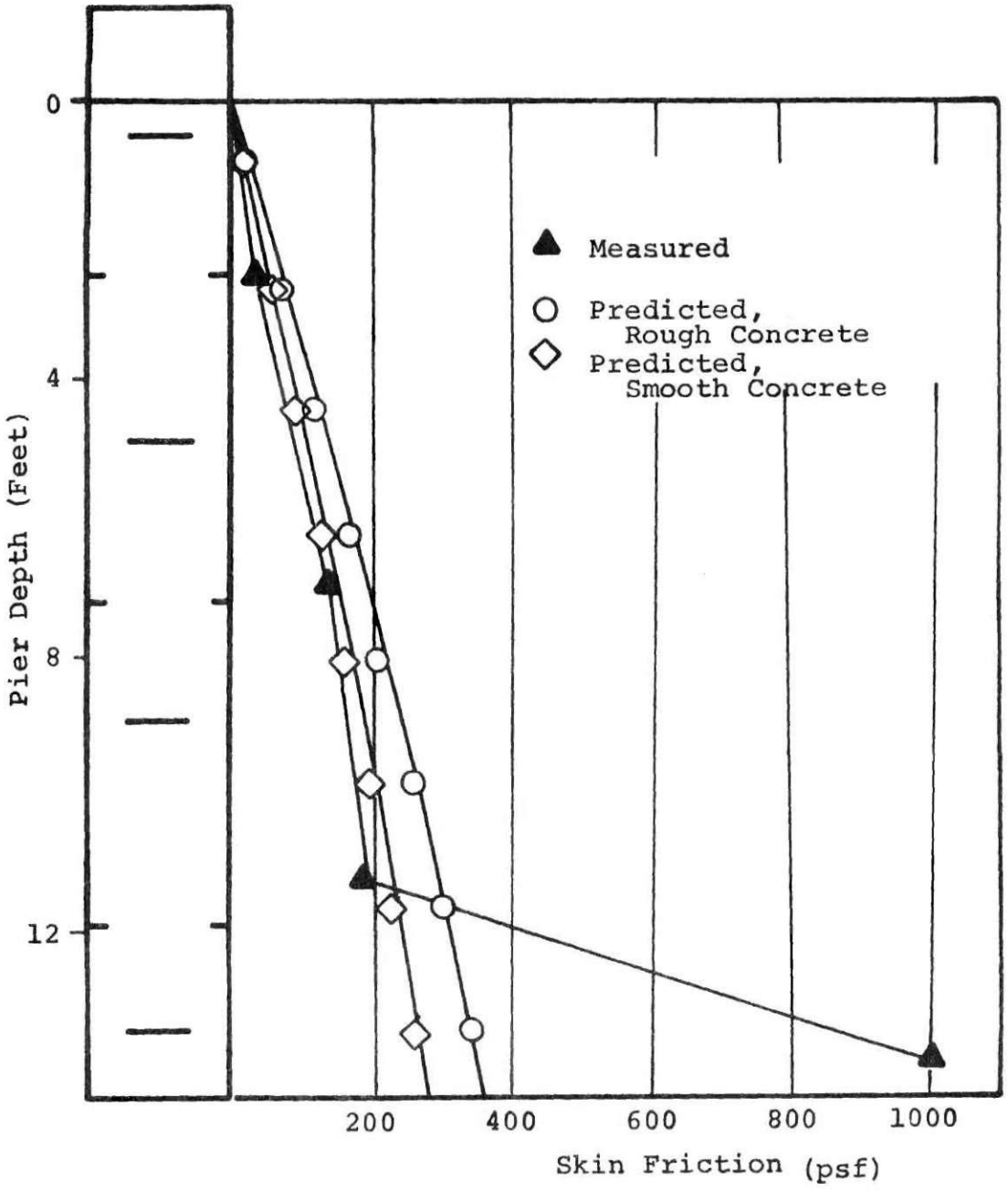

Figure 22. Distribution of Measured and Predicted Skin Friction, Test 1

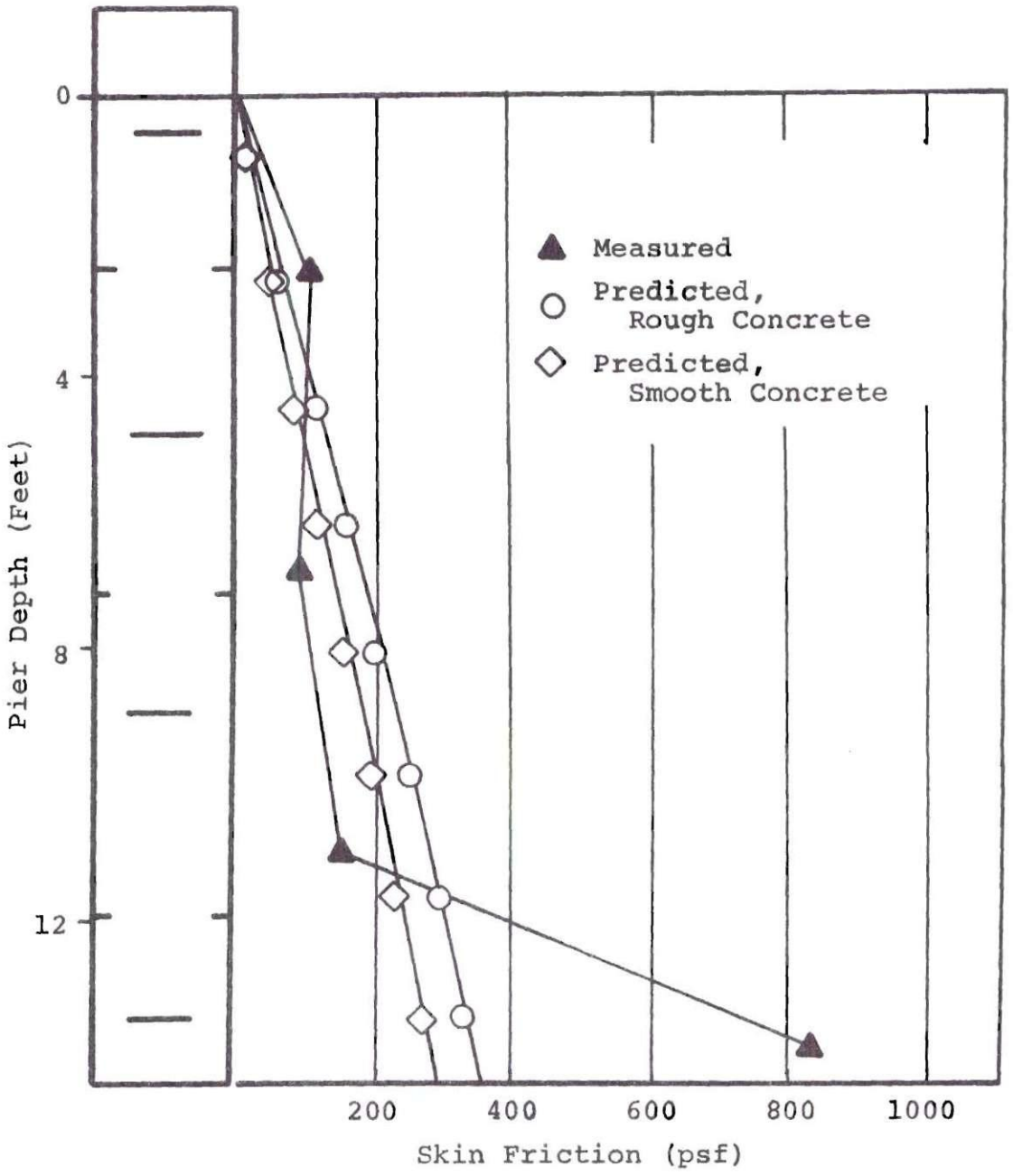

Figure 23. Distribution of Measured and Predicted Skin Friction, Test 2

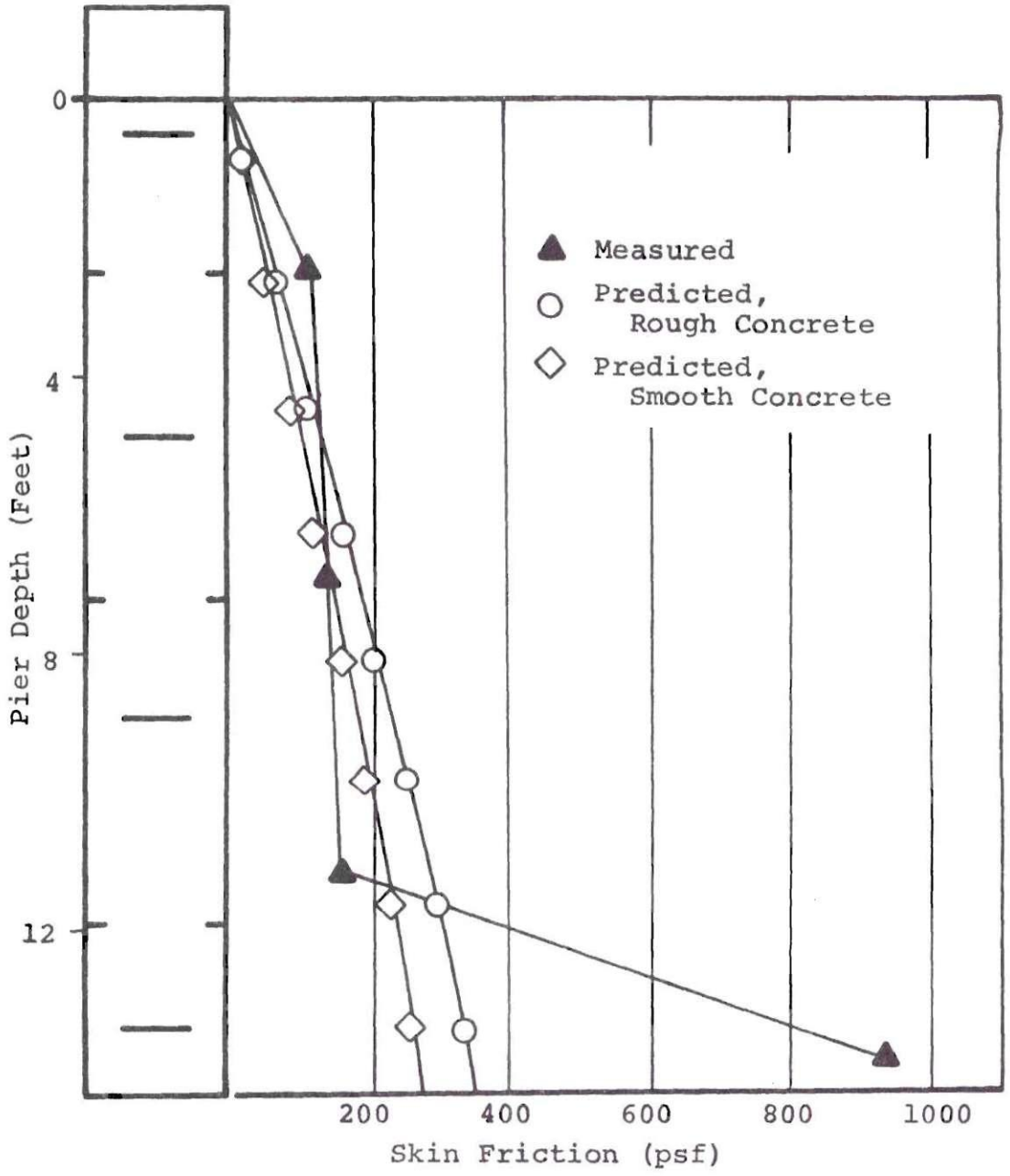

Figure 24. Distribution of Measured and Predicted Skin Friction, Test 3

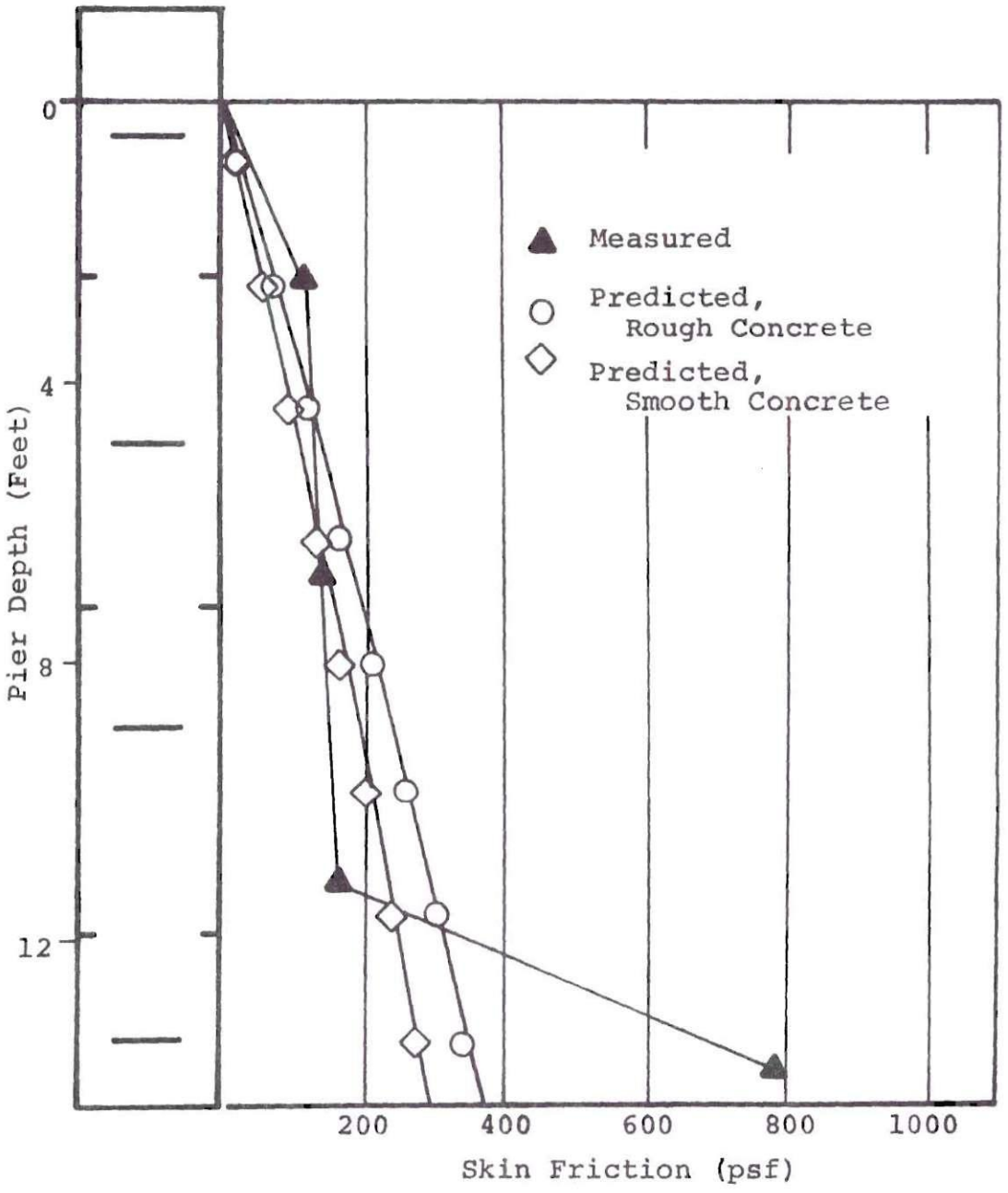

Figure 25. Distribution of Measured and Predicted Skin Friction, Test 4

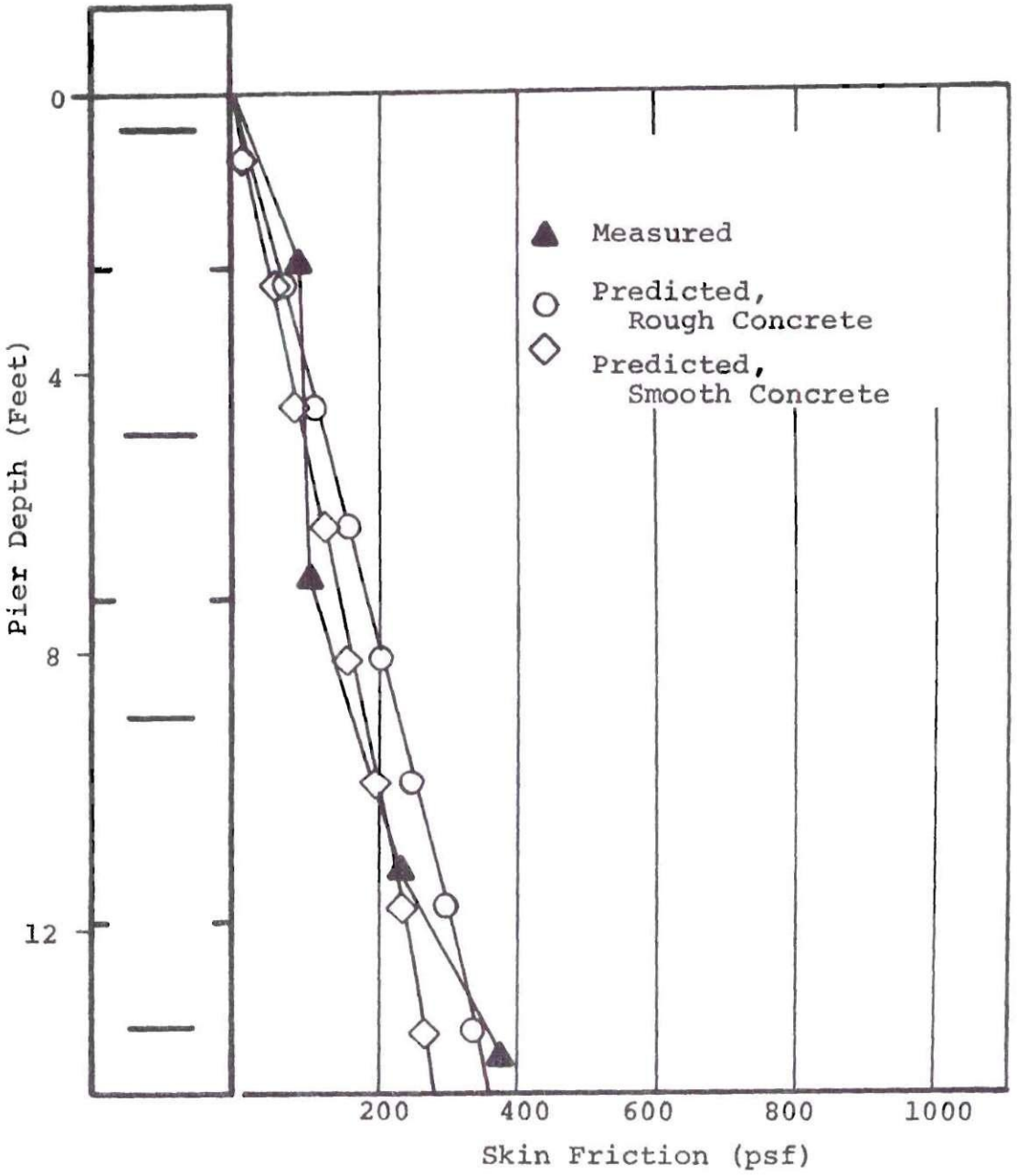

Figure 26. Distribution of Measured and Predicted Skin Friction, Test 5

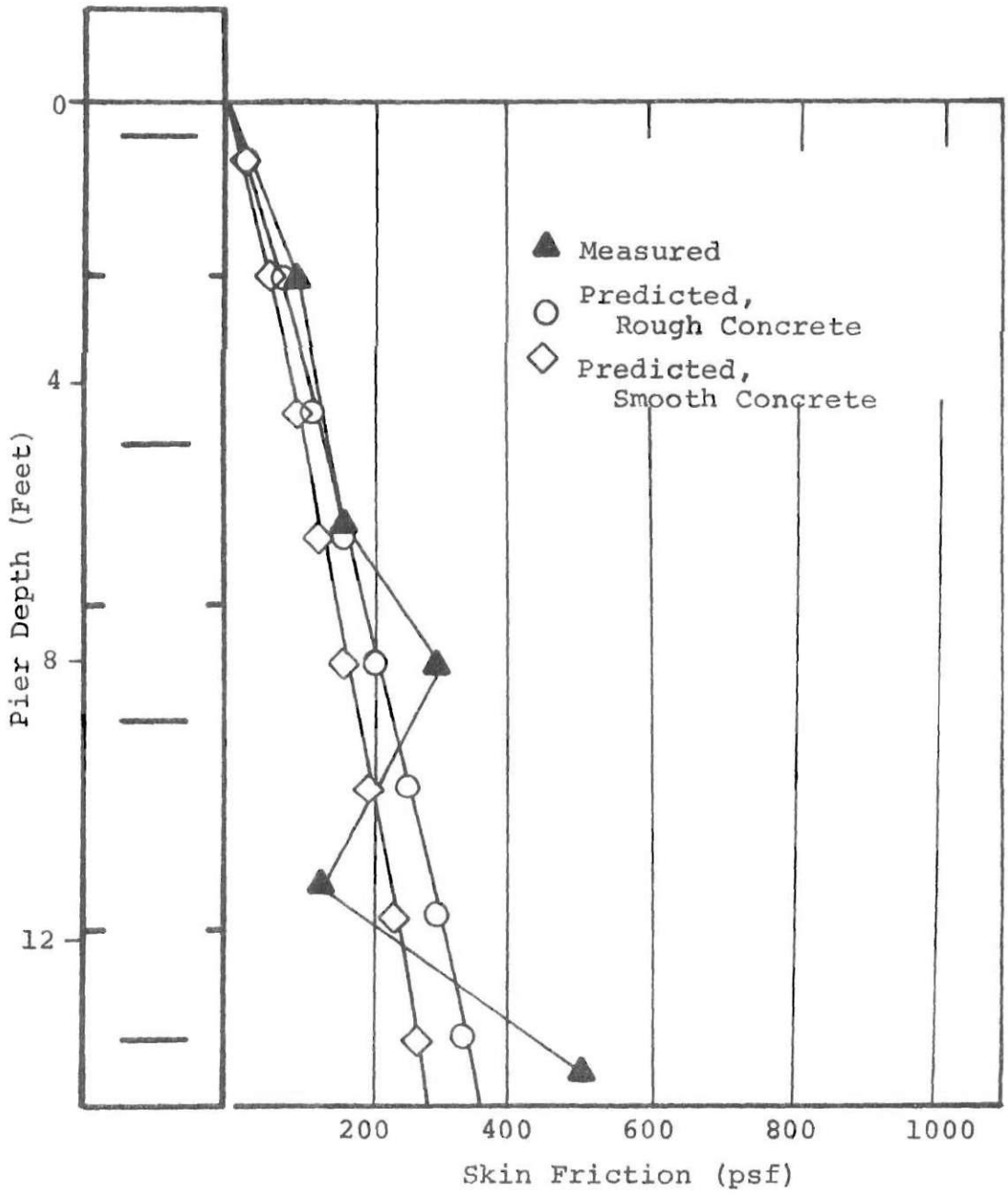

Figure 27. Distribution of Measured and Predicted Skin Friction, Test 1C

for the load were omitted. This was due to erratic values from the strain gages. In most instances, the strain readings at each level were consistent within a few micro-inches/inch of each other.

The effect of the eccentric loading of the pier could not be determined from the reinforcing steel gage output. The individual pairs of gages on each vertical bar showed little difference in strain, and the variation in strain across each level of gages showed no significant bending in the pier.

The waterproofing system proved adequate for the period of testing, which was approximately two months. The gage response was adequate. However, more sensitivity would have given a better defined load distribution. For example, with an applied load of 108,000 pounds, the strain from the top to the bottom of the pier ranged from 182 microinches/inch to 170 microinches/inch. The average value of the modulus of elasticity used for the reinforcing steel was 30×10^6 psi. The average value of the modulus of elasticity for the concrete was 2.60×10^6 psi. The concrete modulus was determined by averaging the calculated moduli of elasticity obtained from the top level of strain gages assuming that the applied load was equal to the load in the pier at the position of the gages. The modulus of elasticity calculated from the test with no sand in the pit was also included in the average. The modulus of elasticity was also

calculated from the concrete strain values from the top set of gages. This average value compared favorably with the modulus determined from stress-strain curves from four of the test cylinders. The average initial tangent value from these tests was 2.76×10^6 psi (Appendix F). A variation of the modulus of elasticity within the measured values did not affect the measured loads a large amount (i.e., for E = 2.60 x 10 psi. The load at the bottom level of gages, Test 2 = 88,800 pounds. For a modulus of elasticity of 2.76×10^6 psi, the load at the bottom level of gages, Test 2 = 92,900 pounds, the difference is 4.6 percent).

Concrete Strain Gages

The results from the six-inch strain gages placed on the outside of the concrete pier were very poor. All of the gages operated with no drift and the resistance remained at approximately 300 ohms throughout the tests. However, the indicated strains for the middle and bottom levels were 10-40 percent of the actual strain. The gages were placed on crack free surfaces. However, the middle and bottom levels were placed directly below the construction joints in the pier. The top level of gages, which were placed on the concrete surface of the topmost pour indicated strains similar to those of the strain gages on the reinforcing steel.

The epoxy coating over the gage surface protected the gages during the placement of the sand and from any moisture that might have gotten to the gage or soldered connections.

These gages and the method of protection were satisfactory, but the location and surface must be carefully selected for suitable results.

Carlson Stress Meters

The Carlson meters were tested extensively prior to placing in the pier and performed satisfactorily. The tests prior to placing in the pier were very similar to tests performed by Hickey [19] for the Bureau of Reclamation. These tests were performed on 18-inch diameter by 36-inch long cylinders of unreinforced concrete to check the performance of the Carlson meters Model PC-800 under standard conditions and also to investigate the effects of weathering and temperature cycles. Hickey found under similar conditions of installation that the Carlson meters indicated the applied stress within seven percent. The calibration tests conducted in this study indicated the meters to be within ten percent of the applied stresses; see Appendix F. After placing in the pier, the resistance of the gages, as well as the resistance ratio, changed only a slight amount. The waterproofing and wiring protected the meters and provided good service throughout the test period. The indicated stresses from the meters were much higher than the applied stresses in all tests. Table 9 gives the results from the meters. The measured stresses were so much in excess of the applied, the results from the meters were not used. The initial resistance of the meters prior to placement and the inplace resistances

were compared for any indication of malfunction in the sensing elements. However, only a slight change was noted. The initial resistance ratios and the final ratio after placing were also in close agreement.

The basic installation procedure used was evidently suitable as indicated by the close coincidence of results with those of Hickey. However, the minimal amount of clearance between the reinforcing steel and the cell may account for the large difference in the applied and measured stresses. During the placing of the concrete on the gage and subsequently upon loading, the meter could have probably become wedged in the reinforcing steel, producing a rigid plate resistance. The effective modulus of elasticity of all the meters is approximately five million psi, as indicated in the suppliers calibration data. Carlson and Pirtz [12] have indicated that the plate shaped meter was designed to have approximately the same compressibility as the surrounding concrete, if placed in a mass of concrete with no surrounding constraints. The meters gave erroneous readings and the data obtained from these meters was not used in the analysis of results, possibly because of the constraining effect of the reinforcing steel.

This type of meter would be quite suitable for mass concrete and measurement of large uniform stress distributions; but in the case of the pier with restricted clearance, the meters did not prove to be satisfactory.

Hydraulic Ram System and LVDT's

The hydraulic ram and pressure monitoring system at the ram tip proved to be satisfactory. The tip load could be monitored within ± 500 pounds throughout all the tests. An initial pressure on the tip ram from the pier, loading plates, top ram and some effect from the sand fill was deducted from each reading during the test to get the exact tip loading.

The monitoring system for the LVDT's sensing the tip movement performed as expected with no problems. However, upon loading the pier with the tip held in a fixed position, the measured deflection at the pier top was more than 100 percent greater than the calculated elastic deflection. This additional deflection was due to the movement of the ram below the pier tip and the support system below the ram. Since the LVDT's were attached to the ram casing and moved downward with the ram upon loading, the pier tip could not be held stationary during loading. Thus, the side friction generated solely from the elastic deflection of the pier could not be investigated.

Theoretical Load Distribution

To demonstrate the reliability of the suggested procedure for estimating the shear transfer in a pier, the hyperbolic predictive technique was applied to the model load tests. The measured deflection for each test and the

computed axial shortening was incorporated into the hyperbolic predictive technique to produce the theoretical skin friction transfer relation. These theoretical distributions for each test are also shown in Figures 22 through 27.

The theoretical skin friction transfer curves were generated using the results of the direct shear tests for a smooth concrete surface and a relative density of 65 percent. The surface of the model pier was carefully inspected prior to placing the sand, and the surface was found to be smooth--the interior surface of the "sleek tube" was paraffin coated and produced a very smooth exterior. The surface texture of the cast in-situ concrete pier in the field would most probably be considered rough. Visual examination of the shafts of cast in place piers after extraction by Reese [38] and others [44] has shown that the surface of the shafts is rough. The surface of the model pier was smooth cast, however, the cardboard form produced small irregular ridges along the pier so that the surface was not entirely smooth. A representative sample of this pier surface was difficult to obtain with the small area used in the direct shear tests, so the tests were conducted on an entirely smooth surface and an entirely rough surface. The actual pier surface condition is probably closer to a smooth surface. The average relative density in the middle of the test pit was 75 percent, but was approximately 10 percent lower in the area adjacent to the pier [10]. The value of ϕ and density used for the theoretical

prediction were those for a relative density of 65 percent.

One of the major assumptions in the theoretical prediction is the distribution of the normal force acting along the pier sides. The most common procedure is to relate this lateral pressure to the overburden stress by a coefficient of lateral earth pressure K. The exact value of this K is unknown for drilled piers. It is most likely less than that for a driven pile, since the soil moves inward during the drilling process rather than being displaced downward and outward during the driving operation. The suggested values for K range from less than the active coefficient of pressure to values greater than the at rest pressure coefficient as shown by Mazurkiewicz [31], Martins [30], Sowa [44], and Reese et al. [42]. The attempt to relate the coefficient to some value of active or passive pressure is not the correct approach since these terms are developed considering an assumption of plane strain. The actual behavior is more closely related to the expansion of cylindrical zone of soil as indicated by Sowers [46]. The information as to the field measured values of side friction in granular soil is scarce; Reese et al. [42] recommends a conservative value of one-third be taken for the value of K for shafts in sand. The value used for this study was that recommended by Jaky [22] to estimate K_o, i.e., $K_o = (1-\sin\phi)$. Using a ϕ of 38° 12', the resulting coefficient of lateral pressure used was 0.35. This provided a conservative value for the coefficient with

some relationship to the physical properties of the sand. This value is within the range of values indicated by Terzaghi [47] for shafts in sand, for $\phi = 40°$. The effect of the assumption of a different value for K (K = 0.4 for a dense sand [45]) is shown in Table 12.

Table 12. Sensitivity of Theoretical Expression to K

Coefficient of Lateral Pressure at D_r = 65%	Predicted Skin Friction Test No. 1 (lbs)	Difference (%)
0.35	8,882	0
0.30	7,621	-14.3
0.40	9,987	+12.5

The final step in applying the hyperbolic model is dividing the pier into segments and determining the load transferred in each segment. The effect of segment size was investigated to find the optimum number which might provide the most accuracy with the least amount of calculations. The number of segments for a particular pier load and deflection was varied from four to fourteen segments. It was found that the agreement of computed load did not improve significantly with a segment number greater than approximately eight to ten sections (1.5 to 2.0 feet in length). This number of

segments provided an accurate estimate of the load (within five percent of the calculated load using 14 segments) with a minimum of computation. Table 13 presents a summary of the effect of segment number.

Table 13. Sensitivity of Theoretical Expression to Number of Segments

Number of Segments	Predicted Skin Friction for Test No. 1 (D_r = 65%, K = 0.35) (lbs)	Difference %
4	8,988	+1.2
8	8,882	0
14	8,870	-0.1
20	8,860	-0.3

The best segment size for use in the field would probably be from one to five feet depending on the length and diameter of the pier.

Measured Load Distribution

Distribution of Load Along Pier Shaft

Figures 16 through 21 are the load distribution curves for all of the tests conducted. The amount of load taken in skin friction for the tests averaged about ten percent of the total load. This small amount of load (approximately 10,000

pounds at a maximum top load of 100,000 pounds) coupled with a relatively low resolution of the reinforcing steel strain gages did not produce as definitive curves as others: Reese [43], Mohan et al. [36]. However, these load distribution curves indicate a definite pattern of a linear increase in skin friction until approximately one diameter above the tip. A sharp increase in the skin friction is noted in this lower part of the pier. Two different instrumentation systems were used to measure the load at the lower portion of the pier, i.e., the strain gages on the reinforcing steel at the bottom level of the pier and the hydraulic ram at the bottom of the pier measured the tip load. The strain gage system was not as reliable as the hydraulic ram; however, results from the preliminary tests, Table 6, indicated that the strain gage system was functioning properly. This sharp increase in load transfer at the bottom of the pier was indicated in all the tests on the model pier, Table 7. In the majority of previous studies, the pier was terminated in a soil mass with some of the load being carried in tip bearing. Touma and Reese [49] have indicated that as the pier tip moves into the sand, two distinct zones are developed; a zone of flow adjacent to the pier tip and a zone of arching above the flow zone, as shown in Figure 28. The zones extend from 0 to 5 pier diameters above the tip. It is postulated that, as sand moves into the failure zone around the pier tip, there will be, as a result of arching, an

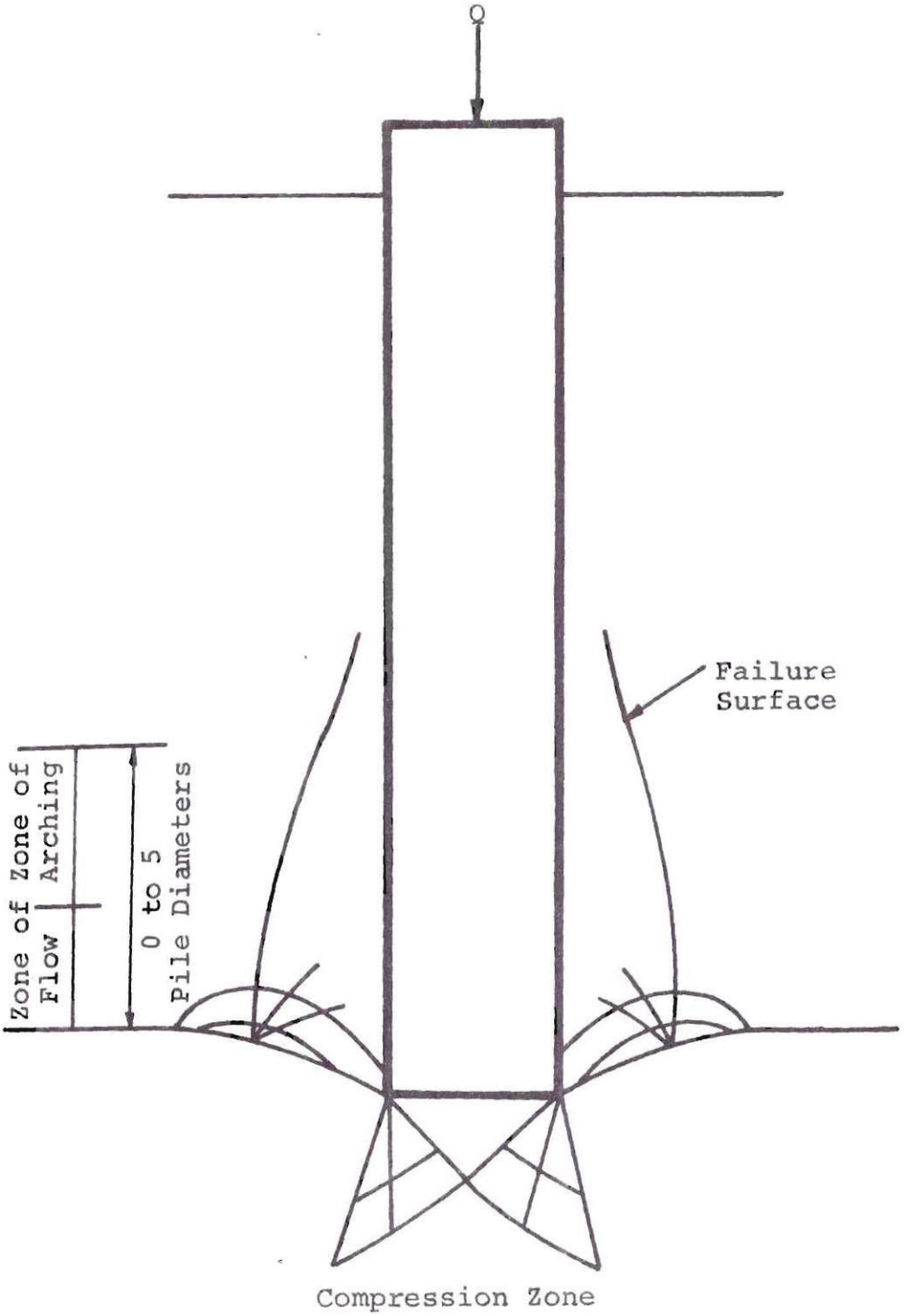

Figure 28. Influence of Tip on the Stresses Around a Bored Pile (After Touma and Reese [49])

increase in the horizontal stresses at the pile wall in this arching zone. An examination of Mindlin's [33] solution for a vertical load applied at a finite distance beneath the surface of an elastic half-space, indicates tensile stresses in the medium above the point of load application. In a real soil medium, these tensile stresses might be interpreted as stresses which would tend to reduce locally the overburden stress, and produce the suggested zone of arching. This application of Mindlin's solution provides some theoretical justification for this zone of "reduced stress." The extent of the zones and magnitude of stress increase are a function of the relative density of the sand. In a loose sand, the tip resistance is small and the influence will be reduced along the sides. In a dense sand, the compression of the sand below the tip takes place at high pressures and the zone of flow and arching may extend for several pier diameters above the tip. Reese presents a typical curve for load transfer versus depth in sand which indicates a large increase in skin friction until approximately 0 to 5 pile diameters above the tip and then a rapid decrease in load transfer due to the arching of the sand near the tip. Vesic [53], Mohan et al. [36], and Kerisel [25] noted this same phenomenon and have indicated that this low skin friction above pile points in sand can be attributed to arching or stress relief in a zone extending to as much as three pile diameters above pile point. In the present study, the

boundary conditions at the pier tip are not the same as those studied by Vesic and Reese. Many of the pier foundations in the southeastern United States have their tips in rock; this was the boundary condition modeled in this study. The results of the tests indicate a reverse phenomenon of that observed by Reese, Vesic and others. The skin friction is greatly increased at the boundary between the sand layers and the rock base. The resulting increase may be due to the confining effect of the rock boundary on the sand mass. The rigid boundary has the effect of increasing the effective horizontal pressure on the pier and results in an increase in the side friction at the tip of the pier. A portion of this increase in shear transfer may be due to the manner in which the model pier and simulated rock base were constructed. The model was constructed such that the pier tip was able to translate downward, however the simulated rock base was unyielding and the rock base remained stationary as the pier tip translated downward.

Load Transfer Curves

O'Neill and Reese [38] and Vijayvergiya et al. [55] have represented the shear transfer along the pier by load-transfer curves. These load-transfer curves are derived from a load distribution curve such as those in Figures 16 through 21. The procedure for obtaining one of the curves at a depth Y_z below the ground surface is illustrated in Figure 29. For a particular load distribution curve, corresponding to a

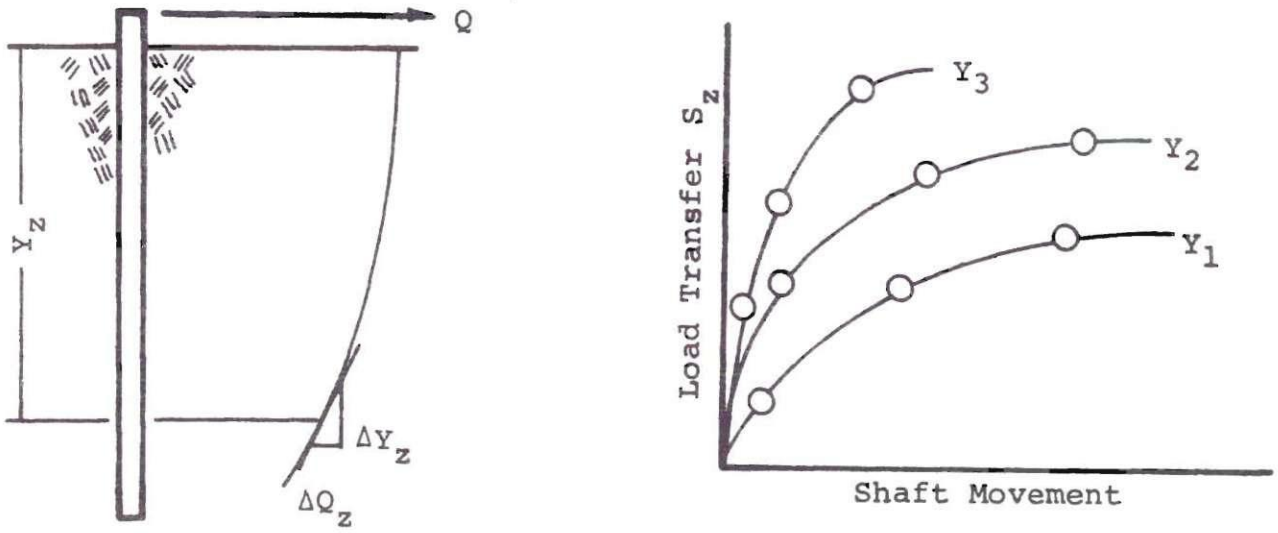

Figure 29. Determination of Load Transfer Curves After Reese [38]

particular load Q_z, the slope of the load distribution curve is obtained at point Y_z. In Figure 29 this slope is indicated as the quantity $\Delta Q_z/\Delta Y_z$. To obtain the load transfer S_z, the quantity is then divided by the shaft circumference at the point Y_z. Thus, the load transfer S_z normally would have the units pound per square foot.

The downward movement of the shaft corresponding to the computed load transfer is the sum of the downward movement of the pier tip and the elastic deflection of the pier at depth Y_z. A typical series of load-transfer curves for the eccentric loading tests is shown in Figure 30. A typical series of load-transfer curves for the concentric load test are shown in Figure 31. A comparison of the generated curves with those of other studies [38, 55, 39] indicates the same general shape. The load transfer increases rapidly with small movements and then gradually reaches a maximum value. The curves also indicate that in the majority of the tests, the pier movement was of such magnitude as to produce the ultimate load transfer between the sand and pier. As indicated, the maximum amount of measured movement was 0.062 inches for the test series prior to allowing the tip to move. Parker and Reese [39] have indicated in their study on small diameter, preplaced piles in sand, that maximum loads were reached at a pier movement of 0.07 inches. They also concluded from their load transfer curves for small diameter piles that the value of pile movement at which the maximum

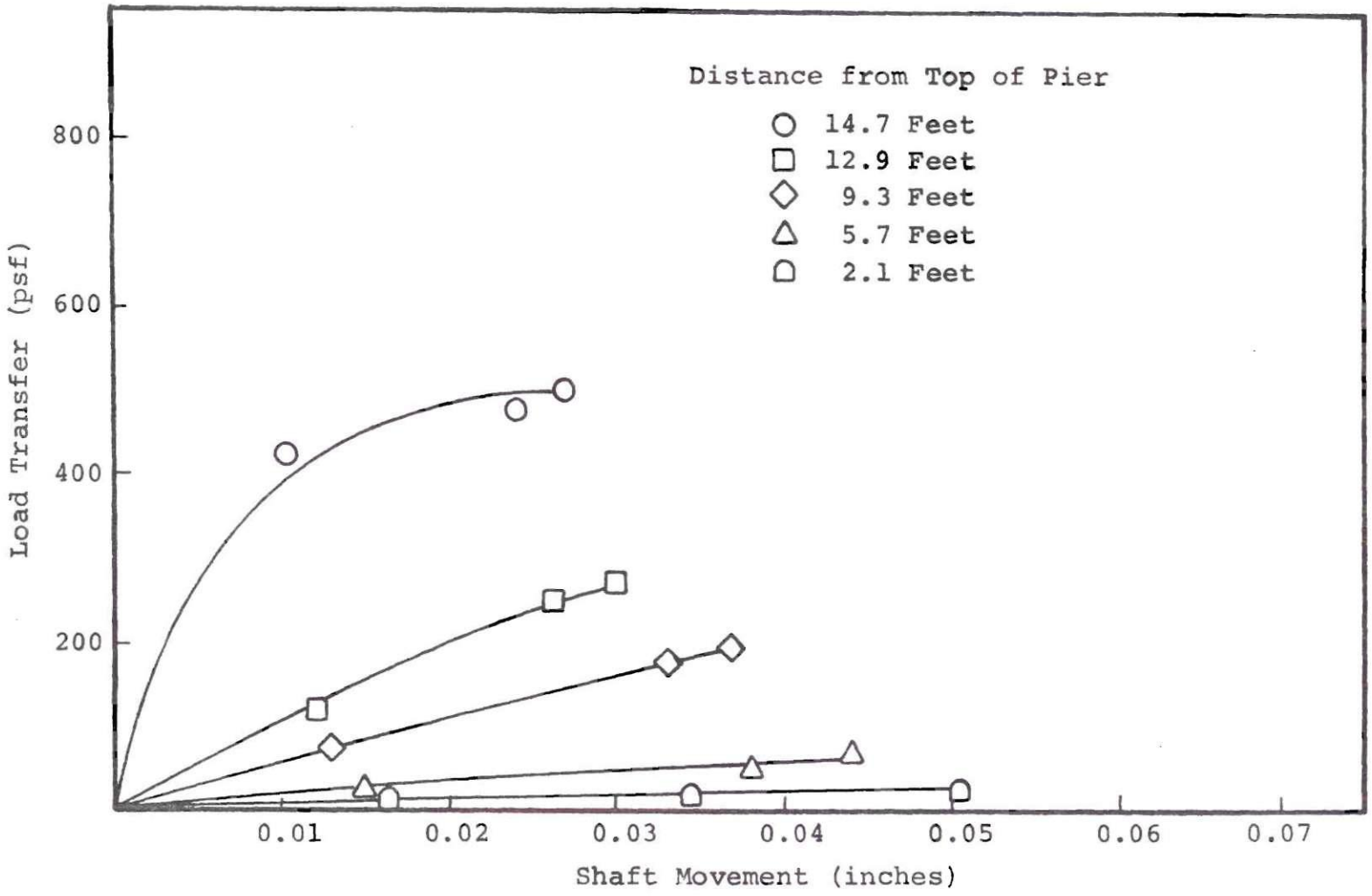

Figure 30. Load Transfer Curves, Test 3

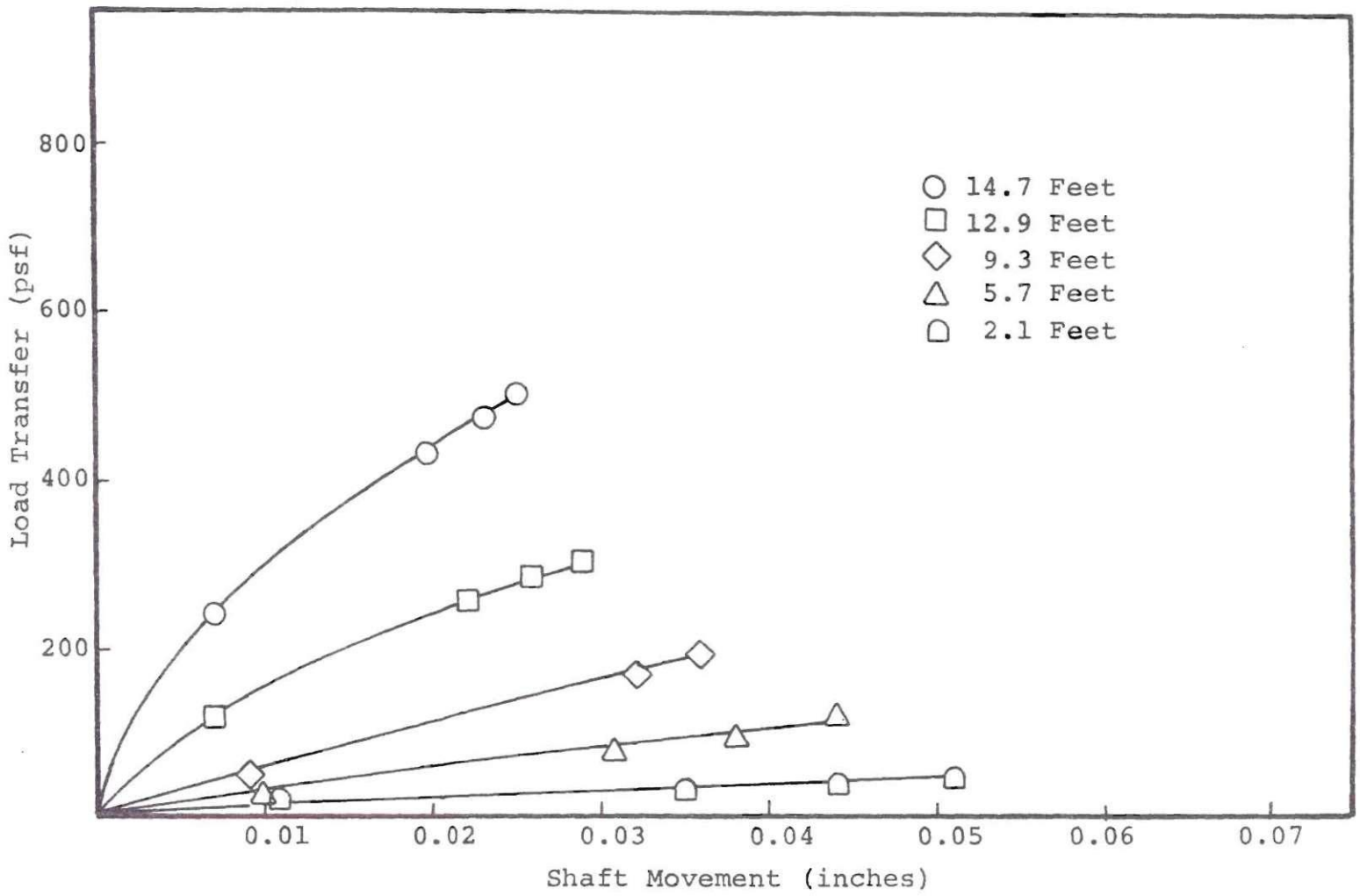

Figure 31. Load Transfer Curves, Test 1C

shear transfer is developed increases as the depth increases.

Comparison of Predicted and Measured Skin Friction

The comparison of the predicted skin friction and the measured values are shown in Table 14 and Figures 22 through 27. Table 14 indicates the percentage difference between the predicted load and the actual load at the maximum applied loads. The final test, in which the pier was loaded and the tip was allowed to move, gave an ultimate skin friction of approximately 10,000 pounds. The ultimate friction was therefore reached in all of the pier tests. The sensitivity of the predicted skin friction to surface roughness of the pier is shown in Table 14. The percentage difference from the measured load for the rough and smooth cases give upper and lower bounds to the predicted value. The pier tested in this study was closer to the case of a smooth concrete surface.

Table 15 shows the amount of load transferred in skin friction due to the elastic deflection of the pier for each test. It can be seen that a substantial portion of the skin friction is generated due just to the elastic deflection of the pier.

The predicted values from Table 14 using the smooth surface averaged 16 percent below the actual measured values for the tests. A study of Figures 22 through 27 will indicate the reason for the low values. These figures are plots of

Table 14. Sensitivity of Predicted Skin Friction to Surface Roughness

Test	Applied Load (lbs)	Measured Skin Friction (lbs)	Predicted Skin Friction			
			Rough Concrete (lbs)	Difference (%)	Smooth Concrete (lbs)	Difference (%)
1	93,630	10,880	11,553	+ 6.9	8,882	-20.0
2	96,030	10,730	11,570	+ 7.8	8,904	-16.0
3	93,660	10,660	11,459	+ 7.5	8,833	-17.1
4	108,770	10,870	11,576	+ 6.5	8,932	-17.8
5	96,730	10,130	11,644	+15.0	8,952	-11.6
1C	100,290	10,190	11,415	+12.0	8,840	-13.3

Table 15. Measured Skin Friction and Predicted Skin Friction

Test	Measured Skin Friction (lbs)	Predicted Skin Friction: Elastic Deflection Only (lbs)	Predicted Skin Friction: Measured Deflection (lbs)	Predicted Skin Friction: Best Estimate* Measured Deflection (lbs)	Difference Between Best Estimate and Measured (%)
1	10,880	6,482	8,882	10,742	-1.3
2	10,730	6,560	8,904	10,783	+0.5
3	10,660	6,490	8,833	10,344	-3.0
4	10,870	6,762	8,932	10,601	-2.5
5	10,130	6,598	8,952	10,620	+4.8
1C	10,190	6,616	8,840	10,364	+1.7

*The best estimate of skin friction was adjusted by doubling the confining pressure for the bottom segment--approximately one diameter.

the average skin friction transferred to the sand along the shaft. The predicted and measured agree until approximately one diameter above the pier tip. Below this point the effect of the rock boundary on the sand is shown by the large increase in shear transfer. The values for skin friction have been empirically adjusted in Table 15 in which the lateral confining stress in the last segment, approximately one diameter, has been doubled to account for the boundary effect. As indicated in Table 15, the predicted and measured loads agree quite well; the average percentage difference is 0.1 percent below the measured values. This purely empirical means of accounting for the boundary effect of the rock layer is suitable for these tests. The boundary effect would not be as effective in the actual installation of a drilled pier to a rock surface. The elastic deflection of the rock layer below the pier tip would tend to reduce the confining effect, however, the amount of rock deflection would be a function of a number of factors including: pier size, depth of rock, soil properties, and method of construction. The basis for application in the field will have to be substantiated from other tests.

Recommended Design Procedure

The step-by-step procedure to be followed for applying the proposed design method for computing the skin friction for a drilled pier is as follows:

(1) Obtain the properties of the soil/pier interface. This would be done by a series of direct shear tests at three or more normal pressures in the range of those that may be encountered in the field. Special care should be given to matching the anticipated characteristics of interface; these characteristics should include surface roughness and such other geotechnical factors as the presence of a free water level. A series of these tests may need to be performed at various densities and degrees of saturation to account for long term environmental changes if a rigorous application of this technique is desired. The size of the sample is not a critical factor as indicated by Lambe [27]. The values of Ψ, R_f, and the relationship of E_i to the normal pressure can be determined.

(2) Using the proposed pier dimensions, divide the pier into one to five foot segments depending on the length and diameter. Using the design load, compute the elastic deflection in each segment and estimate the tip deflection. A sample calculation is shown in Appendix H.

(3) Applying the computed deflections to the hyperbolic model, compute the side friction for each segment and sum for the total load carried in side friction. An empirical correction for the increased load transfer at the tip may be applied, however, further testing and verification of this correction is required.

The proposed design procedure provides a simple, rational means of predicting the side friction developed along a pier. The values provided will be on the conservative side for piers placed to rock as indicated from the measured stress distribution.

CHAPTER IX

CONCLUSIONS

Based upon the results of the load sensor developed and the large scale model study of a pier foundation in sand, the following conclusions can be drawn:

(1) The load cell concept developed for this study proved to be a reliable accurate means of determining the applied axial load and biaxial bending moments. The load cell can be constructed to approximate the structural stiffness properties of typical steel columns and can provide required reliability as a structural element.

(2) The side friction generated in this model study with a dense sand on a smooth pier was approximately ten percent of the applied load on the pier. The proposed prediction technique, accounting for increased confining stress at the base of the pier, predicted shear transfer in side friction to within $\pm$ 3 percent for most cases. Indications are that for rougher piers (i.e., drilled piers) not only in pure sands but also in other predominately frictional soils the shear transfer in side friction may be 20 to 30 percent.

(3) The proposed procedure for estimating the magnitude and distribution of friction in piers seems to be a viable rational technique. The procedure should be applied

with caution since more testing and verification is needed.

(4) The Carlson stress meters did not yield results that were reasonable or that compared well with other data. Future use of Carlson meters in reinforced concrete columns is not recommended.

(5) Results of these tests show that the best single instrumentation technique for determining load distribution in a pier is bonded strain gages on the vertical reinforcing cage. This technique is recommended for use in full scale piers because of its reliability and minimal interference with pier construction operation.

(6) The distribution of the load along the pier shaft indicated that the effect of a resistant layer (e.g., rock) at the pier tip caused the skin friction transfer to be increased for a distance of approximately one diameter above the pier tip. This is probably due to an increased confining stress in this zone and may be due in part to the method used for simulating a "rigid" rock base in the model tests.

The immediate practical significance of this study is to make a drilled pier foundation more economically competitive with other foundation systems. If, for example, the designer can depend on transferring thirty percent of the axial load in skin friction then possibly the size of the pier could be smaller or the need for underreaming may be eliminated. Either of these would result in a substantial cost savings.

CHAPTER X

RECOMMENDATIONS FOR FURTHER STUDY

The development of the model load cell and the large scale study of the model pier have led to numerous other areas to be investigated. Some of the problems needing attention are:

(1) Further testing of the model load cell to determine the degree of accuracy and reliability in the shear and torsional modes of loading.

(2) The construction of a full scale load cell and its inclusion in a multistory building to measure the actual field loads. The instrumentation of the foundation below the load cell would provide a comprehensive study of the applied foundation loads and their distribution through the foundation.

(3) A large scale model study of a pier in a medium with some cohesive properties more closely simulating the saprolitic material in the southeastern United States.

(4) A closer examination of the boundary effect of a rock layer at the pier tip by additional model studies and a finite element study.

(5) A full scale test of an instrumented pier in the field to verify the prediction of side friction using direct shear tests and hyperbolic model.

APPENDIX A

HYPERBOLIC REPRESENTATION OF INTERFACE BEHAVIOR

As shown by Duncan and Chang [16], the nonlinear stress-strain curve for both sand and clay may be approximated by hyperbolae with a high degree of accuracy. The following is the general form of the proposed equation:

$$\sigma = \frac{\varepsilon}{a+b\varepsilon} \tag{14}$$

where a and b are constants determined experimentally. The above general relationship has been applied to the shear force-deflection curves generated from the direct shear tests between the sand and concrete in this study. The basic form of the equation is:

$$\text{Shear force} = \frac{\delta}{a+b\delta} \tag{15}$$

In which δ = the measured deflection and a and b are constants with physical significance. As can be seen from Figure 32, a equals the reciprocal of the initial tangent modulus, and b equals the reciprocal of the asymptotic value of the shear force which the shear force-deflection curve approaches a zero slope.

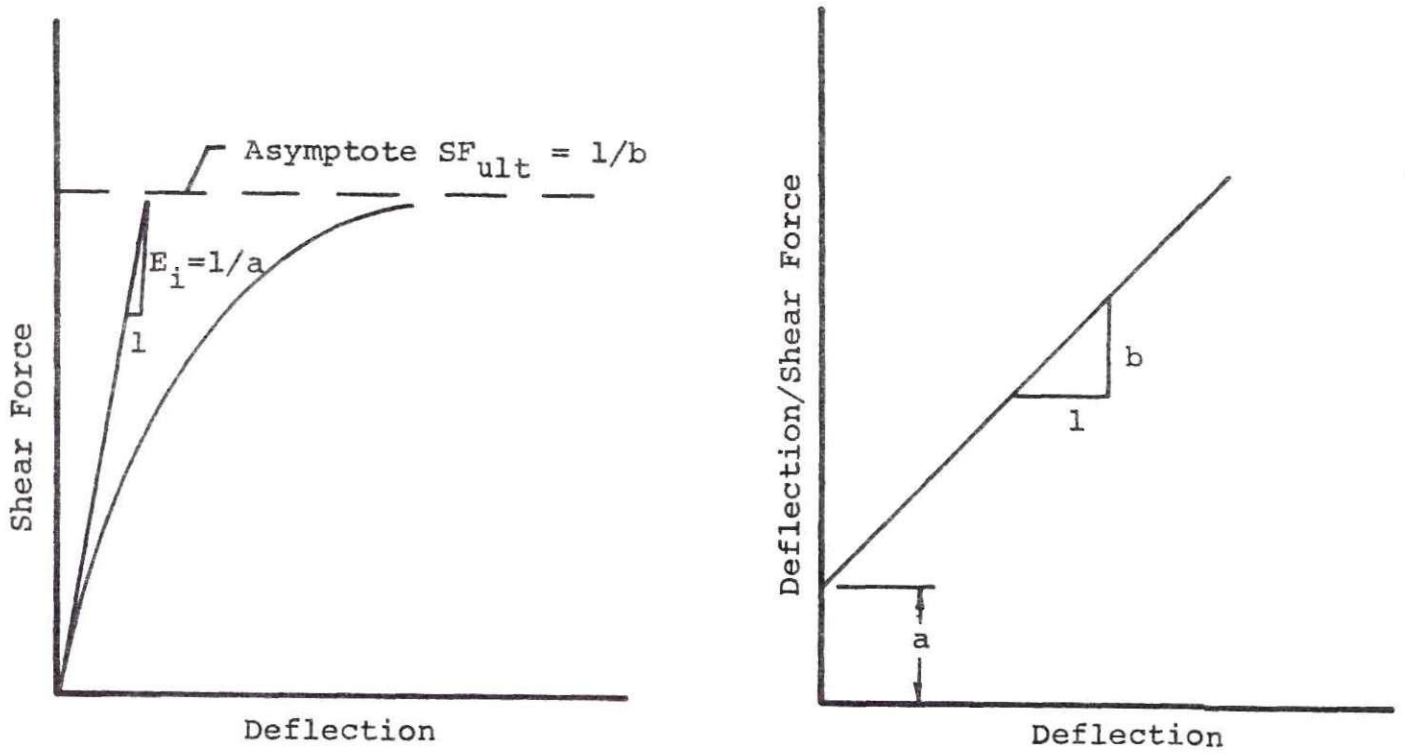

Figure 32. Hyperbolic Force Deflection Curve and Transformed Coordinates

The values of a and b can be readily determined if the shear force-deflection data are plotted in the transformed coordinates as shown in Figures 12, 13, and 14. A regression analysis, using the method of least squares was used to find the best straight line fit for each of the shear force-deflection curves.

After finding the best fit, it is usually found that the asymptotic value of the shearing force is slightly larger than that of the measured value. The asymptotic value may be related to the ultimate shear force by means of a factor R_f as shown by

$$\text{Shear force}_f = R_f(\text{shear force})_{ult} \tag{16}$$

Where shear force_f = shearing force measured at failure and shear force_{ult} = asymptotic value of the shear force. The value of R_f has been found to vary between 0.75 and 1.00 for a number of different soils [16] and to be essentially independent of confining pressure.

The original equation may now be rewritten in the form:

$$\text{Shear force} = \frac{\delta}{[\frac{1}{E_i} + \frac{\delta R_f}{\sigma_n \, \text{Tan}\Psi}]} \tag{17}$$

In which the physical values for a and b have been substituted.

In which:

$$\text{Shear force}_f = \sigma_n \, \text{Tan}\Psi \tag{18}$$

σ_n = normal stress on the failure shear

Ψ = angle of friction between the sand and the concrete pier.

The value of the tangent modulus has been found [16] to vary with the confining pressure employed. Janbu [23] has shown by experimental studies that the relationship between the initial tangent modulus and the confining pressure may be expressed as:

$$E_i = Kp_a(\sigma 3/p_a)^n \tag{19}$$

E_i = Initial tangent modulus

$\sigma 3$ = Minor principal stress

p_a = Atmospheric pressure

K = Modulus number

n = Exponent determining the rate of variation of Ei with $\sigma 3$.

The above relationship is linear when plotted on log-log coordinates. The values obtained from this study were plotted in log-log coordinates as shown in Figure 15

and a linear relationship was found for the relationship of Ei to normal pressure for relative densities at 65 percent and 75 percent.

Using the above relationship for E_i and knowing deformation, the nonlinear relationship of shear force and deformation is completely defined. A summary of the results is shown in Table 5. The application of the hyperbolic relationship to the prediction of the pier performance is discussed in Chapter VIII.

APPENDIX B

DEVELOPMENT OF MODEL LOAD CELL

Dimensional Analysis

A dimensional analysis will determine what parameters must be scaled to insure the validity of the model tests. If all of the requirements from the dimensional analysis are fulfilled, the model will reliably predict the prototype performance. In many cases, all the conditions cannot be satisfied and only a selected few of the model laws are fulfilled.

The general theory of dimensional analysis is detailed by Langhaar [28], Murphy [37], and Bridgeman [8]. The general procedure is:

(a) Determine the variables which will influence the model behavior.

(b) Arrange the groups of variables into dimensionless products.

(c) Consider the resulting dimensionless products and decide which prototype conditions will be modeled.

This procedure was used for an analysis of the static loading and dynamic loading of the cell.

The first case considered will be the static loading,

which is quite simple. The variables considered to be influential in the behavior of the model are: axial deflection, applied force, shear deflection, modulus of elasticity, dimensions of sensors, moment of inertia, and stress.

Listing the applicable quantities:

Quantity	Symbol	Dimensional Units
Deflection	Δ	L
Length	ℓ	L
Modulus of Elasticity	E	F/L^2
Moment of Inertia	I	L^4
Stress	σ	F/L^2
Area	A	L^2

Where F = force, L = length, and T = time and are the basic system of units.

The static behavior of the model is some function of the quantities listed above.

Dimensionless products can be formed as follows:

(a) Any dimensionless product can be written as:

$$\Pi_i = \Delta^{k_1} \ell^{k_2} E^{k_3} I^{k_4} \sigma^{k_5} A^{k_6} \tag{20}$$

The number of dimensionless products may be infinite, but only a specified number of products are independent.

(b) Each variable can be written in terms of its basic dimension as follows:

$$\sigma^{k_5} = (F/L^2)^{k_5} = \frac{F^{k_5}}{L^{2k_5}} = \frac{F^{a_5 k_5}}{L^{b_5 k_5}} \tag{21}$$

where ai, bi, and ci are constants.

(c) The criteria for a product to be dimensionless is:

$$\begin{bmatrix} a_1 & a_2 & \cdots & a_6 \\ b_1 & b_2 & \cdots & b_6 \\ c_1 & c_2 & \cdots & c_6 \end{bmatrix} \begin{bmatrix} k_1 \\ k_2 \\ \cdot \\ \cdot \\ k_6 \end{bmatrix} = 0 \tag{22}$$

The variables may be arranged in a more convenient form:

$$\begin{array}{c} \\ F \\ L \\ T \end{array} \begin{array}{c} \begin{array}{cccccc} k_1 & k_2 & k_3 & k_4 & k_5 & k_6 \\ \Delta & \ell & E & I & \sigma & A \end{array} \\ \begin{bmatrix} 0 & 0 & 1 & 0 & 1 & 0 \\ 1 & 1 & -2 & 4 & -2 & 2 \\ 0 & 0 & 0 & 0 & 0 & 0 \end{bmatrix} \end{array} = 0 \tag{23}$$

The rank of the above matrix is two, since at least one second-order determinant is not equal to zero. Therefore, there will be (n - 2) independent dimensionless products where n = number of variables (six in this case).

To arrive at one set of independent dimensionless

products, operate on matrix $\begin{bmatrix} ai \\ bi \\ ci \end{bmatrix}$

To obtain unity in the diagonal of the last three rows:

$$k_3 + k_5 = 0 \tag{24}$$

$$k_1 + k_2 - 2k_3 + 4k_4 - 2k_5 + 2k_6 = 0 \tag{25}$$

$$k_3 = -k_5;\ k_2 = -k_1 - 4k_4 - 2k_6 \tag{26}$$

		ℓ	E	Δ	I	σ	A
		k_2	k_3	k_1	k_4	k_5	k_6
Π_1	k_1	-1	0	1	0	0	0
Π_2	k_4	-4	0	0	1	0	0
Π_3	k_5	0	-1	0	0	1	0
Π_4	k_6	-2	0	0	0	0	1

(27)

Thus, the four independent dimensionless products:

$$\begin{aligned} \Pi_1 &= \Delta/\ell \\ \Pi_2 &= I/\ell^4 \\ \Pi_3 &= \sigma/E \\ \Pi_4 &= A/\ell^2 \end{aligned} \tag{28}$$

If one defines the model dimension as $\bar{\ell}$ and the prototype as ℓ applying to the dimensionless products:

$$\Pi_1 = \bar{\Delta}/\bar{\ell} = \Delta/\ell\,;\ \bar{\Delta} = \Delta\bar{\ell}/\ell\,;\ \bar{\Delta} = \lambda\Delta\ (\lambda=\bar{\ell}/\ell)$$

$$\Pi_2 = I/\ell^4;\ \bar{I}/I = (\bar{\ell}/\ell)^4;\ \bar{I} = I\lambda^4$$

$$\Pi_3 = \sigma/E;\ \bar{E}/E = \bar{\sigma}/\sigma;\ \bar{F} = \lambda^2 F \qquad (29)$$

$$\Pi_4 = A/\ell^2;\ \bar{A}/A = (\bar{\ell}/\ell)^2;\ \bar{A} = \lambda^2 A$$

The scale chosen for the model was a one-quarter scale (λ=1/4) giving:

$$(1)\quad \bar{\Delta} = \Delta/4$$

$$(2)\quad \bar{I} = I/256$$

$$(3)\quad \bar{F} = F/16 \qquad (30)$$

$$(4)\quad \bar{A} = A/16$$

$$(5)\quad \bar{\ell} = L/4$$

Thus, in the static case all the requirements for the dimensionless analysis can be met, and a geometric reduction of the prototype is possible.

The above analysis assumed at the beginning that the six variables chosen were the most important in affecting the model behavior.

Additionally, a separate analysis of the effect of Poisson's ratio indicates that the additional constraint that $\nu = \bar{\nu}$ must be met for all the stresses to be proportional.

The dynamic loading case is considerably more

complicated, since time effects are considered and body forces must be included, putting additional constraints on the model parameters.

Considering the dynamic loading case for the model, the following variables must be included in the dynamic analysis: (1) time, (2) gravity, and (3) density. Proceeding with the analysis as before, the following independent dimensionless products are derived for the dynamic loading case:

$$\Pi_1 = \Delta/\ell \; ; \; \bar{\Delta} = \lambda\Delta \quad (\lambda = \bar{\ell}/\ell)$$

$$\Pi_2 = I/\ell^4; \; \bar{I} = \lambda^4 I$$

$$\Pi_3 = \sigma/E; \; \bar{\sigma} = \sigma \text{ and } \bar{E} = E$$

$$\Pi_4 = A/\ell^2; \; \bar{A} = \lambda^2 A \tag{31}$$

$$\Pi_5 = gt^2/\ell; \; \lambda gt^2 = gt^2; \text{ if } g = \bar{g}$$

$$(\lambda = \bar{t}^2/t^2; \; \bar{t} = \sqrt{\lambda}t)$$

$$\Pi_6 = \gamma\ell/E = \bar{\gamma}\,\bar{\ell}/\bar{E}; \text{ this implies } \bar{\ell} = \ell,$$

$$\text{if } \bar{E} = E, \text{ then } \bar{\gamma} = \gamma.$$

Thus, for the dynamic loading case, the requirements of the dimensional analysis cannot be completely satisfied, unless a model material of a different unit weight is used.

For this particular study, the static case of loading

was considered of primary interest and the model cell was designed and constructed based on the scale factors derived from the static loading case.

Construction of Model Load Cell

Plate Construction

The construction of the one-quarter scale model load cell was done in the machine shop at Georgia Tech. Figures 2 and 3 give the details and dimension of the model cell including gage location.

The top and bottom plates used for the model are SAE 1040 steel with a yield strength of approximately 60,000 psi. The Rockwell hardness of the plates was 101-E scale and 87-K scale. The plates were both surface ground on both sides with a Blanchard vertical spindle rotary surface grinder.

Sensor Construction

The sensor elements are made of "etd" 150 alloy steel. This steel is made by the La Salle Steel Company of Chicago, Illinois. It is an alloy steel with the same chemical content as an SAE 4100 series steel and is made by an "Elevated Temperature Drawing" process. The properties were developed for the use of this steel in gear and pinion sets. The steel has the following properties [64]:

Table 16. Properties of "etd" 150 Alloy Steel

Chemistry	Amount (%)
Carbon	0.40% min
Manganese	0.75-1.00
Phosphorus	0.35 max
Sulphur	0.04 max
Silicon	0.20-0.35
Chromium	0.80-1.10
Molybdenum	0.15-0.25
Tellurium	0.04-0.05
Mechanical Properties	
Tensile Strength	150,000 psi min
Yield Strength (0.2% offset)	130,000 psi min
Rockwell C Hardness	32 min
Modulus of Elasticity	31.0×10^6 psi

The Rockwell Hardness of the specimen used for the load cell tested in the laboratory was 37 on the C scale.

The modulus of elasticity was determined in the laboratory by use of strain gages and is discussed in the testing section.

The largest diameter round made of "etd" 150 is four inches. The prototype model will be made of "Maxell 3-1/2" steel made by Crucible Steel Co. This is a hot rolled, heat treated, stress relieved steel. It is made in eight inch

diameters and has a minimum tensile yield strength of 103,000 psi. An alternate choice is SAE 4140 hot rolled, annealed alloy steel available in eight-inch diameters with a yield strength of 105,000 psi. The design of the model was based on the use of the lower strength steel but for protection against over stressing during testing, the higher strength material was chosen. The mechanical properties of the materials are similar so that the model and prototype relation will not be influenced.

The load sensors were machined to the proper dimensions in the shop and all four sensors were cut to approximately the same height. Each sensor was placed in a K. O. Lee surface grinder in a vertical position, with the axis of the central portion of the sensor aligned with the vertical. One end of the sensor was then surface ground to a polished smooth surface. After all four sensors had been ground on one end, they were all placed on the magnetic bed of the surface grinder with the ground end on the bed. The other end of the sensors were thus ground simultaneously, producing equal height of all four sensors and a smooth ground surface.

After the first series of tests was conducted, it was discovered that the ends of the sensors were not perpendicular to the axis of the sensor (see discussion in testing section) and regrinding was required. During the first grinding, an aluminum cylinder was used as a spacer to hold the sensors in place and was the cause of the misalignment. The second time,

parallel bars were used as spacers and one end of each sensor was ground perpendicular to the vertical axis. All four sensors were then reground equal height and parallel surfaces. To check the accuracy of the grinding, the sensors were placed in a surface comparator and the variation in height between ends was checked. The maximum variation across the diameter for the sensors was 0.0006 inch.

Instrumentation

Strain Gages

The strain gages used for the model are micro-measurement type EA-06-250BG-120. These gages have 120 ohm resistance, a gage factor of 2.11. They are constantan alloy self temperature compensating and are encapsulated with a flexible polymide coating. The proper alignment on the load sensors was found by using four parallel bars held snugly against the sensors with rubber bands. The sensors were then lightly scored by sliding the parallel bars up and down the sensors. The scored lines were used to align the gages vertically and in the right attitude to provide the placement of gages at 90° intervals on the sensors and aligned properly with the other sensors.

The surface was cleaned and slightly roughened with emery polishing paper and then cleaned with a water based acidic surface cleaner and alkaline neutralizer. The gages were cemented with Eastman 910 cement and allowed to dry for

several hours. The Eastman 910 epoxy was used because of the rapid curing period which facilitated the exact placement of the strain gages. This epoxy is primarily for short term use and would not be suitable for a permanent installation. The leads were then soldered to the gages and wired for use. The details of wiring and the readout is discussed in the testing section.

The vertical distance between the strain gages was measured with a height gage to determine the distance to use in finding the applied shear loads.

The thickness of the gages was determined to be 0.025 inch.

Experimental Stress Analysis

In order to determine the extent of stress disturbance in the load sensors from the point of intersection of the shoulder and the main body of the sensor, a photoelastic coating technique was employed.

The photoelastic technique provides a visible picture of the stress distribution on any type of surface configuration. The method employs a polarized light source, and a plastic material which undergoes a change of index of refraction when stressed. Strain measurements of both magnitude and direction can be made by reflecting polarized light from the surface of a stressed object which has had a photoelastic coating applied to it. The pattern which is

visible by observing the object through an analyzer can be analyzed to determine the direction of principal strains or the magnitude of the strain.

In the case of the load sensor, the main consideration was the location at which the strain became uniform. This qualitative type of measurement can be determined by observing the pattern of color fringes and the change from one point on the sample to another point. If color fringes appear as tightly grouped loops of color patterns going from yellow to red to green, this indicates a rapid increase in strain (i.e. stress concentration), or green-red-yellow would indicate a rapid decrease in strain at one point. However, a single uniform color covering a large area of a test part indicates a uniform strain, i.e., strain is neither increasing nor decreasing from one point to another.

Reference to Figure 33 will illustrate the above discussion. At the edge of the reduced section of the sample there are several rapid changes of color indicating a rapid change of strain, then approximately 0.3 inch below the edge the color becomes uniform for the length of the sample. The uniform red color in the center of the load sensor shows quite clearly the area in which uniform strain occurs with no concentration due the configuration change. The illustrated specimen is under 60,000 pounds of axial compressive load.

Application of Photoelastic Material

The material can be applied with solid flat sheets,

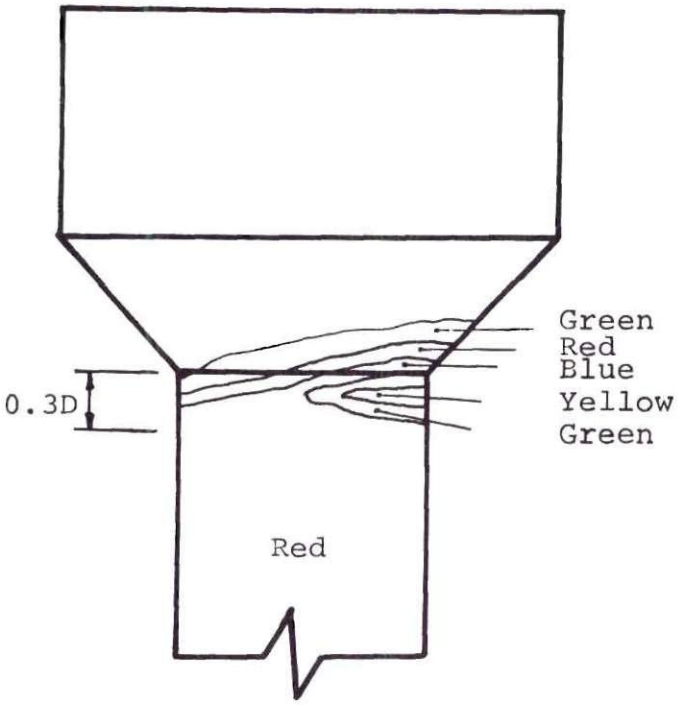

Sketch of Top of Sensor

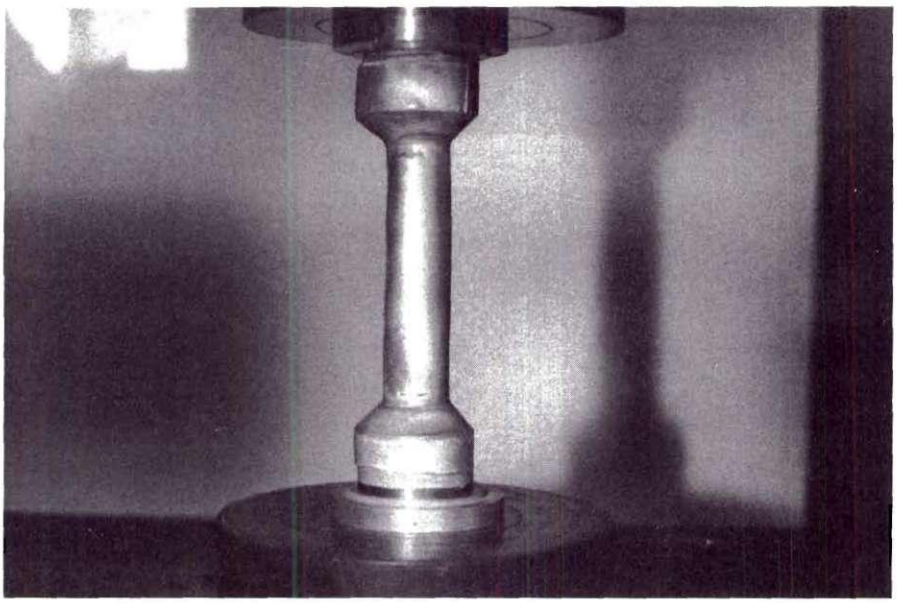

Figure 33. Photoelastic Fringes for Load Sensor
(P = 60,000 lbs)

liquids for contour forming or liquids for spraying. The spray type of application seemed to be the most convenient and easiest type of application. However, this method proved to be most unsatisfactory.

Several cylindrical test specimens were selected to test the spray coating technique. The first coat consisted of a reflective coating to reflect the polarized light back to the analyzer. The photoelastic material was then sprayed on the sample in thin layers allowing each layer to cure properly. Twenty-five coats of the photoelastic spray were applied and then the specimens were allowed to cure properly at temperatures recommended by the manufacturer. Upon completion, the samples were subjected to various types of loading and viewed through the photoelastic analyzer with no success. No fringes were observable at various loading and various types of light settings on the analyzer. A discussion with the manufacturer's representative indicated that the photoelastic coating is dissolved in a solvent for aerosol spray can application; and if the solvent is not completely driven off during the curing process, the coating will not possess photoelastic properties. Thus, the solvents from the coatings were not completely driven off even though the manufacturer's directions were followed exactly.

The liquid for contour forming was applied with success. The method is simple to apply and within forty-eight (48) hours a suitable coating can be applied to a sample for

analyzation.

The thickness of the coating is based on the desired sensitivity, the amount of strain applied, and type of application (dynamic loading, static loading, temperature environment, color or black and white analyzation). In the case of the load sensor, a thickness of 0.100 inches was chosen with a high sensitivity, "K" factor of approximately 0.12, and a modulus of elasticity of approximately 400,000 psi. This coating provided suitable results at the higher levels of stress applied to the sample. After application of the coating, the load sensor was placed in a universal testing machine. The sample was loaded in 10,000 pound increments and observed through the photoelastic analyzer. The fringes appeared well defined at a load of 30,000 pounds, and the distance to the area of uniform stress was approximately 0.3 inch for the entire range of loads (60,000 pounds maximum).

The location of the strain gages was determined from observation of the photographs from the tests. The top of the gages was located a minimum of 0.5 inch from the shoulder of the sensor to insure that there would be no effect from the stress concentration produced by the change in shape of the sensor.

The photoelastic method provided a rapid and most suitable answer to the question of stress distribution in the load sensor, which could have proved to be a time

consuming analytical problem. This method is recommended for application in similar type situations if the liquid contour application is used.

Testing of Model Load Cell

Prior to loading the entire cell, a single sensor was loaded to check the magnitude of strain differences between individual gages which could be expected under axial loading conditions. The sensor was carefully centered in a calibrated testing machine and loaded up to 40,000 pounds with the strain in microinches/inch noted for each gage at every 10,000 pounds. The differences between each gage were small (less than five percent) and indicated that the sensitivity to bending would be excellent.

The modulus of elasticity of the sensors was not indicated in the manufacturer's literature for the "etd" 150 steel. A single sensor was loaded up to 25,000 pounds on a Riehle testing machine in the structures laboratory several times. An average value of strain was found and the modulus of elasticity was found to be 31.0×10^6 psi.

The strain readings in all the tests were taken using a BLH strain indicator using the two-arm Wheatstone bridge. Each strain gage was monitored individually with a temperature compensating gage in series through two 20-channel switching boxes. The individual channels on the switching boxes were preset to a common initial strain and each channel was

monitored during loading increments. Each channel was rechecked prior to testing and the gage factor on the strain box was checked.

A 400,000 pound capacity mechanical feed Riehle testing machine was used throughout all the test series. The accuracy of the load scale was tested with a BLH Type C-1 400,000 capacity load cell and found to be within one percent up to a load of 250,000 pounds.

The testing program for the load cell was conducted in three series: (1) series one consisted of 28 tests with various loading blocks, (2) series two consisted of 31 tests after regrinding the sensors, and (3) series three consisted of 10 tests with two top plates and spacers. The cell was tested with axial and eccentric loads.

The first series of tests consisted of 28 tests loading the single top plate with no spacers through various size loading blocks. The initial tests indicated a large amount of bending in the sensors due to the deflection of the top plate under load. Additional plates were bolted to the top to reduce the bending, but the additional thickness did not reduce the bending significantly. The cell was dismantled and the ends of each sensor were measured in a surface comparator to check if the sensor ends were perpendicular to the vertical axis. The ends were not perpendicular, and the ends were reground carefully and measured to ensure that they were perpendicular to the vertical axis.

The second series consisted of 31 tests with several techniques employed to reduce the bending of the plate. The initial tests again indicated bending of the top plate, which caused large differences of strain on the sensors.

Brass shims (.005-inch thickness) were placed between the load sensor and top plate on the interior portion of the cell to counteract the bending of the plate. This did not eliminate the bending appreciably.

The addition of a second plate with four thin stainless steel spacers centered over each sensor was tested in the third series and proved to be successful in eliminating the bending of the bottom plate and the resulting bending of the sensors. The top plate deflects, but transmits the load through the steel spacers to the lower plate and sensors with very little bending. A series of ten tests were conducted with axial and eccentric loading, which were the final tests.

The results of the third test series indicate that the model load cell can accurately measure the axial component of load within two percent of the actual load.

The results from the eccentric loading tests are outlined in Figure 34. The vertical loads were computed based on elastic theory using the indicated strain from the eight strain gages on each sensor. The total load in each sensor was summed for the total axial load.

The biaxial bending moment was determined by summing moments about the major and minor axes of the load cell as

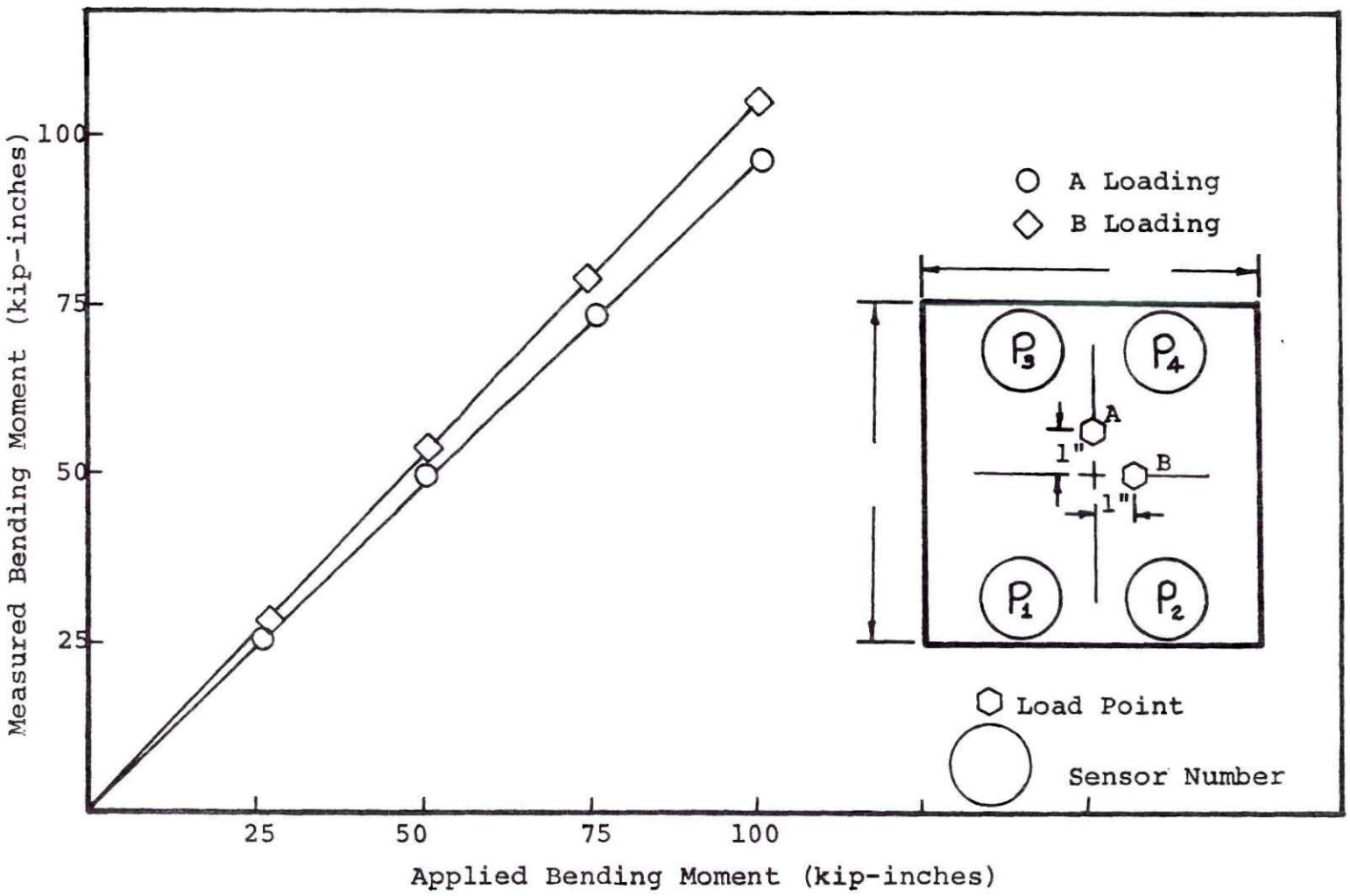

Figure 34. Calibration Curve for Model Load Cell (Eccentric Loading)

shown in Figure 34.

As noted:

$$\text{Vertical Load } P = P_1 + P_2 + P_3 + P_4 \tag{32}$$

P_1, P_2, P_3, P_4 - sensor element loads (P is positive for compressive loads)

Biaxial Bending Moment:

$$P_{ex} = (P_2 - P_4)\ y/2 + (P_1 - P_3)\ y/2 \tag{33}$$

$$P_{ey} = (P_1 - P_3)\ x/2 + (P_2 - P_4)\ x/2 \tag{34}$$

(· positive moment)

The calibration curves in Figure 34 indicate that the biaxial bending moment can be accurately measured within seven percent of various loading configurations.

The horizontal load component can be determined by plotting the moment gradient from the top and bottom level of gages. The moment arm and applied horizontal forces can be calculated from the resulting strains. The torsional loads can be determined from summing moments and horizontal forces for each sensor. The investigator did not have sufficient time to do a complete testing program for the horizontal and torsional load sensing capability of the cell. It is recommended that further testing be applied to the cell to determine the degree of accuracy and reliability in the horizontal and torsional modes of loading.

APPENDIX C

CONSTRUCTION OF MODEL PIER

Pier Construction

The reinforcing steel consisted of six Number six 15-feet long vertical bars. The bars were equally spaced around a 10-inch diameter circle of hoop ties spaced 16 inches apart along the length of the bars. Number three bars were used as hoop ties. The hoops were bent and the bars were tied prior to the placing of the strain gages. After application of the strain gages, the entire reinforcing gage was lowered into the form and centered. Wires were attached to the bars and tied outside the form to hold the cage in correct position. One longitudinal reinforcing bar was untied to facilitate placing of the Carlson meter. This bar was retied into position as the concrete was poured. The form for the pier was a cylindrical paraffin coated cardboard tube with the trade name, "Sleek Tube." The form was placed in the test pit and the bottom was fitted over the bottom steel plate and held in position by a metal hoop which kept concrete from leaking out of the bottom of the form. The form was vertically aligned and supported at two points by wood braces to insure that it did not tip over during the pouring of the concrete. Three 12-inch by 12-inch holes were cut in the form

at the levels where the Carlson meters were to be placed. The "Sleek Tube" form was only 14 feet long and an additional 1.67 feet was added at the top so that the total pier length was 15.67 feet. The concrete pours were from pier tip to 2.58 feet, 2.58 feet to 7.5 feet, 7.5 feet to 12.33 feet and from 12.33 inches to 15.67 feet. Three to four six-inch diameter by twelve-inch cylindrical specimens were taken from each batch for testing. The concrete was mixed in a Worthington Model 6-S electric mixer for approximately ten minutes prior to placing. A slump test was performed on each batch prior to placement. The concrete was placed through the 12-inch holes cut in the form at each level. The first three pours were made by placing the concrete in a steel bucket with a bottom opening. The bucket was hoisted and centered by the five-ton service crane into position above a plywood chute placed such that the concrete flowed into the form openings. The maximum height of fall was approximately four feet, which would cause a minimum of segregation. The concrete was vibrated by an electric immersible vibrator. The operation was repeated for all four pours with the final pour being made directly into the top of the pier. The pier was moist cured for two weeks prior to stripping the form and air cured for another two weeks before any tests were performed.

After the form was stripped and the lower braces removed, the sand fill around the pier was placed. Initially, the sand was placed in the cracks and openings between the

concrete blocks placed in the bottom of the pit to insure a steady and solid base. Two steel plates 0.25-inch thick were placed around the pier prior to placing the sand.

Sand Placement

The sand used was a Chattahoochee River sand [52]. The properties and grain sizes are given in Appendix D. The sand was placed by the "raining" method using an eight-foot diameter perforated pan held a minimum of 30 inches above the surface [52]. The pan bottom consisted of peg board with 0.25-inch holes spaced one inch on center. A 16.5-inch hole was cut in the center of the pan for the pier and the pan was lowered to the bottom of the pit. The sand was placed by sprinkling the sand evenly over the perforated pan, the distribution system can be seen in Figure 4. A three-inch sheet metal collar was placed around the 16.5-inch hold in the pan to keep the sand from falling between the pier and the pan. The sand was placed continuously in layers from two to three feet. The operation was stopped, the pan removed and density measurements were taken in various positions across the pit. A presentation of the density measurements is shown in Figure 6. The density measurements were made with a thin sheet metal cylinder. The cylinder was five inches in diameter and eight inches in length. The middle 3.50 inches were used to measure the density. The metal cylinder was gradually forced into the soil until the top surface was

even with the sand surface. The sand inside the tube was removed until the top line of the measured section was reached. The surface was leveled and the sand excavated until the bottom reference line was reached. The surface was again leveled and the sand removed from the 3.5-inch section was weighed and the density computed. The volume of the tube was measured and calculated and checked by the volume of water required to fill the measured volume.

After completion of the sand filling, the loading frame was swung into position and leveled prior to testing. The bottom of the loading frame was found to be bent, thus the base of the 400,000 pound Simplex ram did not fit evenly across the frame. A layer of quick setting mortar, approximately one inch thick was placed between the ram and the loading frame in order to spread the load evenly from the loading frame to the ram. After several tests, the entire loading frame was releveled and the mortar pad was removed and replaced by a series of steel and brass spacers. The ram and spacers were moved by trial and error until the model load cell indicated no eccentric loading from the ram.

APPENDIX D

PROPERTIES OF SAND USED IN PIER TESTS

The sand used for the model pier test was a medium sand from the Chattahoochee River near Atlanta, Georgia. The sand was sieved through a window screen (equivalent to 1.4 mm openings). The sand was composed primarily of subangular quartz particles with mica particles. A grain size curve of the sand is shown in Figure 35. The maximum and minimum densities of this sand were found using standard procedures. These values agreed with those found by Vesic [52] and are listed, along with porosity and void ratio, in Table 17.

The specific gravity was determined using ASTM procedure D854-52 and is given in Table 17.

The average water content was 0.11 percent determined from moisture contents at several levels in the pit.

Shear strength properties were determined by standard triaxial tests [52]. The values of ϕ and c are given for average relative densities of 65 and 75 percent in Table 17.

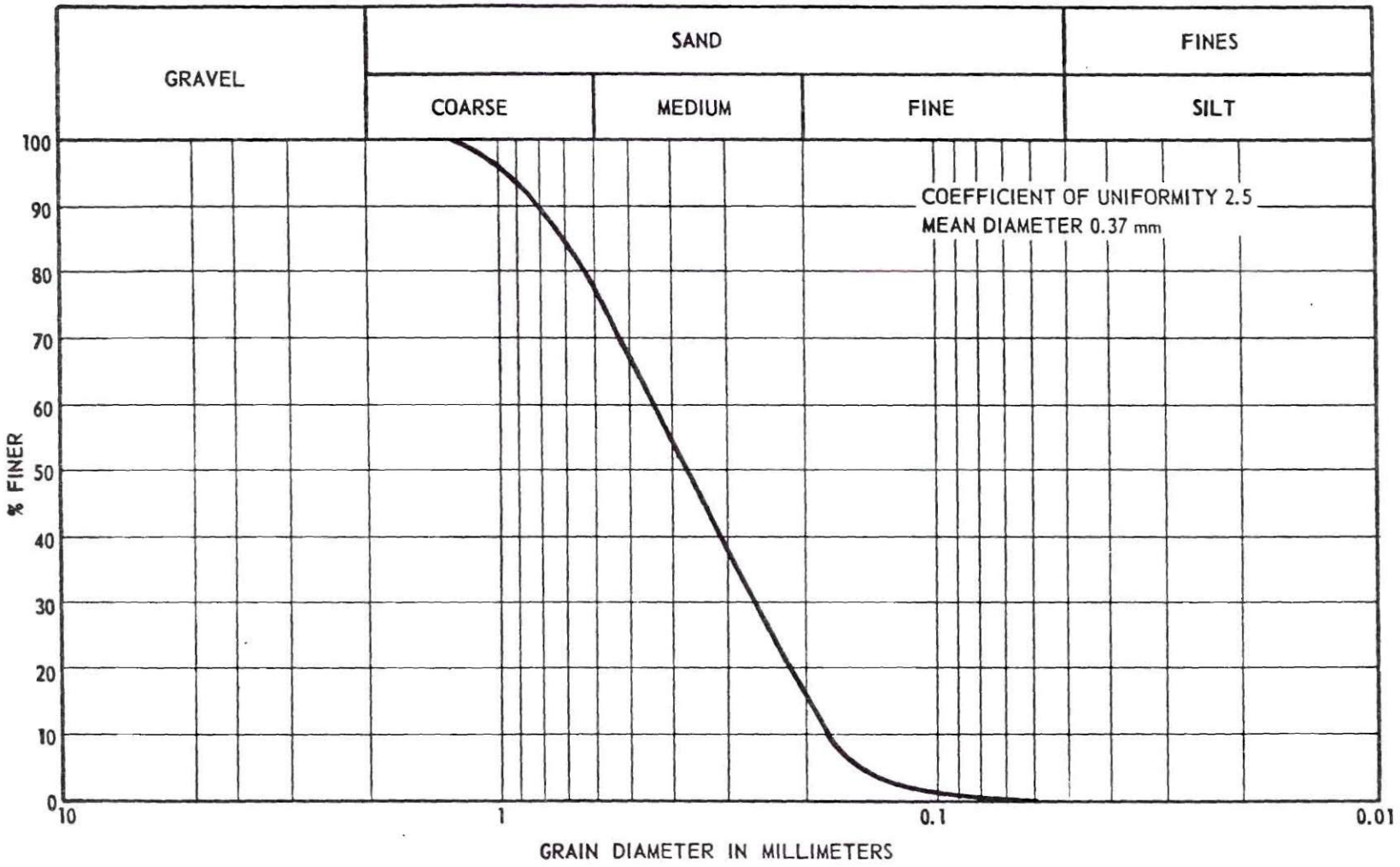

Figure 35. Grain Size Curve for Chattahoochee River Sand (After Vesic [52])

Table 17. Properties of Chattahoochee River Sand

Density	Dry Unit Weight (pcf)	Void Ratio	Porosity
		e	n
Maximum	79.0	1.10	52.4%
Minimum	102.5	0.615	38.1
Specific gravity--Average (three tests)--2.63			
		ϕ	c
Relative density	65%	38°12'	0
Relative density	75%	42°54'	0
Smooth Concrete:			
Relative density	65%	Ψ = 30°25'	
Rough Concrete:			
Relative density:	65%	Ψ = 38°12'	

Ψ equals coefficient of friction between sand and concrete.

APPENDIX E

INSTRUMENTATION IN PIER

Each instrumentation system will be described in the subsections of this Appendix.

Electric Strain Gages on the Reinforcing Steel

The electric strain gages placed on the reinforcing steel were SR-4 universal type 40. These gages are paper backed, Constantan wire gages, with a 0.4-inch gage length, 120 ohm resistance, and a gage factor of 2.08. The gages were placed at four levels along the pier shaft--1.67 feet, 6.17 feet, 10.17 feet and 14.67 feet below the top.

Six strain gages were placed at each level, on alternate bars, with two gages on each bar, one on the inside and one on the outside. Each gage was wired separately to the switching box so that any bending moment in a particular bar could be sensed. Also, if one gage was defective, the strain on the bar would not be completely undetected. The bars were spaced at 120 degrees around the pier circumference.

The gages were bonded to the reinforcing bars using a two-part epoxy, BLH EPY-150, and cured at room temperature for 24 hours. Solder tabs were also epoxyed to the reinforcing steel at the ends of the gages. The EPY-150 epoxy was recommended for use by the manufacturer as a stable, long

lasting epoxy which would withstand the temperature and moisture variations during construction and testing of the pier.

The deformations on the reinforcing steel were filed off over an area large enough for the strain gages and solder tabs to be epoxyed down. The surface was then smoothed with emery cloth and cleaned with an acid based cleanser and neutralizer. The gage and tabs were epoxyed and allowed to cure. The lead wires and wires from the strain gages were soldered to the tabs and waterproofed with Micro Measurements M-Coat C, a rubber based waterproofing agent. After allowing to cure, a one-inch wide strip of "Barrier E", a waterproofing material manufactured by BLH Electronics, Inc., was placed on the gage and lead wires to insure waterproofing and protection from any physical damage. The "Barrier E" consists of a rubber sheet with a layer of soft gummy rubber material approximately 0.125 inches thick which can be applied to the gages and compressed around the wires and gage providing positive physical protection as well as moisture protection. After both gages on each bar were completed, electrical insulating tape was wrapped around the gages. The lead wires were numbered and taped at intervals up the length of the reinforcing steel to the top. Figures 36 and 37 are photographs of the reinforcing steel cage with the gages attached and a close up of the gages. The method of waterproofing proved to work quite well with only three gages rendered

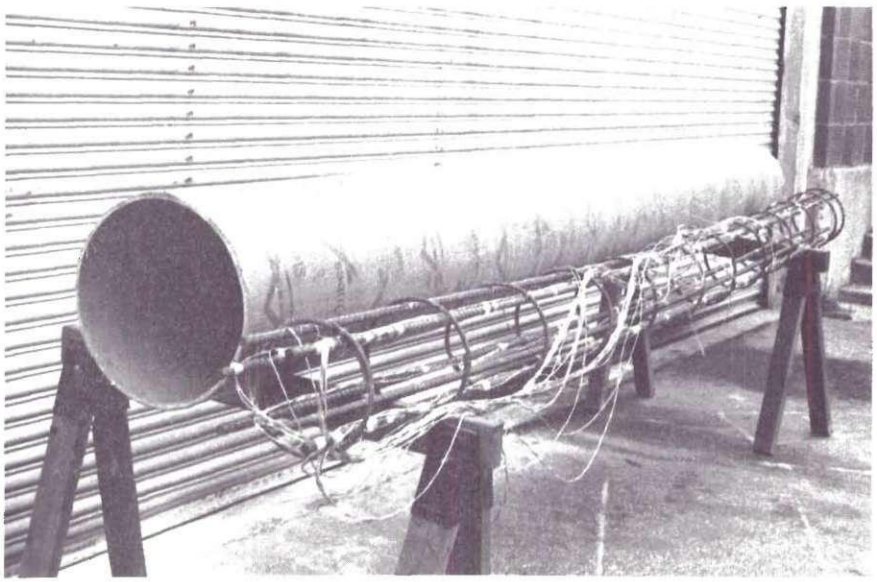

Figure 36. Reinforcing Steel and "Sleek Tube" Form

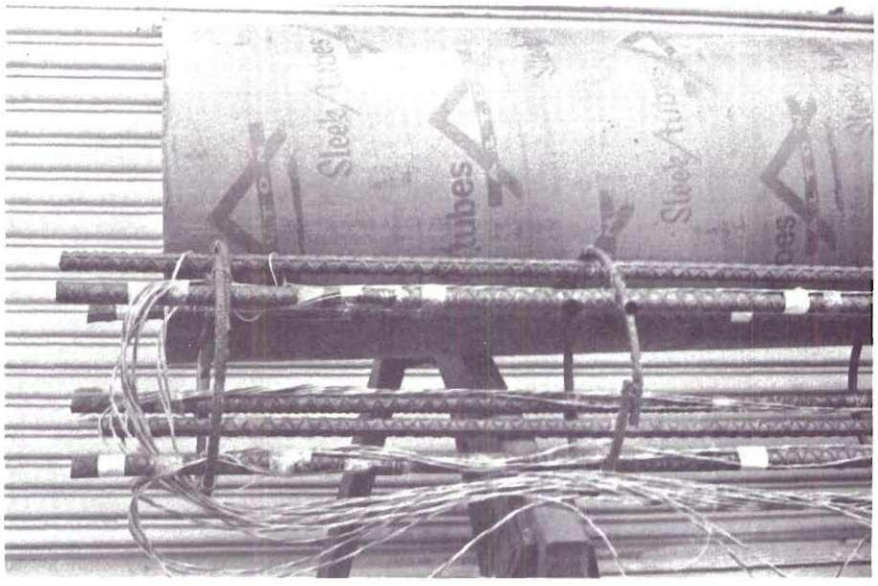

Figure 37. Close Up of Strain Gage Protection

inoperative due to moisture during the testing phase.

After completion of the pier construction, the strain gages were attached to a Baldwin 20-channel switching box which read the gages individually with a compensating gage wired to the other leg of the strain box bridge. The compensating gage was attached to a six-inch length of reinforcing steel, waterproofed and cast in a cylindrical concrete specimen six inches in diameter and twelve inches long, and placed in the sand pit adjacent to the pier.

Electric Strain Gages on the Concrete

The strain gages placed on the exterior of the pier were SR-4, Type A-9. These gages are paper backed, Constantan wire with a gage length of six inches, 300 ohms resistance and a gage factor of 2.12. The gages were placed at three levels along the pier shaft--3.83 feet, 8.50 feet and 13.17 feet from the pier top. These gages were placed at approximately the same level as the Carlson meters in order to compare the load results from each. Three gages were placed at each level 120 degrees apart and in the same radial orientation as the strain gages on the reinforcing steel.

The concrete surface on which the gages were to be placed was carefully examined to insure that no cracks were present. The gages were placed close to the cold joints that occurred where each Carlson meter was placed. The surface was wire brushed and cleaned of all loose debris. The gages were

bonded to the concrete with an industrial two part epoxy. They were held to the pier with a piece of Teflon along the length of the gage held in place by elastic tape wrapped around the circumference of the pier. The gages were allowed to cure for 24 hours and then a coating, approximately one-eighth inch thick, of the same epoxy was applied to the entire gage to protect the gage from moisture and the abrasive action of the sand. The lead wires for each gage were soldered with three inches of wire taped to the pier at each gage such that verticalmmovement of the pier would not break the soldered connection. The lead wires were run out horizontally from each gage when sand was placed up to the gage level and the wires were then taped up the side of the test pit. The gages were connected to a ten-channel Budd switching box, so each one could be read separately. A compensating gage was epoxyed on the outer surface of the same six-inch by twelve-inch concrete cylinder used for the compensating gage for the steel strain gages.

Linear Variable Differential Transformers (LVDT)

The two LVDT's used for sensing bottom movement were G. L. Collins Model SS-207 attached to the hydraulic ram and connected in series to a Sorenson Model ORD 60-5130-1 power supply and a NLS digital voltmeter Series MX-3. The voltage required for these LVDT's is 24 VDC. The connecting wires were placed in a six foot length of six-inch diameter PVC

running from the center of the pier to the edge where a vertical access port to the pier base allowed the wires to be run up to the top of the test pit. The Model SS-207 has a linear range of ±1.00 inch from the null position. The LVDT's were mounted such that approximately 1.5 inches of downward travel of the tip could be measured. The LVDT's were calibrated in series using two specially adapted .0001 inch micrometers and with the same power supply and digital voltmeter used during the tests. After calibrating with the micrometers, the LVDT's were attached to the hydraulic ram and placed in the Riehle testing machine. The ram was held at a constant height by monitoring the LVDT signal on the digital voltmeter. The exact position of the ram head could be held within ±0.0005 inches. The calibration curve is shown in Figure 38.

Hydraulic Ram

The hydraulic ram placed at the tip of the pier was a Simplex Jenny Model No. 1003A, 200,000 pound capacity hydraulic ram. The travel distance for the ram was 3.25 inches which was considered sufficient for tip movement of the pier. The bottom of the test pit was not level, and a level base was constructed. A three-foot by four-foot concrete pad was placed in the center of the pit, with two steel wide flange beams, eight inches in depth, cast into the pad and carefully leveled. A one-inch steel plate was bolted to the top of the

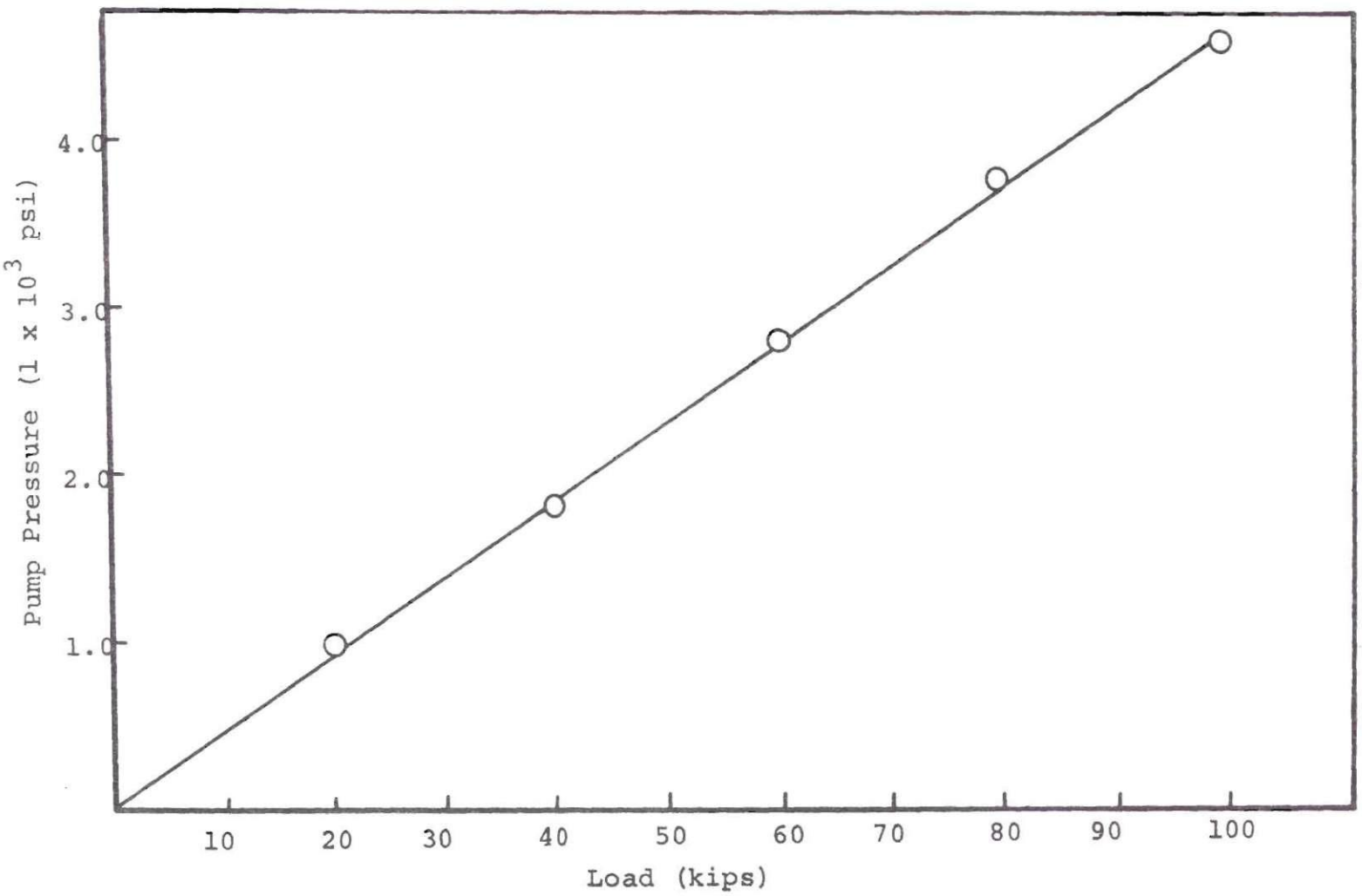

Figure 38. Calibration Curve for 200,000 Pound Simplex Ram

wide flange beams and the hydraulic ram was centered by means of a plumb bob from the top of the pit. After centering and leveling the ram, three small steel blocks were tack welded around the ram base to hold it in the center of the plate. The ram supported a series of welded circular plates, the largest being the diameter of the pier which supported the pier tip, as can be seen from Figure 39. The ram was connected by 10,000 psi reinforced high pressure hose to a pressure sensing and generating device constructed at the Georgia Institute of Technology. The pressure sensors are calibrated Bourdon pressure gages of varying ranges up to 10,000 psi. The pressure is generated by air pressure supplied to an air hydraulic pressure pump with valving arrangements which allow two positive displacement pistons to be included in the pressure line such that the hydraulic pressure can be monitored and regulated to within 10 psi. A picture of the hydraulic pressure device is included in Figure 8.

After completion of the calibration of the ram and LVDT's, they were placed in the pit, leveled and centered. The hose and all the wires were connected and fed through the protective PVC tubing to the access port and up to the top of the test pit. Prior to placing the sand, the ram was encased with a cylindrical sheet metal casing to protect the ram and LVDT's from the sand.

The loading at the top of the pier was done by a 40,000 pound capacity hydraulic Simplex ram which reacted against a steel reaction frame. The ram was calibrated in the Riehle

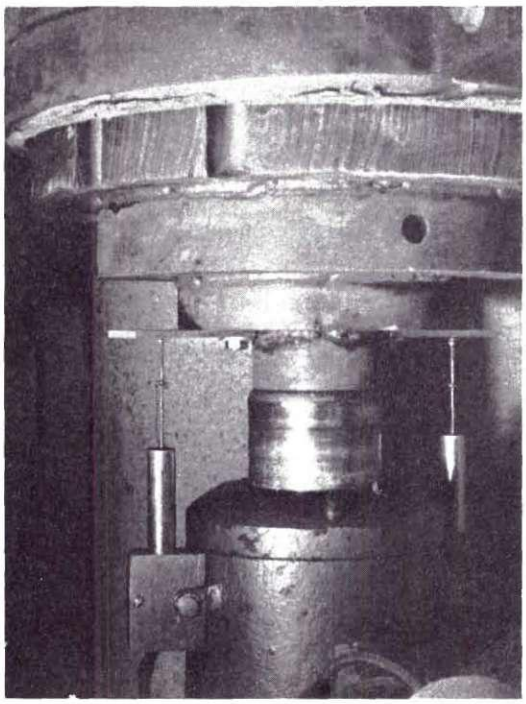

Figure 39. View of Bottom Ram, LVDT's, and Supporting Blocks

testing machine prior to being used in the test. The ram applied the load through the model load cell and several steel spreader plates to the top of the pier. The plates, load cell, and ram were leveled and centered individually on the pier top. The model load cell could sense any eccentric loading applied to the pier.

Deflection Gages

The pier deflection was measured by several .0001 inch micrometer dial gages mounted on three sides of the pier. The dial gages were attached to a cross beam resting on the outer edge of the test pit and free from any movement due to loading of the pier. The gages reacted against aluminum clips epoxyed to the pier at 90 degree intervals around the pier. Three gages were used to monitor the pier movement.

Four other gages were mounted on an additional support beam and measured the deflection of the sand surface one foot and one and one-half feet from the pier at 90 degree intervals. Figure 7 gives a view of these gages.

Carlson Stress Meters

The description, calibration and preliminary testing of these meters is included in Appendix F. The meters were placed at three levels in the concrete pier, and the installation was done in accordance with the manufacturer's recommendations. These recommendations require that the meters be placed against a previously hardened concrete

surface. To accomplish this, a 12-inch by 12-inch opening was cut in the pier form at each level where the Carlson meters were to be placed. After reaching the level for the first meter, the pour was stopped and the concrete was allowed to cure for several days. After hardening, the meter was placed in the center of the pier according to the manufacturer's recommendations and the next level of concrete was placed.

The placement of the meters was difficult due to the small amount of clearance between the reinforcing steel and the outer diameter of the Carlson meter. The rubber gasket material around the Carlson meter edge was trimmed off in order to fit the meter into the center of the pier. The rubber gasket and metal edge of some of the meters actually touched the vertical reinforcing steel.

The cables from the cells were attached to the reinforcing steel and brought out through the side of the pier at the top. After completing the pier, all the cells were checked and the resistance readings were correct. The results of the tests are indicated in Appendix F with a sample form indicating the application of temperature corrections.

APPENDIX F

CONCRETE MIX DESIGN FOR PIER

The mix design was based on a 28-day strength of 5,000 psi. The minimum recommended is 3,000 psi [38].

The maximum water-cement ratio for the probable exposure conditions is 0.5 [63]. The design slump was a minimum of six inches as recommended by O'Neill and Reese [38]. This high slump is recommended to make sure that the concrete is free flowing enough to fill all the voids in the pier cavity as the casing is removed. Since this slump is used in the field, the model was designed also based on this criterion.

The following quantities were used to determine the mix design by absolute volume:

Non-Air Entrained Concrete:

Water/cement Ratio	0.50	
Maximum Aggregate Size	0.75	inch
Air Content	2.0	percent
Slump	6	inches
Fineness Modulus of Fine Aggregate	1.98	
Fine Aggregate Specific Gravity	2.64	
Coarse Aggregate Specific Gravity	2.63	
Dry Rodded Density of Coarse Aggregate	96	PCF

The trial mix design based on the above quantities:

Cement	360 pounds
Water	720 pounds
Fine Aggregate	990 pounds
Coarse Aggregate	1,800 pounds

After mixing a trial batch, the above quantities were found suitable.

The typical batch weights for one of the pours:

Volume No. 4 (7.00 cubic feet):

Cement	93 pounds
Water	186 pounds
Fine Aggregate	255 pounds
Coarse Aggregate	467 pounds

The total batch weight was limited to a maximum of 500 pounds. The mixer operated with the most efficiency at this level. Table 18 gives the water-cement ratio and slump for each batch and volume. Since Type 1A Portland cement was used for Volumes 2-4, the mix design was adjusted to account for the air-entraining cement.

The concrete samples were cured in a moisture room for 28 days and comprehensive strength tests were conducted on cylinders from each of the four volumes. The results are shown in Table 19.

The tangent modulus of elasticity was measured for the stress range from 0 to 1,000 psi which was the stress range for the pier. The values are given in Table 19. The

Table 18. Slump, Water-Cement Ratio and Number of Samples for Concrete Pier

	Slump (inches)	W/C Ratio	Number of Samples (6 inch x 12 inch cylinders)
Volume 1 (5.00 cubic feet)			
Batch 1	5	0.48	3
Batch 2	7	0.51	2
Volume 2 (8.50 cubic feet) - Type 1A Cement			
Batch 1	6	0.53	2
Batch 2	7	0.55	2
Batch 3	7	0.54	2
Volume 3 (8.50 cubic feet) - Type 1A Cement			
Batch 1	5	0.53	2
Batch 2	7	0.55	2
Batch 3	6	0.58	2
Volume 4 (7.00 cubic feet)			
Batch 1	6.5	0.50	1
Batch 2	4.5	0.50	3
Batch 3	5	0.47	1

deflection of the cylinders was measured by a mechanical lever system using .001 inch micrometer dial gages.

Table 19. Twenty-Eight Day Compressive Strength of Concrete Cylinders

Cylinder-Volume Number	Failure Stress (psi)	Modulus of Elasticity (psi)
1	6050	2.86×10^6
2	5990	2.78×10^6
3	5300	3.33×10^6
4	5170	2.63×10^6

APPENDIX G

CARLSON STRESS METERS

These meters have been used extensively in concrete dams and large structures to measure both the vertical and horizontal stresses in large masses of concrete with good results [41]. The meter consists of a plate shaped device 7.25 inches in diameter and 0.5-inches thick as shown in Figure 40. One side of the plate is a flexible diaphragm with a mercury filled chamber. A cylinder protruding from one side of the plate contains a small elastic wire strain meter which senses changes in the mercury pressure. The range of the PC-800 meter is 0-800 psi and the sensitivity is five psi [12]. The change in stress is indicated by the resistance ratio measured by a sensitive decade resistance meter also supplied by the manufacturer of the meters.

The installation instructions [11] indicate that the meter cannot be placed in a mass of fresh concrete and be expected to suitably measure vertical stresses because, as the concrete cures, water migrating upward through the concrete collects on the underside of the meter. This collection of water underneath the meter creates an imperfect contact between the meter and concrete resulting in considerable under registration of the applied stress. The recommended

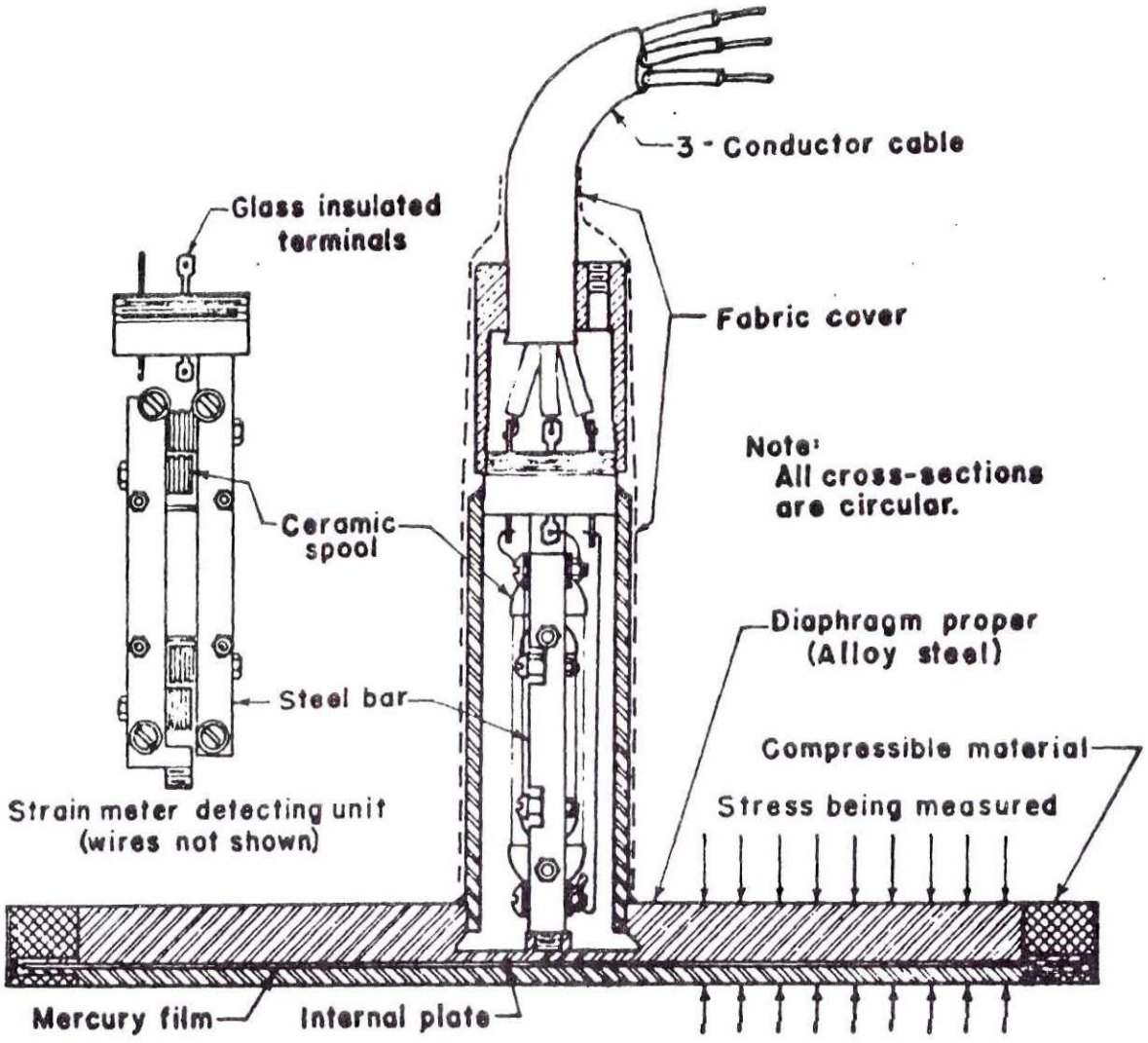

Figure 40. Carlson Stress Meter
(After Carlson [12])

procedure is to place the back of the meter against a previously hardened mass of concrete.

The meters were to be placed at the third points of the pier; 2.5 feet, 7.5 feet and 12.5 feet and in the center to measure the vertical stress. Originally, the meters were to be placed in the mass concrete. However, since it was likely that water would collect under the meter, an alternate method of placement was investigated. In order to prevent the accumulation of water under the meter, a cone of concrete was precast around the bottom of the meter and the stem as shown in Figure 41. Water migrating upward through the concrete mass would be deflected around the meter without collecting underneath the cell. A cone was precast on one of the meters, and to verify that this method would work, the meter and cylinder were cast in a twelve inch diameter cylinder, twenty-four inches long. The cylinder was cured for twenty-one days and then placed in a loading machine and tested. The meter under registered the applied stresses as much as 50 percent. The meter was removed from the cylinder and void spaces were found both below the cone and on the diaphragm face. The cone was removed from the meter and the recommended method of placement [11] on a previously hardened surface was tested. A twelve inch diameter cylinder twelve inches long had been previously cast and cured. The Carlson meter was placed on this hardened surface with a small amount of paste below the diaphragm and twenty-four inches of concrete was placed above

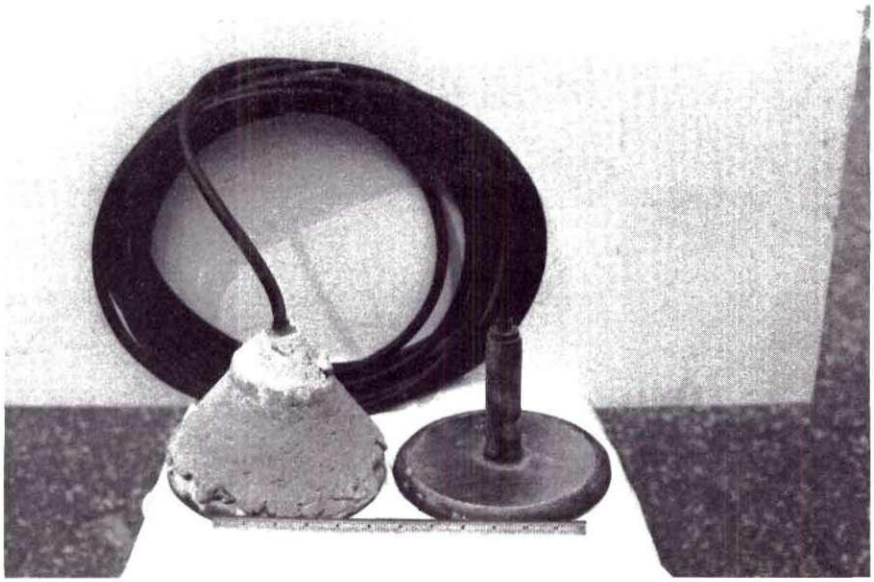

Figure 41. Carlson Stress Meters With and Without Concrete Cone

the meter. After curing, the 36-inch long cylinder was loaded and the stress levels indicated by the Carlson meter were within ten percent of those applied. As a result, the pier was cast in three separate sections in order to insure proper placement of the Carlson meters. Following the recommended procedure for the placement of the meters was considered to be of more importance than the effect of the construction joints in the pier.

The cable attached to the meters was a three conductor, 16 gage type 50 cable recommended by the cell manufacturer. The three wires were soldered to the correct terminals and coated with MM waterproofing agent. The space around the wires was filled with Presstite permagum waterproofing agent and the protective casing was placed over the wires. The meters were each checked for the correct resistance and resistance ratio prior to placing in the pier. The meter resistance and resistance ratio was checked after casting the pier and was found to be unchanged.

Carlson Meter Readings

The results of the Carlson meters have been discussed in Chapter VIII. This portion of the Appendix is included to indicate the computations and corrections required to determine the stress. Also included are the typical results from one of the tests.

The calibration constant for stress as supplied by the

manufacturer must be corrected for the extra resistance added by the conductor cable. The equation for the correction is as follows:

$$C' = C + \frac{y\ C\ (0.89)}{R} \qquad (35)$$

C' = New calibration constant

C = Calibration constant supplied by manufacturer

y = Resistance of a pair of conductor cables

R = Meter resistance at 0°F.

This resistance for the additional cable was 0.28 ohms for all three meters. The original calibrations and the corrected calibrations were:

Meter No.	Original Calibration	Corrected Calibration
125	5.23	5.40
126	5.19	5.36
127	5.23	5.40

A temperature correction is also required each time the meter is read. This correction is usually small and is deducted from the final stress. The correction is as follows:

$$T.C. = -[(80T/D + 6.7)10^{-6} - K]EF \qquad (36)$$

D = Thickness of stress meter

T = Thickness of mercury film

K = Coefficient of thermal expansion of concrete

E = Sustained modulus of elasticity of the concrete

F = Dependence factor of the stress meter (usually 0.07).

This correction was evaluated and applied to each reading for the stress meter.

Table 20 gives the results of the Carlson stress meters for Test 4.

Calibration Test

Prior to placing the meters in the model pier, one of the meters was cast in a concrete cylinder, twelve inches in diameter and twenty-four inches high. The meter was placed according to the manufacturer's recommendations. The cylinder was cured and loaded in a calibrated testing machine. The results are shown in Table 21.

Table 20. Results of Carlson Stress Meter for Test 4, Meter No. 127 (Middle of Pier)

Applied Stress (psi)	Temperature (°F)	Resistance Ratio	Resistance Ratio	Measured Stress (psi)	Temperature Correction (psi)	Corrected Measured Stress (psi)
0	64.5	109.94	0	0	-	0
92		104.58	0.36	195	4	199
196		104.11	0.83	448	4	452
292		103.82	1.02	550	4	554
386		103.59	1.35	729	4	733
485		103.32	1.62	875	4	879
541		103.18	1.76	950	4	954

As can be seen from an inspection of the table, the measured stresses are much higher than the actual applied stresses throughout the test. This difference was noted in all the tests with all the Carlson meters.

Table 21. Calibration Test of Carlson Meter

Applied Stress (psi)	Measured Stress (psi)	Percentage Difference (%)
0	0	0
50	54	8.0
200	196	2.0
400	372	7.0
500	470	6.0

APPENDIX H

SAMPLE CALCULATION FOR SKIN FRICTION

The following sample calculations are presented to indicate the steps involved in predicting the skin friction.

Test 2

The following data was generated from the direct shear test (smooth concrete):

$$\Psi = 30°25'$$

$$\text{Tan}\Psi = 0.5871 \qquad \frac{R_f}{\text{Tan}\Psi} = 1.47 \qquad (37)$$

$$R_f = 0.87$$

$$\gamma = 92.8$$

Using an average value of K = 0.35.

Determining E_i:

Section	Depth (ft)	Lateral Stress (σ_h) (psi)	E_i (pci)	$1/E_i$ (1/pci)
1	0.9	0.202	107	0.0093
2	2.7	0.61	221	0.0045
3	4.5	1.01	320	0.0031
4	6.3	1.42	390	0.00256
5	8.1	1.83	457	0.00219
6	9.9	2.24	525	0.00190
7	11.7	2.64	582	0.00172
8	13.5	3.04	640	0.00156

Table 22. Tabular Calculation of Skin Friction for Test 2 (Deflection Data Determined from Test 2)

Section	δ (in)	$1/E_i$ (1/pci)	1.47δ (in)	$1.47\delta/\sigma_h$ (in^3/lb)	(Sum) $1/E_i + 1.47\delta/\sigma_h$	δ/sum_2 (lb/in^2)	Skin Friction* (lbs)
1	0.0551	0.0093	0.0810	0.400	0.409	0.135	147
2	.0515	.0045	.0757	.124	.129	.401	435
3	.0480	.0031	.0706	.070	.073	.657	714
4	.0444	.00256	.0653	.046	.0486	.911	989
5	.0409	.00219	.0601	.0329	.0351	1.16	1,265
6	.0373	.00190	.0548	.0245	.0264	1.41	1,531
7	.0337	.00172	.0495	.0187	.0204	1.65	1,792
8	.0302	.00156	.0444	.0146	.0162	1.87	2,031
							8,904 pounds

*Skin Friction = δ/sum (area)

Section area = 1,086 in^2

BIBLIOGRAPHY

1. Aldrich, Hari P., Jr., "Importance of the Net Load to the Settlement of Buildings in Boston," *Journal of the Boston Society of Civil Engineers*, Volume 39, Number 2, April, 1952, pages 370-394.

2. Arthur, J. R. F. and Roscoe, K. H., "An Earth Pressure Cell for the Measurement of Normal and Shear Stresses," *Civil Engineering and Public Works Revue*, Volume 56, Number 659, 1961, pages 765-770.

3. Babichev, Z. V., "Stress and Deformation in Pile Foundations of Large-Panel Houses," *Osnovaniya*, Fundamenty i Mekhanika Gruntov, Number 5, September-October, 1966, pages 11-13.

4. Babichev, Z. V. and Yushin, A. I., "Combined Action of a Pile Foundation and the Boxing of a Large-Panel Frameless Building," *Osnovaniya*, Fundamenty i Mekhanika Gruntov, Number 6, November-December, 1970, pages 410-415.

5. Barker, W. R. and Reese, L. C., "Instrumentation for Measurement of Axial Loads in Drilled Shafts," *Research Report 89-6, Center for Highway Research*, The University of Texas at Austin, Austin, Texas, 1969.

6. Bozozuk, M., Personal Communication, 1971.

7. Bozozuk, M., "Field Instrumentation of Soil," *Proceedings, Conference on Design and Installation of Pile Foundations and Cellular Structures*, Lehigh University, Bethlehem, Pennsylvania, 1970, pages 145-157.

8. Bridgeman, P. W., *Dimensional Analysis*, Yale University Press, 1931.

9. Brumund, W. F., "Experimental Study of Static and Dynamic Friction Between Sand and Typical Construction Materials," *Journal of Testing and Evaluation*, 1973.

10. Brumund, W. F., "Subsidence of Sand Due to Surface Vibrations," Ph.D. Thesis, Purdue University, Lafayette, Indiana, 1969.

11. Carlson, R. W., "Manual for the Use of Stress Meters, Strain Meters, and Joint Meters in Mass Concrete," *Terrametrics*, Golden, Colorado, 1966, Part 1.

12. Carlson, R. W. and Pirtz, D., "Development of a Device for the Direct Measurement of Compressive Stress," *Journal of the American Concrete Institute*, November, 1952, pages 201-215.

13. Davisson, M. T., "Static Measurements of Pile Behavior," *Proceedings, Conference on Design and Installation of Pile Foundations and Cellular Structures*, Lehigh University, Bethlehem, Pennsylvania, 1970, pages 159- .

14. DeBeer, E. E., "The Scale Effect on the Phenomenon of Progressive Rupture in Cohesionless Soils," *Proceedings of the Sixth International Conference on Soil Mechanics and Foundation Engineering*, Montreal, Canada, Volume II, 1965, pages 13-17.

15. DuBose, L. A., "Load Studies of Drilled Shafts," *Proceedings, Highway Research Board*, Volume 34, Washington, D. C., 1955.

16. Duncan, J. M. and Chang, C. Y., "Nonlinear Analysis of Stress and Strain in Soil," *Journal of Soil Mechanics and Foundation Division*, ASCE, Volume 96, Number SM5, 1970, pages 1629-1654.

17. Fellenius, B. H. and Haagen, T., "New Pile Force Gauge for Accurate Measurements of Pile Behavior During and Following Driving," *Canadian Geotechnical Journal*, Volume 6, Number 3, August, 1969, pages 356-362.

18. Gupta, B. K., Edwards, A. D., and Loveday, R. W., "The Development and Use of a Force-Moment Transducer," *Magazine of Concrete Research*, Cement and Concrete Association, Volume 20, Number 64, September, 1968, pages 177-182.

19. Hickey, K. B., "Studies of Carlson Stress Meters in Concrete," *Report No. REC-ERC-71-19, Engineering and Research Center*, Bureau of Reclamation, Denver, Cclorado, 1971.

20. Hirsch, T. J., Coyle, H. M., Lowery, L. L., Jr., and Samson, C. H., Jr., "Instruments, Performance and Method of Installation," *Proceedings, Conference on Design and Installation of Pile Foundations and Cellular Structures*, Lehigh University, Bethlehem, Pennsylvania, 1970, pages 173-190.

21. Horner, J. M., "Uplift Resistance of Straight Auger and Belled Auger Footings in Sandy Silt," United States Department of the Interior, Bureau of Reclamation, Denver, Colorado, November, 1969.

22. Jaky, J., "The Coefficient of Earth Pressure at Rest," *Journal of the Society of Hungarian Architects and Engineers*, 1944, pages 355-358.

23. Janbu, N., "Soil Compressibility as Determined by Oedometer and Triaxial Tests," European Conference on Soil Mechanics and Foundations Engineering, Wiesbaden, Germany, Volume 1, pages 19-25, 1963.

24. Jimenez, Salas J. A., "Tests on Models Related to the General Topic of the Conference," *Proceedings, Conference on Deep Foundations*, Mexican Society of Soil Mechanics, Volume I, Mexico City, 1964.

25. Kerisel, J. L., "Deep Foundations--Basic Experimental Facts," *Proceedings, Conference on Deep Foundations*, Mexican Society of Soil Mechanics, Volume I, Mexico City, 1964, pages 5-44.

26. Konder, R. L. and Zelasko, J. S., "A Hyperbolic Stress-Strain Formulation for Sands," *Proceedings, Second Pan-American Conference on Soil Mechanics and Foundation Engineering*, Brazil, Volume I, 1963, pages 289-324.

27. Lambe, T. W., *Soil Testing for Engineers*, John Wiley and Sons, Inc., New York, 1951, page 93.

28. Langhaar, H. L., *Dimensional Analysis, and Theory of Models*, John P. Wiley and Sons, Inc., New York, 1951.

29. Mabry, R. E., Discussion, *Journal of the Soil Mechanics and Foundations Division*, ASCE, Volume 95, SM2, March, 1969, pages 668-673.

30. Martins, J. B., "Pile Load Tests on the River Pungue," *Proceedings, Third Regional Conference for Africa on Soil Mechanics and Foundation Engineering*, The Rhodesian Institution of Engineering, Salisbury, 1963, pages 157-160.

31. Mazurkiewicz, B. K., "Skin Friction on Model Piles in Sand," *Danish Geotechnical Institute*, Bulletin No. 25, 1968, pages 13-47.

32. Meyerhoff, G. G., Session 1, *Conference on Deep Foundations*, Mexican Society of Soil Mechanics, Volume II, Mexico City, 1964, page 416.

33. Mindlin, R. D., "Force at a Point in the Interior of a Semi-Infinite Solid," *Physics*, Volume 7, May, 1936.

34. Mohan, D. and Chandra S., "Frictional Resistance of Bored Piles in Expansive Clays," *Geotechnique*, Volume XI, Number 4, London, December, 1961.

35. Mohan, D. and Jain, G. S., "Bearing Capacity of Bored Piles in Expansive Clays," *Proceedings of the Fifth International Conference on Soil Mechanics and Foundation Engineering*, 1961.

36. Mohan, D., Jain, G. S. and Kuman, V., "Load-Bearing Capacity of Piles," *Geotechnique*, Volume 13, Number 1, Institution of Civil Engineering, London, March, 1963, pages 76-86.

37. Murphy, G., *Similitude in Engineering*, The Ronald Press Company, New York, 1950.

38. O'Neill, M. W. and Reese, L. C., "Behavior of Axially Loaded Drilled Shafts in Beaumont Clay," *Research Report 89-8, Parts 1, 2, 3, 4, and 5, Center for Highway Research*, The University of Texas at Austin, Austin, Texas, December, 1970.

39. Parker, F., Jr., and Reese, L. C., "Experimental and Analytical Studies of Behavior of Single Piles in Sand Under Lateral and Axial Loading," *Research Report 117-2, Center for Highway Research*, The University of Texas at Austin, Austin, Texas, 1970.

40. Potyondy, J. G., "Skin Friction Between Various Soils and Construction Materials," *Geotechnique*, Volume II, Number 4, Institution of Civil Engineers, London, 1961.

41. Raphael, J. M. and Carlson, R. W., "Measurement of Structural Action in Dams," *Terrametrics*, Golden, Colorado, 1965, Part 2.

42. Reese, L. C., Brown, J. C. and Dalrymple, H. H., "Instrumentation for Measurements of Lateral Earth Pressure in Drilled Shafts," *Research Report 89-Z, Center for Highway Research*, The University of Texas at Austin, Austin, Texas, 1968.

43. Reese, L. C. and Hudson, R. W., "Field Testing of Drilled Shafts to Develop Design Methods," *Research Report 89-1, Center for Highway Research*, The University of Texas at Austin, Austin, Texas, 1968.

44. Sowa, V. A., "Pulling Capacity of Concrete Cast in Situ Bored Piles," *Canadian Geotechnical Journal*, Volume 7, Number 4, November, 1970, pages 482-493.

45. Sowers, G. B. and Sowers, G. F., *Introductory Soil Mechanics*, The Macmillan Company, New York, 1970, page 338.

46. Sowers, G. F., Session, I., *Conference on Deep Foundations*, Mexican Society of Soil Mechanics, Volume II, Mexico City, 1964, page 306.

47. Terzaghi, K., "Theoretical Soil Mechanics," John Wiley and Sons, Inc., New York, 1943, pages 202-206.

48. Tjechman, A., "Skin Friction of a Model Pile Driven in Sand," *Danish Geotechnical Institute*, Bulletin No. 29, 1971, pages 5-26.

49. Touma, F. T. and Reese, L. C., "Behavior of Bored Piles in Sand," *Proceedings, ASCE Annual and National Environmental Engineering Meeting*, Houston, Texas, 1972.

50. Vanderbilt, D. M., "Structural Reaction Dynamometers," *Journal of the Structural Division*, ASCE, Volume 97, Number ST6, 1971, pages 1701-1713.

51. Vesic, A. S., "Load Transfer in Pile-Soil Systems," *Proceedings, Conference on Design and Installation of Pile Foundations and Cellular Structures*, Lehigh University, Bethlehem, Pennsylvania, 1970, pages 47-73.

52. Vesic, A. S., "A Study of Bearing Capacity of Deep Foundations," Engineering Experiment Station, Georgia Institute of Technology, *Project B-189 Final Report*, 1967.

53. Vesic, A. S., "Investigation of Bearing Capacity of Piles in Sand," *Proceedings, Conference on Deep Foundations*, Mexican Society of Soil Mechanics, Volume I, Mexico City, 1964.

54. Vesic, A. S., "Model Testing of Deep Foundations and Scaling Laws," *Proceedings, Conference on Deep Foundations*, Mexican Society of Soil Mechanics, Volume II, Mexico City, 1964.

55. Vijayvergiya, V. N., Hudson, R. W. and Reese, L. C., "Load Distribution for a Drilled Shaft in Clay Shale," *Research Report 89-5, Center for Highway Research*, The University of Texas at Austin, Austin, Texas, 1968.

56. Ward, H. S., "Some Reasons and Techniques for Measuring Large Structural Displacements," *The Engineering Journal*, Volume 54/6, June, 1971, pages 14-21.

57. Watt, W. G., Kurfurst, P. J. and Zeman, Z. P., "Comparison of Pile Load-Test--Skin Friction Values and Laboratory Strength Tests," *Canadian Geotechnical Journal*, Volume 6, Number 3, August, 1969, pages 339-352.

58. Watson, F. X., "An Investigation of the Development of Skin Friction of Drilled Piers in Decomposed Rock," Ph.D., Thesis, Georgia Institute of Technology, Atlanta, Georgia, 1970.

59. Whitaker, T. and Cooke, R. W., "An Investigation of the Shaft and Base Resistance of Large Bored Piles in London Clay," *Proceedings of the Symposium on Large Bored Piles*, Institution of Civil Engineers, London, February, 1966.

60. Whitaker, T. and Cooke, R. W., "100 Ton Load Cell for Pile Loading Tests," *Engineering*, Volume 194, Number 5040, London, November 23, 1962, pages 693-695.

61. Whitaker, G. M. J. and Colman, R. B., "The Design of Piles and Cylindrical Foundations in Stiff Fissured Clay," *Proceedings, Sixth International Conference on Soil Mechanics and Foundation Engineering*, Volume II, 1963.

62. Woodward, R. J., Lundgren, R. and Boitano, J. D., Jr., "Pile Loading Tests in Stiff Clay," *Proceedings of the Fifth International Conference on Soil Mechanics and Foundation Engineering*, 1961.

63. --------, "Design and Control of Concrete Mixtures," Portland Cement Association, Skokie, Illinois, 1968.

64. --------, "etd 150 Alloy Steel Bars," *Helpful Data Bulletin No. 41*, LaSalle Steel Company, Chicago, Illinois, 1968.

VITA

Samuel Patton Clemence was born on May 23, 1939, in Knoxville, Tennessee. He graduated from Druid Hills High School, Atlanta, Georgia, in 1957. He received a Bachelor of Science in Civil Engineering (cooperative plan) from the Georgia Institute of Technology in 1962, and a Master of Science from the Georgia Institute of Technology in 1964. Upon completion, he entered the United States Navy as an officer in the Civil Engineer Corps. His assignments included serving as assistant operations officer for a Seabee Battalion in Guam and Viet Nam. He served as officer in charge of a Seabee team deployed to northeast Thailand engaged in the construction of an earth dam and roadway. He served as assistant resident officer in charge of construction for the construction of a naval hangar and support facilities at Rota, Spain, and as assistant public works officer at the Naval Amphibious Base in Little Creek, Virginia. During his work on his Ph.D., he has served as graduate research assistant and graduate teaching assistant at the Georgia Institute of Technology.

His professional activities include membership in the American Society of Civil Engineers, Society of American Military Engineers, Highway Research Board, Sigma Xi and Chi Epsilon.